

Electromagnetic Bandgap Structures (EBGSs) Assisted Microstrip Bandpass Filter

by

Abu Talha Sadi

A thesis submitted in partial fulfillment of the requirement for the degree of Master of
Science in Electrical and Electronic Engineering



Khulna University of Engineering & Technology

Khulna 920300, Bangladesh.

August 2015 alha Sadi

Declaration

This is to certify that the thesis work entitled “*Electromagnetic Bandgap Structures (EBGSs) Assisted Microstrip Bandpass Filter*” has been carried out by *Abu Talha Sadi* in the *Department of Electrical and Electronic Engineering*, Khulna University of Engineering and Technology, Khulna Bangladesh. The thesis work or any part of this work has not been submitted anywhere for the award of any degree or diploma.

Signature of Supervisor
(Prof. Dr. Md. Nurunnabi Mollah)

Signature of Author
(Abu Talha Sadi)

Approval

This is to certify that the thesis work submitted by *Abu Talha Sadi* entitled “*Electromagnetic Bandgap Structures (EBGSs) Assisted Microstrip Bandpass Filter*” has been approved by the board of examiners for the partial fulfillment for the degree of *Master of Science in Electrical & Electronic Engineering* in the Department of *Electrical & Electronic Engineering*, Khulna University of Engineering & Technology, Khulna, Bangladesh in August, 2015.

Board of Examiners

1. Chairman
(Supervisor)

Dr. Md. Nurunnabi Mollah
Professor
Department of Electrical & Electronic Engineering
Khulna University of Engineering & Technology

2. Member

Head
Department of Electrical & Electronic Engineering
Khulna University of Engineering & Technology

3. Member

Prof. Dr. Md. Shahjahan
Department of Electrical & Electronic Engineering
Khulna University of Engineering & Technology

4. Member

Prof. Dr. Mohammad Shaifur Rahman
Department of Electrical & Electronic Engineering
Khulna University of Engineering & Technology

5. Member
(External)

Prof. Dr. Md. Maniruzzaman
Electronics and Communication Discipline
Khulna University, Khulna

Acknowledgment

It is a great pleasure for me to express unbound indebted gratitude to my respected supervisor **Professor Dr. Md Nurunnabi Mollah**, Department of Electrical and Electronic Engineering, Khulna University of Engineering & Technology (KUET), for his numerous helpful, constructive suggestion, scholastic guidance, constant inspiration, valuable advices and kind co-operation for the successful completion of the work on “*Electromagnetic Bandgap Structures (EBGSs) Assisted Microstrip Bandpass Filter*”. I have received continuous motivation and suggestions from him regularly. In my academic life, I am boasting of having such a dynamic and punctual supervisor. This work could not be possible without his help.

My thanks go to all teachers, technicians and staff of Communication Lab for their assistance and support throughout the completion of this thesis work.

I convey my special thanks to my mother for her constant encouragements, devotion and moral support to complete my M. Sc. degree.

Space does not allow me to mention each person by name, but I am deeply grateful to my friend Mr. G. M. Rafiquzzaman Shohag who helped me in different ways. I also wish to complement all the respected concern teachers, staffs & friends of my Department for their direct and indirect co-operation at different times.

Author
Abu Talha Sadi

Abstract

In high performance of wireless communication and advanced modern technologies, the demand for large bandwidth, high efficiency radio frequency devices, ease of installation, low profile antennas with the microwave devices are required tremendously. To meet these requirements the new technique Electromagnetic Bandgap Structures (EBGSs) have been introduced as potential means of improving the performances of existing RF active and passive devices. EBGSs are periodic structures those exhibit distinct passband and stopband properties. These are the unique properties of this structure.

The thesis concern the planner EBGS in forms of conventional circular, square, rectangular and dumbbell shaped defected ground structures (DGSs). The investigations into different types of EBGSs that yield better passband, return loss, insertion loss, low ripple and wider stopband have been carried out. The parametric study of different shaped EBGSs have been conducted with their inter element spacing, width, length and the size of the slots. From the investigation, it is clear that 1-D EBGS yield similar performance like 2-D EBGS. It is also found that dumbbell shaped DGS is more compact than the conventional EBGS. For conventional EBGS, it found that etching area is an important factor for producing stopband. In case of dumbbell shaped DGS, narrower slot and its position play important role to produce stopband.

The novel design is used in asymmetric coupled line bandpass filters. It is found that EBGSs suppress second and third harmonics by about 40 dB. This illustrates the significance of EBGSs in suppression of higher order harmonics of the bandpass filters. It has been found that the non - uniform distribution of EBGSs is more effective to suppress higher order harmonics than the conventional uniform EBGSs. Dumbbell shape DGSs are very effective for simultaneous suppression of both 2nd and 3rd harmonics due to their very wide stopband performances. This phenomenon of dumbbell shaped DGSs has been demonstrated in various designs of asymmetric coupled line bandpass filters.

Contents

Title Page	i
Declaration	ii
Approval	iii
Acknowledgments	iv
Abstract	v
Contents	vi
List of Figures	ix
List of Tables	xv
List of Abbreviations	xvi
List of Major Symbols	xviii
CHAPTER I Introduction	1
1.1 Introduction	1
1.2 Objective of the Thesis	2
1.3 Thesis Outline	4
CHAPTER II Literature Survey	5
2.1 Introduction	5
2.2 Application of EBGs	6
2.3 EBG Tuned Microwave Devices	10
2.4 Miniaturization	10
CHAPTER III Filter Terminologies and Conventional Filters	12
3.1 Introduction	12
3.2 Filter	12
3.3 Microwave Filter	13
3.4 Classification of Filter	15
3.5 Different Types of Filter	17
3.6 Advantages and Uses of Filters	18
3.7 Network Variables	19
3.8 Definition of Different Terminologies	25

3.9	Periodic Structures	28
3.10	Conventional Filter Design	32
3.10.1	Filter Design by the Image Parameter Method	33
3.10.2	Filter Design by the Insertion Loss Method	40
3.10.3	Filter Implementation	44
3.11	Coupled Line Filters	46
3.12	Design of Coupled Line Bandpass Filter	49
3.13	Conclusion	56
CHAPTER IV	Electromagnetic Bandgap Structures (EBGSs)	57
4.1	Introduction	57
4.1.1	Classification of EBG Structures	57
4.1.2	Types of EBG Structures On The Basis of Dimensions	64
4.2	Microstrip Lines	66
4.3	Analysis methods for EBG structures	70
4.4	Defected ground Structure	71
4.5	Design of Microstrip Transmission Line over Uniform PBGS (uniform circular PBGS)	74
4.5.1	Designing equation	74
4.5.2	Designs of Uniform Circular PBGSs	75
4.5.3	Designs of Uniform Square Patterned PBGSs	77
4.5.4	Designs of Dumbbell shaped Defected Ground Structures (DGSs)	78
4.6	Simulated S-parameter Performances)	78
4.7	Conclusion	84
CHAPTER V	EBGS Assisted Bandpass Filter	85
5.1	Introduction	85
5.2	Compact EBG assisted Bandpass filter	85
5.3	Uniform PBGS assisted Bandpass filter	88
5.3.1	Reference Bandpass Filter	88
5.3.2	Design of Uniform PBGS assisted Bandpass Filter	90

5.3.3 Performances of Uniform PBGS assisted Bandpass Filter	92
5.4 Uniform Dumbbell Shaped DGS assisted BPF for Harmonic Suppression	96
5.5 Non-Uniform Dumbbell Shaped DGS assisted Bandpass Filter for Harmonic Suppression	98
5.5.1 Theory of Non-uniform 1-D Microstrip PBGSs	98
5.5.1.1 Binomial Distribution	98
5.5.1.2 Chebyshev Distribution	99
5.5.2 Binomially Distributed Dumbbell Shaped DGS assisted Bandpass Filter	100
5.5.3 Chebyshev Distribution Dumbbell Shaped DGS assisted Bandpass Filter	101
5.6 Conclusion	105
CHAPTER VI Conclusion	106
6.1 Conclusion	106
6.2 Recommendation for Future Work	107
References	109

LIST OF FIGURES

Figure No	Description	Page
Fig. 2.1	(a) Schematic of UC-PBG metallic pattern. (b) Unit cell of the UC-PBG structure	08
Fig. 2.2	Schematic diagram of a BPF	09
Fig. 3.1	Electromagnetic spectrum	13
Fig. 3.2	Different types of filters	15
Fig. 3.3	Conventional lowpass filter	16
Fig. 3.4	Conventional highpass filter	16
Fig. 3.5	Conventional bandpass filter	17
Fig. 3.6	Conventional bandstop filter	18
Fig. 3.7	Two-port network showing network variables	19
Fig. 3.8	Symmetrical two-port networks with (a) even-mode excitation, and (b) odd-mode excitation	21
Fig. 3.9	Periodic structures. (a) Periodic stubs on a microstrip line. (b) Periodic diaphragms in a waveguide	28
Fig. 3.10	Equivalent circuit of a periodically loaded transmission line. The unloaded line has characteristic impedance Z_0 and propagation constant k	28
Fig. 3.11	(a) Equivalent circuit model of a unit cell, (b) a transmission line cascaded by unit cells. The unit cell may be divided into three parts as a transmission line of length $d/2$ on either side of normalized susceptance B	30
Fig. 3.12	A two-port network terminated in its image impedances	33
Fig. 3.13	A two-port network terminated in its image impedances and driven with a voltage generator	34
Fig. 3.14	Low-pass constant- k filter sections in T and π forms. (a) T-section (b) π –section	36
Fig. 3.15	Typical passband and stopband characteristics of the low-pass	

	constant- k sections of Fig. 3.6	37
Fig. 3.16	High-pass constant- k filter sections in T and π forms. (a) T-section. (b) π –section	37
Fig. 3.17	Development of an m -derived filter section from a constant-k section	38
Fig. 3.18	m-Derived filter sections (a) Low-pass T-section (b) High-pass T-section	38
Fig. 3.19	Typical attenuation responses for constant-k , m -derived, and composite filters	39
Fig. 3.20	A bisected π -section used to match $Z_{i\pi}$ to Z_{iT}	40
Fig. 3.21	The final four-stage composite filter	40
Fig. 3.22	Maximally flat and equal-ripple low-pass filter responses ($N = 3$)	42
Fig. 3.23	Elliptic function lowpass filter response	42
Fig. 3.24	The process of filter design by the insertion loss method	43
Fig. 3.25	Richards' transformation. (a) For an inductor to a short-circuited stub. (b) For a capacitor to an open-circuited stub	45
Fig. 3.26	The Four Kuroda Identities ($n^2 = 1 + Z_2/Z_1$)	46
Fig. 3.27	Definitions pertaining to a coupled line filter section. (a) A parallel coupled line section with port voltage and current definitions. (b) A parallel coupled line section with even- and odd-mode current sources. (c) A two-port coupled line section having a bandpass response	48
Fig. 3.28	Equivalent circuit of the coupled line section of Fig. 3.27c	50
Fig. 3.29	Development of an equivalent circuit for derivation of design equations for a coupled line bandpass filter. (a) Layout of an ($N + 1$)-section coupled line bandpass filter. (b) Using the equivalent circuit of Figure 8.44 for each coupled line section. (c) Equivalent circuit for transmission lines of length 2θ . (d) Equivalent circuit of the admittance inverters. (e) Using results of (c) and (d) for the $N = 2$ case. (f) Lumped-element circuit for a bandpass filter for $N = 2$	51
Fig. 4.1	Different EBG structures	58
Fig. 4.2	Bumpy metal sheet: (a) electric field extends across the bumps and	

	(b) electric field wraps around the bumps	58
Fig. 4.3	Corrugated metal surface	59
Fig. 4.4	Periodic metal connected to ground with via holes to yield high impedance surface	59
Fig. 4.5	UC-PBG structure (b) Unit cell	60
Fig. 4.6	Three-dimensional view of a substrate perturbed by uniform circular slots	61
Fig. 4.7	Triangular slots with square lattice	62
Fig. 4.8	The geometry of 2-D square slots having square lattice structure	62
Fig. 4.9	2-D geometry of a substrate having uniform circular slots with square lattice	63
Fig. 4.10	Uniform circular slots with triangular lattice arrangement	63
Fig. 4.11	Uniform circular slots with rectangular lattice	64
Fig. 4.12	Three dimensional EBG structure	65
Fig. 4.13	Two dimensional EBG structure	65
Fig. 4.14	One dimensional EBG structure	66
Fig. 4.15	General microstrip structure	67
Fig. 4.16	A microstrip transmission line	68
Fig. 4.17	Characteristic impedance and effective permittivity of microstrip line	70
Fig. 4.18	Lumped LC model for EBG analysis	71
Fig. 4.19	Periodic transmission line method for EBG analysis	71
Fig. 4.20	Geometry of a unit cell of a dumbbell shape DGS. The arm length of a larger square patterned slot is 'b'. The vertical rectangular slot has width, w and gap g	73
Fig. 4.21	The equivalent circuit of dumbbell shaped DGS unit	74
Fig. 4.22	Geometry of a standard 50Ω Tx-line	76
Fig. 4.23	(a) Geometry of a 50-ohm microstrip transmission line where 2-D (three lines) uniform circular PBGSs are etched in the ground plane. (b) The filling factor (FF) explanation ($FF = r/a$)	76
Fig. 4.24	Geometry of a standard 50-ohm transmission line with 1-D uniform circular PBGSs etched in the ground plane	77

- Fig. 4.25 2-D (three lines) of square patterned PBGSs under standard 50 ohm transmission line. Substrates: $\epsilon_r = 2.45$ and height (h) = 31 mils and $\tan\delta = 0.002$. The inter-element spacing, $a = 10.43$ mm, element width and length, $b = 5.215$ mm 77
- Fig. 4.26 1-D square patterned periodic structures under standard 50-ohm transmission line. The substrate is Taconic having dielectric constant of 2.45 and height of 31 mils. The inter-element spacing, $a = 10.43$ mm, element width and length, $b = 5.215$ mm 78
- Fig. 4.27 1-D Dumbbell shaped DGSs patterned periodic structures under standard 50-ohm transmission line. The substrate is Taconic having dielectric constant of 2.45 and height of 31 mils. The inter-element spacing, $a = 10.43$ mm, element width and length, $b = 5.215$ mm 78
- Fig. 4.28 IE3D simulated S-parameters versus frequency of an ideal 50-ohm transmission line. The substrate is Taconic having height of 31 mils and the dielectric constant is 2.45 79
- Fig. 4.29 Simulated S-parameter performances of a standard 50- ohm transmission line perturbed by 2-D (three lines) uniform circular PBGSs in the ground plane. The substrate is Taconic having height of 31 mils and dielectric constant of 2.45. The uniform circular PBGSs are of 2.6075 mm and the period is 10.43 mm (FF=0.25) 80
- Fig. 4.30 Simulated S-parameter performances of a standard 50 ohm transmission line perturbed by 1-D (one line) uniform circular PBGSs in the ground plane 81
- Fig. 4.31 S-parameters performances of three lines uniform square-patterned PBG structures. The substrate is Taconic having dielectric constant of 2.45 and height of 31 mils. The inter-element spacing is 10.43 mm and FF is 0.50 82
- Fig. 4.32 Simulated S-parameter performances of a standard 50 ohm transmission line perturbed by 1-D (one line) uniform rectangular PBGSs in the ground plane 83
- Fig. 4.33 S-parameters performances of three lines uniform Dumbbell shaped DGS structures. The substrate is Taconic having dielectric

	constant of 2.45 and height of 31 mils. The inter-element spacing is 10.43 mm and FF with respect to larger element is 0.50	84
Fig. 5.1	The schematic of a microstrip BPF on the UC-PBG ground	86
Fig. 5.2	Measured S-parameters of the PBG BPF. The S_{21} of a conventional BPF is also plotted for comparison (indicated by BPF / REF)	87
Fig. 5.3	Geometry of a reference 4 section parallel coupled line band pass filter with unperturbed on RT/Duroid 6010 substrate. Dielectric constant, $\epsilon_r = 10.2$, thickness, $h = 25$ mils, $\tan\delta = 0.0002$ and $W = 24$ mils	89
Fig. 5.4	S-parameters performance of an unperturbed 4 section parallel coupled line band pass filter according to Fig 5.3	89
Fig. 5.5	BPF with PBGSs (0.25 FF) under two extreme 50 ohm lines	90
Fig. 5.6	BPF with PBGSs (0.25 FF) under all lines assisted BPF	91
Fig. 5.7	BPF with PBGSs (0.30 FF) under all lines assisted BPF	91
Fig. 5.8	BPF with PBGSs (0.25 FF) under all lines assisted BPF	91
Fig. 5.9	BPF with PBGSs (0.45 FF) under all lines assisted BPF	92
Fig. 5.10	Simulated S-parameters performances of a BPF where two 50-ohm lines are only perturbed with uniform circular PBGSs. Substrate is RT/Duroid having dielectric constant of 10.2 and height of 0.635 mm	92
Fig. 5.11	Theoretical S-parameters performances of a BPF when uniform circular PBGSs are situated under all the lines. Substrate is RT/Duroid having dielectric constant of 10.2 and height of 0.635 mm	93
Fig. 5.12	S-parameters performances of a BPF when uniform circular at 0.30FF (design 3) PBGSs are situated under all the lines. Substrate is RT/Duroid having dielectric constant of 10.2 and height of 0.635 mm	94
Fig. 5.13	S-parameters performances of a BPF when uniform square at 0.40FF PBGSs are situated under all the lines. Substrate is RT/Duroid having dielectric constant of 10.2 and height of 0.635	

	mm	95
Fig. 5.14	S-parameters performances of a BPF when uniform square at 0.45FF PBGSs are situated under all the lines. Substrate is RT/Duroid having dielectric constant of 10.2 and height of 0.635 mm	96
Fig. 5.15	Geometry of a dumbbell shaped DGS assisted BPF. 6 dumbbell shaped DGSs are used under two 50 Ω transmission line	97
Fig. 5.16	Simulated S-parameters performances of a dumbbell shaped DGS assisted BPF having total 6 DGS (3+3) lying under two 50 Ω transmission lines	97
Fig. 5.17	Pascal's Triangle	99
Fig. 5.18	Geometry of a binomially distributed dumbbell shaped DGS assisted BPF. 6 dumbbell shaped DGSs are used under two 50 Ω transmission line	101
Fig. 5.19	Simulated s-parameter performances of a band pass filter perturbed by binomially distributed dumbbell shaped DGS in the ground plane. The substrate is RT/Duroid having height of 25 mils and dielectric constant of 10.2	101
Fig. 5.20	Geometry of a chebyshev distributed dumbbell shaped DGS assisted BPF. 10 dumbbell shaped DGSs are used under two 50 Ω transmission line	102
Fig. 5.21	Simulated s-parameter performances of a band pass filter perturbed by chebyshev distributed dumbbell shaped DGS in the ground plane. The substrate is RT/Duroid having height of 25 mils and dielectric constant of 10.2	103

LIST OF TABLE

Figure No	Description	Page
Table. 3.1	Chart of the electromagnetic spectrum	14
Table 5.1	A comparison table of the different designs and its s-parameter performances.	103

List of Abbreviations

FF	Filling factor
PBG	Photonic bandgap
PBGSs	Photonic bandgap structures
UPBGS	Uniform PBGS
BPF	Bandpass filter
PCB	Printed circuit board
DGS	Defected ground structure
TEM	Transverse Electric and Magnetic
TM	Transverse magnetic
TE	Transverse electric
UC-PBG	Uniplanar compact-photonic bandgap
EM	Electromagnetic
EBGS	Electromagnetic bandgap structure
PC	Photonic crystal
1-D, 2-D, 3-D	One dimensional, two dimensional, three dimensional
RF	Radio frequency
FET	Field effect transistor
VLSI	Very large scale integration
dB	Decibel
BW	Bandwidth
ACPA	Aperture coupled patch antenna
VSAT	Very small aperture terminal

LED	Light emitting diode
LPF	Lowpass filter
LO	Local oscillator
GPS	Global positioning system
HF	High frequency
VHF	Very high frequency
VNA	Vector network analyzer
MSAT	Mobile satellite
HMIC	Hybrid microwave integrated circuit
MMIC	Monolithic microwave integrated circuit

List of Major Symbols

ϵ_r	Dielectric constant
ϵ_{eff}	Effective relative permittivity
C_0	Speed of light in free space
γ	Propagation constant
β	Phase Constant
π	Pi = 3.1415927
ω	Angular frequency
k	Wave number (/m)
α	Attenuation constant
λ_g	Guided wavelength
λ_0	Wavelength in air
Z_0	Characteristic impedance
f_0	Center frequency
S	Scattering parameters

CHAPTER I

Introduction

1.1 Introduction

In high performance of wireless communication and advanced modern technologies, the demand for large bandwidth, high efficiency radio frequency devices, ease of installation, low profile antennas with the microwave devices are required tremendously. To meet these requirements the new technique Electromagnetic Bandgap Structures (EBGSs) have been introduced as potential means of improving the performances of existing RF active and passive devices. EBGSs are periodic structures those exhibit distinct passband and stopband properties. These are the unique properties of this structure.

Planar photonic bandgap structures (PBGSs) are a class of periodic structure with ability to control the propagation of electromagnetic wave [1]. Electromagnetic (EM) waves behave in substrates as electrons behave in semiconductors. Due to these characteristic PBGSs are also known as electromagnetic bandgap structures (EBGSs). EBGS is also called electromagnetic crystal and exhibit a frequency-selective behavior similar to carrier transport in semiconductors. The perturbation in the ground plane of a structure is widely known as defected ground structure (DGS) [2]. When the perturbation in the ground plane is uniform, then it is known as PBGS. Also, they exhibit wide band-pass and band-rejection properties at microwave and millimeter-wave frequencies and have offered tremendous applications in active and passive devices [3-8]. They allow shifting the rejected frequency band by simply changing the geometry parameters of the EBG element.

Introducing periodic perturbation such as dielectric rods, holes and patterns in waveguides and microstrip substrates forms PBG materials. While various configurations have been proposed in literature, only the planar etched PBG configurations are attracting much interest due to their ease of fabrication and integration with other circuits with photolithographic processes [9-12]. The passband of PBGSs is used as a slow wave

medium that is useful for compact design. On the other hand the stopband is used to suppress the surface wave, leakage and spurious transmission [13-16]. Due to these unique properties of PBG structures, they find potential application in filter, antennas, waveguides, phased arrays and many other microwave devices and components [17].

Dumbbell shaped DGS differs from the PBG structures, both in configuration and in principle of operations. Dumbbell shaped DGSs are formed from 2-D regular square patterned PBGSs with narrow vertical slot connections. They are known as dumbbell shaped DGSs [2], [18]. In principle, PBGSs follow Bragg's condition to generate the stopband. On the other hand the behavior of dumbbell shaped DGSs is controlled by current path around the DGS element.

Nonlinear distribution in EBGs provides smoother transmission passband and dumbbell shaped defected ground structures (DGSs) provide wider stopband [19-22]. These two concepts are combined to design EBGs assisted bandpass filter (BPF) to suppress the 2nd and 3rd order harmonics which will be investigated in this paper. Both binomially and chebyshev distribution will be used to investigate the performances. From there we will be able to conclude that how much our designs are capable of suppressing the higher order harmonics.

1.2 Objective of the Thesis

The goal of this thesis is to design EBG assisted microstrip transmission lines and filters. EBG assisted transmission lines are investigated to see their improved performance in terms of wider stopband and ripple free smoother transmission thorough the passband. In case of EBG assisted filter the bandstop property will be utilized in harmonic suppression. EBGs will be implemented into the conventional lines and filters. The choice of the proper EBG structure is a vital issue to achieve better performance of the designed components for all the conventional designs. Therefore, the first goal is proper selection of EBG/PBG units, which will yield distinct passband and stopband characteristics of the designed frequency. The EBGs have different forms and their lattice structures are different. The investigations will be confined mainly to circular and square patterned EBG structures. Uniform EBG structures have constraints of filling factor (FF). FF is defined to

be the volumetric ratio of one unit cell to the single EBG element. FF controls the width and depth of the stopband [23]. The general concept of increasing the stopband is the enhancement of FF. But after some value of FF the passband transmission suffers from the worst performances. The passband contains huge ripples with large dimension of the EBG patterns. The passband return loss performance is also very poor. To alleviate these problems uniform circular EBGs with an optimized value of 0.25 [23] and uniform square EBGs with an optimized value of 0.50 are used. For non-uniform patterned PBGSs, the central elements have the largest radii of ' r_0 ' and the radii of the adjacent circles decrease proportionally to the amplitude co-efficients of the polynomials.

Then dumbbell shaped DGSs will be investigated. In the open literature, researchers used uniplanar compact photonic bandgap structure (UC-PBGS) or DGSs to improve the performance of the Bandpass Filter (BPF) designs. T. Itoh et al. [24] have proposed UC-PBGS in the ground plane of parallel couple lined BPF and we will use the BPF as our reference filter. Such structures/configurations need careful attention for both top and bottom layers of planar substrates. Attention will be devoted to develop wide bandgap and BPF performance by the perturbed ground plane only. Intensive investigation will be carried out on non-uniform dumbbell shaped DGS structures. In the case of non-uniform distributions dumbbell shaped DGS structures with *Binomial* [25] and *Chebyshev* [26] distributions will be investigated. The amplitudes of the EBG elements will be calculated as the proportional of the co-efficients of the distributions.

The thesis has the following objectives:

Novel EBG elements that will provide broadband, distinct passband and stopband characteristics will be designed. The main objectives are as follows.

- Implementation of uniform circular, square EBG elements in harmonic suppression of bandpass filter.
- Implementation of dumbbell shaped DGS on reference BPF for higher order harmonics suppression.
- Implementation of dumbbell shaped DGS in harmonic suppression of bandpass filter. In the present research the dumbbell shaped DGS with *Binomial* and *Chebyshev* distributions will be focused.

1.3 Thesis Outline

The followings are the outline of the thesis.

- In chapter 1, the introduction of the thesis is reported. This chapter elucidates the goal and proposition of the dumbbell shaped DGS assisted bandpass filter.
- In chapter 2, a comprehensive literature survey of different kinds of filters and the application of EBGs.
- In chapter 3, the basic theory of conventional filters and different periodic structures are presented. Different terminologies are present and discussed in this chapter. Also, conventional BPF is explained there.
- In chapter 4, EBGs are explained clearly. The design equations are presented. To get the idea about the passband-stopband phenomena of the EBGs, numerical result for dispersion diagram has been reported. This chapter shows some S-parameters performances of uniform circular and square patterned PBGs.
- In chapter 5, performance of a coupled line BPF will be focused. Both square and circular EBGs with uniform distribution have been reported to see their improved performance over coupled line BPF. Dumbbell shaped DGS will also be used in harmonic suppression on BPF which will be reported. The binomially and Chebyshev distributed dumbbell shaped DGS will be applied to suppress 2nd and 3rd harmonics.
- In chapter 6, conclusions and recommendation for future work have been presented.

CHAPTER II

Literature Survey

2.1 Introduction

Microwave engineers are working with the concept of electromagnetic waves interacting with periodic structures. Periodic structures in either closed metallic or open waveguides have been used for many years, for example, in filters and travelling-wave tubes. Planar versions of these can be found in the form of frequency selective surfaces (FSS) and phased array antennas. In the late 1980s a fully 3-D periodic structure, working at microwave frequencies, was realized by Yablonovitch and his co-workers by mechanically drilling holes into a block of dielectric material [1]. This so-called material Yablonovite, prevents the propagation of microwave radiation in any three dimensional spatial direction whereas the material is transparent in its solid form at these wavelengths. These artificially engineered materials are generically known as photonic bandgap (PBG) materials or photonic crystals. Although photonic” refers to light, the principle of bandgap” applies to electromagnetic waves of all wavelengths. Consequently, there is a controversy in the microwave community about the use of the term “Photonic, and the name Electromagnetic bandgap (EBG) material or Electromagnetic crystal [27].

EBG materials are presently one of the most rapidly advancing sectors in the electromagnetic arena. They allow us to manipulate the propagation of electromagnetic waves to an extent that was previously not possible. The rapid advances in both theory and experiment together with substantial technological potential have driven the development of EBG technology. Emphasis is now placed on finding tangible applications combined with detailed modeling. Owing to the tremendous potential of EBGs there is a plethora of applications in which they can be used [17].

Various works on the recent development of EBGs have been reported in this chapter. EBG structures are found to play vital roles in enhancing the performance of the

microwave components and devices. The stopband characteristic causes the significant improvement in the performance by suppressing surface waves, leakage and spurious transmission [16]. Filling factor (FF) is one of the important controlling factors to yield wider and distinct stopband that should be optimized to maintain a smoother transmission in the passband. In the literature for uniform circular and rectangular patterned PBGSs the optimum filling factors are considered. In case of uniform circular EBG element the optimum FF is considered to 0.25 [23]. But for non-uniform EBG elements, it has been stretched up to 0.45~0.50 [28]. These types of designs are considered as the conventional PBG structure design. Besides, the researchers have worked out on dumbbell shaped EBGs.

2.2 Application of EBGs

The modern microwave communication system requires high performance, compact size and low cost devices. To fulfil the requirement and to enhance performance some new structures like EBGs, dumbbell shaped DGS, Substrate integrates waveguide (SIW) etc. are existing on the communication system. Recently, many researchers paid more attention to PBGSs due to their unique properties. A summary of their works in this section are briefly discussed in this section.

❖ Power amplifiers

EBGs can create a spatially periodic variation of the effective dielectric constant of the line, which produces the desired stopbands and passbands. Broad-band operation of power amplifiers requires harmonic filtering and tuning that is typically difficult to realize. The wide stopband characteristic of microstrip on EBG ground plane can be used as broad-band harmonic tuner for power amplifiers to increase power added efficiency [29].

❖ Resonators

Resonators based on EBG technology have been recently proposed as an alternative to current technologies [30-33]. Resonator structures can be fabricated on different laminates by using inexpensive standard printed circuit board (PCB) processing techniques and can be used in commercial products. Tim Eular and John Papapolymeror proposed a micro-

machined resonator at 45 GHz based on defect induced EBG laminate with high quality factor and low losses [30].

❖ **Filters**

EBG structures have also been demonstrated. For example, Rumsey et al. [34] presented a lowpass filter with a wide high frequency rejection bandwidth using cascaded sections of EBG structures with different lattice periods. Horii et al. [35] presented a microstrip patch antenna with PBG ground plane to suppress radiation at harmonic frequencies while Deal et al. [36] used the same structure to reduce power lost to surface waves. Chang et al. demonstrated EBG resonators for microstrip line and CPWs [37].

Some other researchers also designed high quality factor filters [30, 31], with high isolation [32] and low insertion losses [32, 33] with wide bandwidth. The concept of EBGs has been utilized to develop the devices of high isolation with high quality factor that can integrate monolithically with other components. According to the demands, Chappel and his co-workers designed 2, 3 and 6 pole filters using metallodielectric EBG lattice. Chappel also designed a wide bandgap structure using the high-k ceramics, which was embedded into a polymer to create an EBG substrate. J. C Vardaxoglu et. al. also proposed a tunable wide bandgap using metallo-dielectric EBGs [38]. Hell and his team proposed a reconfigurable EBG cavity resonator with low insertion losses [39]. The use of EBG circuits for filter applications [23, 40-44] in microwave technology has been proposed in different ways. Vesna Radistic designed the EBG by etching a 2-D structure of holes in the ground plane of the microstrip circuit [31].

❖ **UC-PBG Structure applied to BPF**

The crystal structure previously described has planar geometry and is effective; however, it has the drawback of being large in terms of wavelength. This problem has been overcome by the recent development of the UC-PBG structure sketched in Fig. 2.1 (a). The UC-PBG structure is comprised of a square lattice of square metallic pads, each one connected to the four adjacent ones through a narrow strip. Figure 2.1 (b) shows a single unit cell of the crystal. The narrow strips together with insets at connections introduce lumped inductive elements, while the gaps between neighboring pads introduce lumped

capacitors. The effect of the two-dimensional periodic LC-network is that of reducing the wavelength of an electromagnetic wave propagating along the structure.

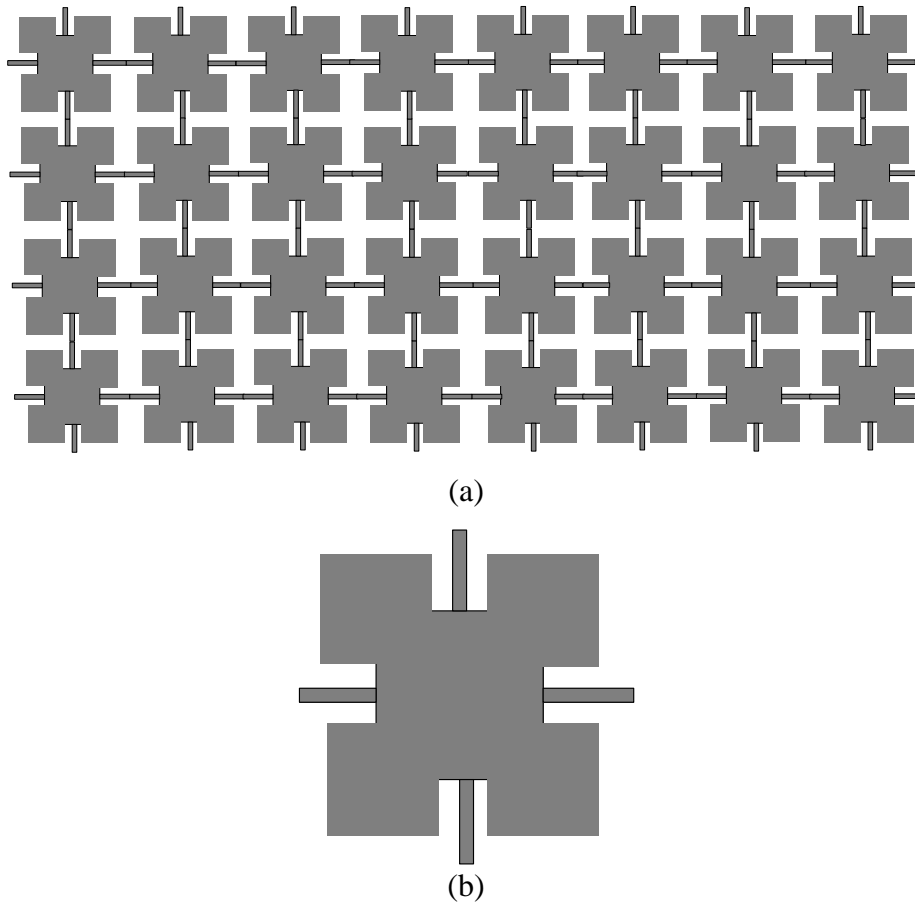


Fig. 2.1: (a) Schematic of UC-PBG metallic pattern. (b) Unit cell of the UC-PBG structure.

❖ Spurious-Free Microstrip Filters

The previous structure can be exploited to suppress spurious passband always present in conventional microstrip filters [44], [45]. The sharp cutoff can be exploited to improve the roll-off of a lowpass filter [45], meanwhile, the slowwave effect reduces the resonator length of the filter integrated with UC-PBG ground plane [44].

❖ Harmonic Tuning in Power Amplifier

Harmonic tuning in power amplifier using the UC-PBG has been demonstrated [46]. A S-band class AB power amplifier integrated with UC-PBG microstrip have been investigated [29]. Improved performance with harmonics suppression had achieved.

❖ Aperture Coupled Patch Antenna on UC-PBG Substrate

Microstrip patch antennas are extensively used in communication systems for their low profile, low cost and easy fabrication [34]. Patch antennas are usually built on low permittivity substrates for optimum performance, since surface waves are excited on a high dielectric constant substrate. On the contrary, MIC and MMIC are usually built on high dielectric constant substrates to reduce the dimensions. To achieve a high degree of integration for both circuits and antenna is desirable to realize planar antennas with good performance on high dielectric substrates. The complete stopband provided by the UC-PBG structure can be employed to reduce surface wave losses of patch antennas on high dielectric constant substrate [47 - 49].

❖ Bandpass Filters (BPF)

Conventional parallel-coupled band pass filters (BPF) need extra filters to suppress the spurious transmission that results the increase of insertion loss. It is reported [50] that the use of extra filters can be avoided by just applying PBG to obtain a compact microstrip BPF with intrinsic spurious rejection. The well-matched microstrip on the UC-PBG ground plane is suited as a low-loss transmission line. The generated spurious passbands at higher harmonics can be suppressed with the aid of PBGS as it provides a wide and deep

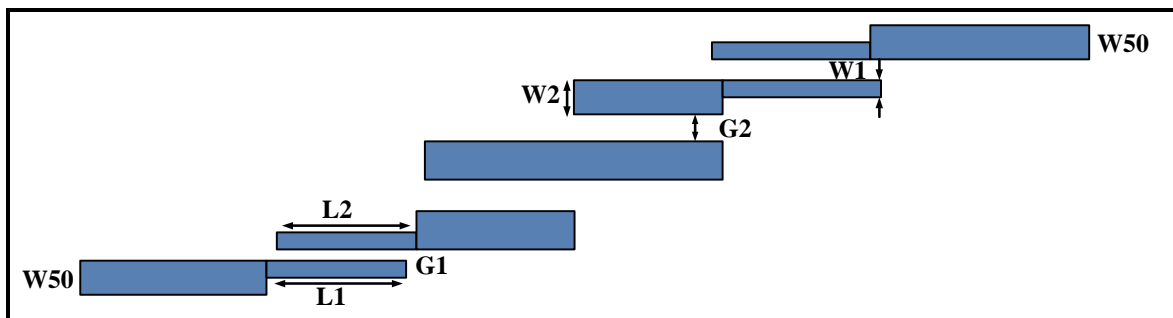


Fig. 2.2: Schematic diagram of a BPF

stopband. The physical length of the filter circuit is reduced as well due to the slow-wave effect of the UC-PBG structure. Fig. 2.2 shows the schematic of a microstrip BPF on the UC-PBG ground. The reference [51] narrates the standard design procedures of the parallel-coupled BPF.

2.3 EBG Tuned Microwave Devices

In micro electro mechanical systems (MEMS) fabrication technologies, the position of the switches and membrane was modified electrically and local properties of the EBG components were modulated. In the fourth alternative, they use different dielectric substrates are used in which the EBG structures were designed. By changing the permittivity and the permeability of the substrate, by using external electric or magnetic field, they achieve tuning in the EBG components is achieved.

A tunable filter using fractural electromagnetic bandgap structure was designed, simulated and fabricated, and its tuning was achieved using micro-machined capacitive bridge [52]. Another ultra wide bandstop filter was designed and tuned using MEMS switches based on EBG co-planar waveguides [51]. Tunable electromagnetic bandgap structures are based on ferroelectric or ferromagnetic thin films were also reported in the literature [53]. To achieve tunable EBG performance ferroelectric capacitors are also considered [52- 55].

In addition, to achieve tunable electromagnetic bandgap EBG performance, ferroelectric varactors are considered in LC circuits, for periodically loading coplanar waveguides (CPWs). Asymmetric or symmetric tuning of the bandgap width was achieved by changing the capacitance of the varactors in LC circuits [54]. Yongje Sung presented a novel approach to obtain the electromagnetic bandgap structure with a wide tunable stopband filter using defected ground structure (DGS) [56]. Miguel and researcher also proposed a multiple frequency tuned photonic bandgap microstrip structure [57].

2.4 Miniaturization

Miniaturization of microwave devices and antennas has become increasingly important in recent years. Modern wireless communication systems require small microwave elements that are relevant to high-level integrated into compact lightweight systems.

Miniaturization can be achieved by several techniques. Roger and his co-workers designed a magnetic conductor and to reduce its size and cost. In order to do that, they integrated some capacitance of the FSS without resorting to a second layer of overlapping patches [58]. By increasing the capacitor and inductor in Sivenpiper High Impedance Surface, the

size of the EBG cell was reduced [59]. Feresidis et. al. introduced the concept of closely coupled metallo dielectric electromagnetic band-gap structure, and designed 2-D double layer dipole arrays. These arrays are closely packed [60].

It is well known that at certain frequencies outside the band gap, periodic structures support waves, commonly termed as slow waves, with reduced phase velocity and guided wavelength with respect to the wave propagating in a comparable homogeneous medium. This property can be exploited for the miniaturization of microwave elements, such as the triple array elements [61]. An approach to this is to examine the elements with periodic loading. Multiple-order periodic loading of basic elements possesses a good degree of flexibility in the design [60-61].

Fractal-type structures are subsequently produced using a second order loading. This can also be used for multiband Artificial Magnetic Conductor (AMC) designs [62]. Another way of increasing the length of the loading stubs without increase the unit cell and at the same time to increasing the capacitive coupling between successive elements are in the inter digital topology. The loadings of successive dipoles are shifted so that they can extend to the full length allowed by the array geometry.

The technological potential of electromagnetic crystals for developing such novel components and subsystems offers a very promising alternative that could potentially overcome the limitations of current technology. EBG technology is a breakthrough, mainly due to their ability to guide and control efficiently electromagnetic waves. As long as primary EBG components emerge with functional efficiency, the realization of a complete system would become a distinct possibility.

Chapter III

Filter Terminologies and Conventional Filters

3.1 Introduction

A two-port component is used to provide frequency selectivity in satellite and mobile communications, radar, electronic warfare, metrology, and remote-sensing systems operating at microwave frequencies (1 GHz and above). Microwave filters perform the same function as electric filters at lower frequencies, but differ in their implementation because circuit dimensions are on the order of the electrical wavelength at microwave frequencies. For designing, developing, improving and understanding the filter, it is needed to study elaborately. For this purpose this chapter is going to describe different filters, two port network concepts, network parameters, periodic structures and provide equations that are useful for the analysis of filter networks.

3.2 Filter

Filter is a device or material for suppressing or minimizing waves or oscillations of certain frequencies. It is a network that is designed to attenuate certain frequencies but pass others without loss. Inductor and capacitor are important elements for filter design.

According to Webster's Definition recited by Berlin, "A filter is a device or substance that passes electric currents at certain frequencies or frequency ranges while preventing the passage of others." Based on the frequencies they pass, the filters are classified as low-pass filter (LPF), highpass filters (HPF), bandpass filters (BPF) and bandstop filters (BSF).

A filter is an AC circuit that separates some frequencies from others within mixed frequency signals [62]. Filter can limit any band of frequencies depending on the design. Designer can capable to select one frequency or range of frequencies out of a mix of different frequencies in a circuit.

Filter networks are widely used in communication systems specially microwave communication. Audio equalizers and crossover networks are two well-known applications of filter circuits. It is also applicable in radar, measurement system, telemeter equipment and impedance matching etc. where it is necessary to transmit or attenuate a limited range of frequencies [63].

3.3 Microwave Filter

Microwave filter is a two-port network used to control the frequency response at a certain point in a microwave system by providing transmission at frequencies within the pass band of the filter and attenuation in the stop band of the filter.

Here is the term - Microwaves refers to alternating current signals with frequencies between 300 MHz (3×10^8 Hz) and 300 GHz (3×10^{11} Hz), with a corresponding electrical wave-length between, $\lambda = c / f = 1\text{m}$ and $\lambda = 1\text{mm}$, respectively [51]. It is used in microwave communication, radar, or test and measurement system.

Microwave lies within the electromagnetic spectrum which is the range of all possible frequencies of electromagnetic radiation. The electromagnetic spectrum extends from below the low frequencies used for modern radio communication to gamma radiation at the short-wavelength (high-frequency) end, thereby covering wavelengths from thousands of kilometers down to a fraction of the size of an atom. The limit for long wavelengths is the size of the universe itself, while it is thought that the short wavelength limit is in the vicinity of the Planck length. Below there is an image of electromagnetic spectrum.

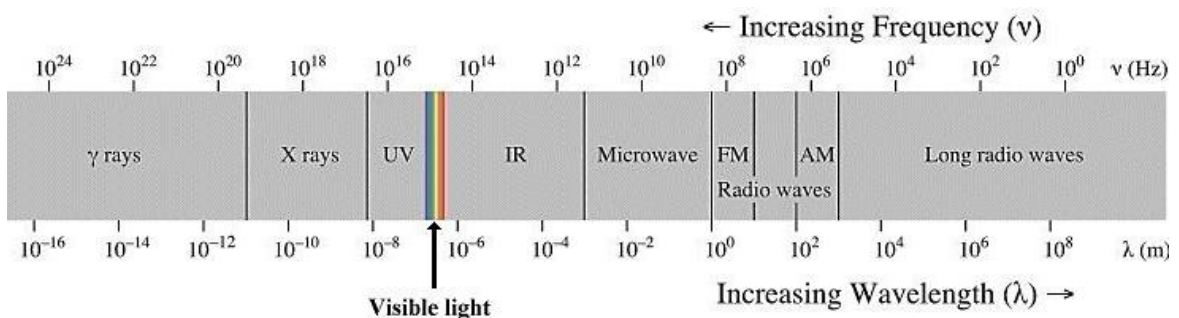


Fig. 3.1: Electromagnetic spectrum

Frequency Band		Frequency	Frequency Band Use
Radio and Broadcast		600KHz to 1.6 MHz	AM radio
		88 to 108 MHz	FM radio
		54 to 700 MHz	TV broadcast
Microwave	L band	1 to 2 GHz	Cell phones 0.9-2.4 GHz Microwave 2.4 GHz Wireless Data 2.4 GHz Radar 1- 100 GHz
	S band	2 to 4 GHz	
	C band	4 to 8 GHz	
	X band	8 to 12 GHz	
	K _u band	12 to 18 GHz	
	K band	18 to 26.5 GHz	
	K _a band	26.5 to 40 GHz	
	Q band	30 to 50 GHz	
	U band	40 to 60 GHz	
	V band	50 to 75 GHz	
	E band	60 to 90 GHz	
	W band	75 to 110 GHz	
	F band	90 to 140 GHz	
D band	110 to 170 GHz		
Terahertz		1 to 10 THz	Bio Imaging
Infrared		300 to 400 THz	Remotes, night vision
Visible Light		400 to 800 THz	
Ultraviolet		800 THz to 30 PHz	Dental curing, tanning
X-ray		30 PHz to 30 EHz	Baggage screening
Gamma		>30 EHz	PET imaging

Table. 3.1: Chart of the electromagnetic spectrum.

All possible frequencies range of electromagnetic radiation which is shown in the above table. Electromagnetic radiation interacts with matter in different ways across the spectrum. These types of interaction are so different that historically different names have been applied to different parts of the spectrum, as though these were different types of radiation. Thus, although these "different kinds" of electromagnetic radiation form a quantitatively continuous spectrum of frequencies and wavelengths, the spectrum remains divided for practical reasons related to these qualitative interaction differences [55].

3.4 Classification of Filter

Conventional filter can be classified as four types. These are shown in below:

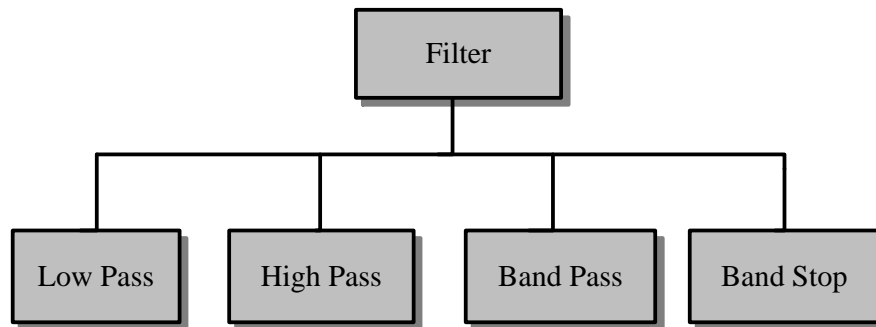


Fig. 3.2: Different types of filters.

3.5 Different Types of Filter

The frequency response can be classified into a number of different band forms describing which frequency bands the filter passes (the passband) and which it rejects (the stopband).

On the basis of band, filter can be classified which is already shown. The short descriptions of them are given below.

3.5.1 Lowpass Filter (LPF)

A low-pass filter is a filter that passes low-frequency signals and attenuates (reduces the amplitude of) signals with frequencies higher than the cutoff frequency. The actual amount of attenuation for each frequency varies depending on specific filter design. It is sometimes called a high-cut filter, or treble cut filter in audio applications. A low-pass filter is the opposite of a high-pass filter. Low-pass filters provide a smoother form of a signal, removing the short-term fluctuations, and leaving the longer-term trend.

Lowpass filter passes all frequencies up to the cut-off frequency f_{c2} and attenuates all other frequencies greater than f_{c2} . This transmits currents of all frequencies from zero up to the cut-off frequency. This band is called pass band or transmission band whose range between 0 to f_{c2} . The frequency range over which transmission does not take place is called the stop band or attenuation band. The stop band for a lowpass filter is the frequency range above f_{c2} [51].

The attenuation characteristic of a lowpass filter is shown in below:

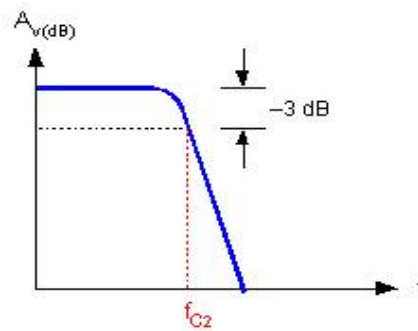


Fig. 3.3: Conventional lowpass filter

The cutoff frequency for a low-pass filter is that frequency at which the output (load) voltage equals 70.7% of the input (source) voltage. Above the cutoff frequency, the output voltage is lower than 70.7% of the input & vice versa.

3.5.2 Highpass Filter (HPF)

A high-pass filter's task is just the opposite of a low-pass filter that offers easy passage of a high-frequency signal and difficult passage to a low-frequency signal.

A highpass filter passes high frequency signal above cut-off frequency, f_{C1} and attenuates all frequencies below, f_{C1} . Thus the pass band of this filter is the frequency range above f_{C1} and the stop band is the frequency range below f_{C1} . High-pass filters can be used as blocking DC signal or RF devices. They can also be used in conjunction with a low-pass filter making a bandpass filter [51].

The attenuation characteristic of a highpass filter is shown below:

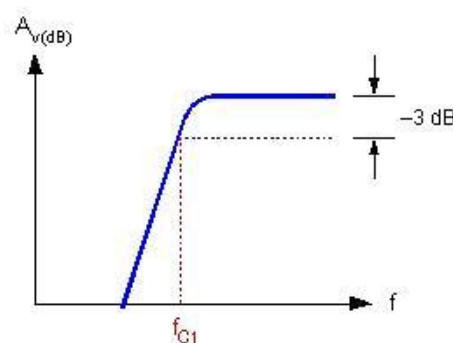


Fig. 3.4: Conventional highpass filter

The cutoff frequency for a high-pass filter is that frequency at which the output (load) voltage equals 70.7% of the input (source) voltage. Above the cutoff frequency, the output voltage is greater than 70.7% of the input and vice versa.

3.5.3 Bandpass Filter (BPF)

A bandpass filter is an electronic device or circuit that allows signals between two specific frequencies to pass, but that discriminates against signals at other frequencies. An ideal bandpass filter would have a completely flat pass band (e.g. with no gain/attenuation throughout) and would completely attenuate all frequencies outside the pass band. They can be designed by combining the properties of low-pass and high-pass into a single filter.

The attenuation characteristic of a bandpass filter is shown below:

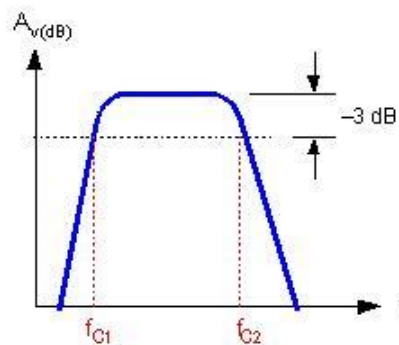


Fig. 3.5: Conventional bandpass filter

A bandpass filter has two cut-off frequencies. One is called the lower cut-off frequency denoted by f_{c1} , while f_{c2} is called the upper cut-off frequency. The bandwidth of the filter is simply the difference between the upper and lower cut-off frequencies that is $f_{c2} - f_{c1}$ [51].

3.5.4 Bandstop Filter (BSF)

Bandstop filter also known as band-elimination, band-reject, or notch filters passes all frequencies above and below a particular range set by the component values. It can be made out of a low-pass and a high-pass filter. It is the opposite of a band-pass filter. It has

also two cut-off frequencies f_{C1} , f_{C2} . f_{C1} is lower cut-off frequency and f_{C2} is upper cut-off frequency. Between these two cut-off frequencies attenuation band is found [51].

The attenuation characteristic of a bandstop filter is shown below:

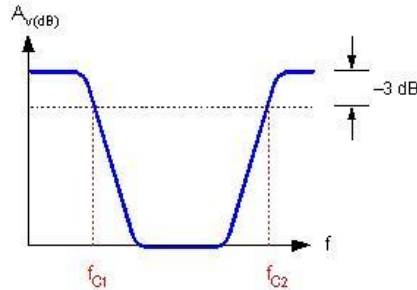


Fig. 3.6: Conventional bandstop filter

3.6 Advantages and Uses

Due to the unique properties advantages of PBG engineered structures; they find many potential applications in microwave components and devices which will be described in bellow.

3.6.1 Advantages of Filters

Filters are at the heart of many design problems. They are used to separate or combine signals of different frequencies, such as in multichannel communications systems, or in components such as frequency converters. The electromagnetic spectrum is limited and has to be shared; filters are used to confine the radiation from high-power transmitters within assigned spectral limits; conversely, other filters are used to protect receivers from interference outside their operating bands. Filter like networks occur in impedance matching, as between two transmission lines of different characteristic impedances; or between a resistive generator and a reactive load. Sometimes it is necessary to obtain certain phase characteristics, for example, to compensate for the phase distortion produced by another filter or dispersive structure components whose design benefits from filter theory range from directional couplers to circular polarizers [55].

3.6.2 General Use of Filter Principles in Terms of Microwave Components

As can be readily seen by extrapolating from discussions in preceding sections, microwave

filter design techniques when used in their most general way are fundamental to the efficient design of a wide variety of microwave components. Generally, these techniques are basic to the designs when selecting, rejecting or channeling of energy of different frequencies is important. It is also important to achieve energy transfer with low reflection over a wide band and to achieve a controlled time delay. The possible specific practical situations where such considerations arise are too numerous and varied to permit any attempt to treat them individually herein [55].

3.7 Network Variables

Filter networks are essential building elements in many areas of RF/microwave engineering. Such networks are used to select/reject or separate/combine signals at different frequencies in a host of RF/microwave systems and equipment. In this section to various network concepts are described and provided equations that are useful for the analysis of filter networks for better understanding.

3.7.1 Two Port Network

A two-port network (a kind of four-terminal network or quadripole) is an electrical network (circuit) or device with two pairs of terminals to connect to external circuits. Most RF/microwave filters and filter components can be represented by a two-port network, as shown in Fig. 3.7, where V_1 , V_2 and I_1 , I_2 are the voltage and current variables at the ports 1 and 2, respectively, Z_{01} and Z_{02} are the terminal impedances, and E_s is the source or generator voltage. Note that the voltage and current variables are complex amplitudes when we consider sinusoidal quantities. For example, a sinusoidal voltage at port 1 is given by

$$v_1(t) = |V_1| \cos(\omega t + \phi) \quad (3.1)$$

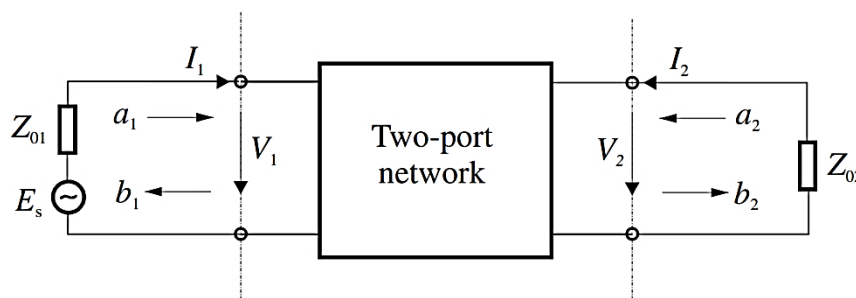


Fig. 3.7: Two-port network showing network variables [65].

We can then make the following transformations:

$$v_1(t) = |V_1| \cos(\omega t + \phi) = \text{Re}|V_1|e^{j(\omega t + \phi)} = \text{Re}V_1e^{j\omega t} \quad (3.2)$$

Where, Re denotes “the real part of” the expression that follows it. Therefore, one can identify the complex amplitude V_1 defined by

$$V_1 = |V_1| e^{j\phi} \quad (3.3)$$

It is difficult to measure the voltage and current at microwave frequencies, the wave variables a_1 , b_1 and a_2 , b_2 are introduced, with ‘a’ indicating the incident waves and ‘b’ the reflected waves. The relationships between the wave variables and the voltage and current variables are defined as

$$V_n = \sqrt{Z_{0n}}(a_n + b_n) \quad \text{For } n= 1 \text{ and } 2 \quad (3.4a)$$

$$I_n = \frac{1}{\sqrt{Z_{0n}}}(a_n - b_n)$$

$$a_n = \frac{1}{2} \left(\frac{V_n}{\sqrt{Z_{0n}}} + \sqrt{Z_{0n}}I_n \right) \quad \text{For } n= 1 \text{ and } 2 \quad (3.4b)$$

$$b_n = \frac{1}{2} \left(\frac{V_n}{\sqrt{Z_{0n}}} - \sqrt{Z_{0n}}I_n \right)$$

The above definitions guarantee that the power at port n is

$$P_n = \frac{1}{2} \text{Re}(V_n \cdot I_n^*) = \frac{1}{2} (a_n a_n^* - b_n b_n^*) \quad (3.5)$$

Where, the asterisk denotes a conjugate quantity. It can be recognized that $a_n a_n^*/2$ is the incident wave power and $b_n b_n^*/2$ is the reflected wave power at port n [65].

3.7.2 Symmetrical Network Analysis

A network is symmetrical if its input impedance is equal to its output impedance. Most often, but not necessarily, symmetrical networks are also physically symmetrical. If a network is symmetrical, it is convenient for network analysis to bisect the symmetrical network into two identical halves with respect to its symmetrical interface. When an even

excitation is applied to the network, as indicated in Fig. 3.8(a), the symmetrical interface is open-circuited, and the two network halves become the two identical one-port, even-mode networks, with the other port open-circuited. In a similar fashion, under an odd excitation, as shown in Fig. 3.8 (b), the symmetrical interface is short-circuited and the two network halves become the two identical one-port, odd-mode networks, with the other port short-circuited. Since any excitation to a symmetrical two-port network can be obtained by a linear combination of the even and odd excitations, the network analysis will be simplified by first analyzing the one-port, even- and odd-mode networks separately, and then determining the two-port network parameters from the even- and odd-mode network parameters [65].

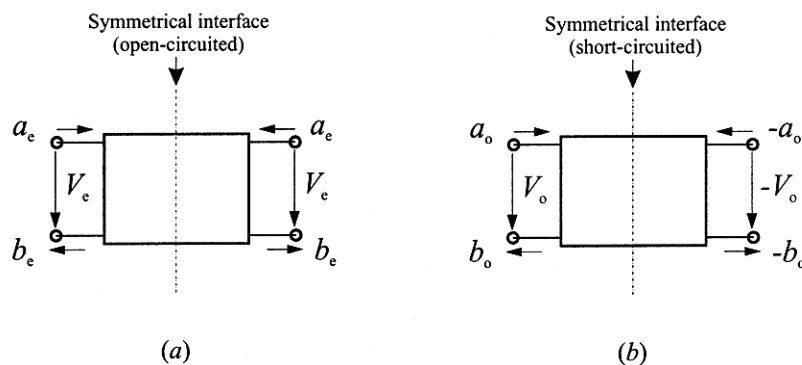


Fig. 3.8: Symmetrical two-port networks with (a) even-mode excitation, and (b) odd-mode excitation.

For example, the one-port, even- and odd-mode S parameters are

$$S_{11e} = \frac{b_e}{a_e} \quad S_{11o} = \frac{b_o}{a_o} \quad (3.6)$$

Where, the subscripts e and o refer to the even mode and odd mode, respectively. For the symmetrical network, the following relationships of wave variables hold

$$b_1 = b_e + b_o \quad b_2 = b_e - b_o \quad (3.7)$$

Letting $a_2 = 0$, we have from (3.6) and (3.7) that

$$\begin{aligned} a_1 &= 2a_e = 2a_o \\ b_1 &= S_{11e}a_e + S_{11o}a_o \\ b_2 &= S_{11e}a_e - S_{11o}a_o \end{aligned} \quad (3.8)$$

Substituting these results into the definitions of two-port S-parameters gives

$$S_{11} = \left. \frac{b_1}{a_1} \right|_{a_2=0} = \frac{1}{2}(S_{11e} + S_{11o}), \quad S_{21} = \left. \frac{b_2}{a_1} \right|_{a_2=0} = \frac{1}{2}(S_{11e} - S_{11o}) \quad (3.9)$$

$$S_{22} = S_{11} \text{ and } S_{21} = S_{12}$$

Let, Z_{ine} and Z_{ino} represent the input impedances of the one-port, even- and odd-mode networks. According to scattering parametric equation, the reflection coefficients in (3.6) can be given by

$$S_{11e} = \frac{Z_{ine} - Z_{01}}{Z_{ine} + Z_{01}} \quad \text{and}, \quad S_{11o} = \frac{Z_{ino} - Z_{01}}{Z_{ino} + Z_{01}} \quad (3.10)$$

3.7.3 Scattering Parameters

The scattering or S parameters of a two-port network are defined in terms of the wave variables as

$$S_{11} = \left. \frac{b_1}{a_1} \right|_{a_2=0} \quad S_{12} = \left. \frac{b_1}{a_2} \right|_{a_1=0} \quad (3.11)$$

$$S_{21} = \left. \frac{b_2}{a_1} \right|_{a_2=0} \quad S_{22} = \left. \frac{b_2}{a_2} \right|_{a_1=0}$$

Where $a_n = 0$ implies a perfect impedance match (no reflection from terminal impedance) at port n. These definitions may be written as

$$\begin{bmatrix} b_1 \\ b_2 \end{bmatrix} = \begin{bmatrix} S_{11} & S_{12} \\ S_{21} & S_{22} \end{bmatrix} \begin{bmatrix} a_1 \\ a_2 \end{bmatrix} \quad (3.12)$$

Where, the matrix containing the S parameters is referred to as the scattering matrix or S matrix, which may simply be denoted by [S].

The parameters S_{11} and S_{22} are also called the reflection coefficients, whereas S_{12} and S_{21} the transmission coefficients. These are the parameters directly measurable at microwave frequencies. The S parameters are in general complex, and it is convenient to express them in terms of amplitudes and phases, i.e., $S_{mn} = |S_{mn}| e^{j\phi_{mn}}$ for $m, n = 1, 2$. Often their amplitudes are given in decibels (dB), which are defined as

$$20 \log |S_{mn}| \text{ dB} \quad m, n = 1, 2 \quad (3.13)$$

Where, the logarithm operation is base 10. For filter characterization, we may define two parameters:

$$\begin{aligned} IL &= -20 \log |S_{mn}| \text{ dB} \quad m, n = 1, 2 \quad (m \neq n) \\ RL &= -20 \log |S_{nn}| \text{ dB} \quad n = 1, 2 \end{aligned} \quad (3.14)$$

Where, IL denotes the insertion loss between ports n and m and RL represents the re-turn loss at port n. Instead of using the return loss, the voltage standing wave ratio *VSWR* may be used. The definition of *VSWR* is

$$VSWR = \frac{1 + |S_{nn}|}{1 - |S_{nn}|} \quad (3.15)$$

Whenever a signal is transmitted through a frequency-selective network such as a filter, some delay is introduced into the output signal in relation to the input signal. There are other two parameters that play role in characterizing filter performance related to this delay. The first one is the phase delay, defined by

$$\tau_p = \frac{\phi_{21}}{\omega} \text{ seconds} \quad (3.16)$$

Where, ϕ_{21} is in radians and is in radians per second. Port 1 is the input port and port 2 is the output port. The phase delay is actually the time delay for a steady sinusoidal signal and is not necessarily the true signal delay because a steady sinusoidal signal does not carry information; sometimes, it is also referred to as the carrier delay [65]. The more important parameter is the group delay, defined by

$$\tau_d = \frac{d\phi_{21}}{d\omega} \text{ seconds} \quad (3.17)$$

This represents the true signal (baseband signal) delay, and is also referred to as the envelope delay.

In network analysis or synthesis, it may be desirable to express the reflection parameter S_{11} in terms of the terminal impedance Z_{01} and the so-called input impedance $Z_{in1} = V_1 / I_1$, which is the impedance looking into port 1 of the network. Such an expression can be deduced by evaluating S_{11} in (3.11) in terms of the voltage and current variables using the relationships defined in (3.4b). This gives

$$S_{11} = \left. \frac{b_1}{a_1} \right|_{a_2=0} = \frac{V_1/\sqrt{Z_{01}} - \sqrt{Z_{01}}I_1}{V_1/\sqrt{Z_{01}} + \sqrt{Z_{01}}I_1} \quad (3.18)$$

Replacing V_1 by $Z_{in1} I_1$ results in the desired expression

$$S_{11} = \frac{Z_{in1} - Z_{01}}{Z_{in1} + Z_{01}} \quad (3.19)$$

Similarly, we can have

$$S_{22} = \frac{Z_{in2} - Z_{02}}{Z_{in2} + Z_{02}} \quad (3.20)$$

Where, $Z_{in2} = V_2 / I_2$ is the input impedance looking into port 2 of the network. Equations (3.19) and (3.20) indicate the impedance matching of the network with respect to its terminal impedances. The S parameters have several properties that are useful for network analysis. For a reciprocal network $S_{12} = S_{21}$. If the network is symmetrical, an additional property, $S_{11} = S_{22}$, holds. Hence, the symmetrical network is also reciprocal. For a lossless passive network the transmitting power and the reflected power must equal to the total incident power [65]. The mathematical statements of this power conservation condition are

$$\begin{aligned} S_{21}S_{21}^* + S_{11}S_{11}^* &= 1 \text{ or } |S_{21}|^2 + |S_{11}|^2 = 1 \\ S_{12}S_{12}^* + S_{22}S_{22}^* &= 1 \text{ or } |S_{12}|^2 + |S_{22}|^2 = 1 \end{aligned} \quad (3.21)$$

3.7.4 ABCD Parameters

The ABCD parameters of a two-port network are given by

$$\begin{aligned} A &= \left. \frac{V_1}{V_2} \right|_{I_2=0} & B &= \left. \frac{V_1}{-I_2} \right|_{V_2=0} \\ C &= \left. \frac{I_1}{V_2} \right|_{I_2=0} & D &= \left. \frac{I_1}{-I_2} \right|_{V_2=0} \end{aligned} \quad (3.22)$$

These parameters are actually defined in a set of linear equations in matrix notation

$$\begin{bmatrix} V_1 \\ I_1 \end{bmatrix} = \begin{bmatrix} A & B \\ C & D \end{bmatrix} \begin{bmatrix} V_2 \\ -I_2 \end{bmatrix} \quad (3.23)$$

Where, the matrix comprised of the ABCD parameters is called the ABCD matrix. Sometimes, it may also be referred to as the transfer or chain matrix. The ABCD parameters have the following properties:

$$AD - BC = 1 \quad \text{For a reciprocal network} \quad (3.24)$$

$$A = D \quad \text{For a symmetrical network} \quad (3.25)$$

A network is said to be reciprocal if the voltage appearing at port 2 due to a current applied at port 1 is the same as the voltage appearing at port 1 when the same current is applied to port 2. If the network is lossless, then A and D will be purely real; B and C will be purely imaginary [65].

3.8 Definition of Different Terminologies

In microwave engineering we use lots of terms for better understanding the microwave engineering. So for clearly understanding the microwave engineering we should know the terminologies elaborately.

3.8.1 Insertion Loss (IL)

Insertion loss is equal to the difference in dB power measured at the filter input and at the filter output. The power measured at the filter input is equal to the measured Power when the filter is replaced by a properly matched power meter or network analyzer. The input impedance of the measuring instrument should be equal to the characteristic impedance of the filter or system. Unless otherwise specified, Mini-Circuits filters are designed for 50 ohm systems. Similarly, the power measured at the filter output is equal to the measured power when the filter is terminated by the same measuring instrument as discussed. The insertion loss will be equal to the sum of three loss factors. One is the loss due to the impedance mismatch at the filter input, the second is due to the mismatch at the filter output, and the third is due to the dissipative loss associated with each reactive element within the filter [51].

Mathematically, insertion loss means 10 times of the logarithmic value of the ratio of transmitting power to the incident power.

$$\text{Insertion Loss (IL)} = 10 \log_{10} \left(\frac{p_t}{p_i} \right) \quad (3.26)$$

In terms of voltage,

$$\text{Insertion Loss (IL)} = 20 \log_{10} \left(\frac{V_r}{V_i} \right) = 20 \log_{10} \Gamma_V \quad (3.27)$$

Where V_r is the reflected voltage and V_i is the incident voltage of a two port network.

3.8.2 Return Loss (RL)

Return loss is the loss of power in the signal returned/reflected by a discontinuity in a transmission line. This discontinuity can be a mismatch with the terminating load or with a device inserted in the line. It is usually expressed as a ratio in decibels (dB). Return loss is related to both standing wave ratio (SWR) and reflection coefficient (Γ). Increasing return loss corresponds to lower SWR. Return loss is a measure of how well devices or lines are matched. A match is good if the return loss is high. A high return loss is desirable and results in a lower insertion loss [51].

Mathematically, insertion loss means 10 times of the logarithmic value of the ratio of reflecting power to the incident power.

$$\text{Return Loss} = 10 \log_{10} \left(\frac{p_r}{p_i} \right) \quad (3.28)$$

In terms of voltage

$$\begin{aligned} \text{Insertion Loss (IL)} &= 20 \log_{10} \left(\frac{V_i}{V_r} \right) \quad (3.29) \\ &= 20 \log_{10}(1/\Gamma_V) \end{aligned}$$

Where V_r is the reflected voltage and V_i is the incident voltage of a two port network.

3.8.3 Pass Band

Pass band is equal to the frequency range for which the filter insertion loss is less than a specified value. For example, most of the Mini-Circuits' low-pass filter (LPF) models are specified to have a maximum insertion loss value of 1 dB within the pass band [51].

3.8.4 Stop Band

Stop band is equal to the frequency range at which the filter insertion loss is greater than a specified value. For example, most of the Mini-Circuits' low-loss filter (LPF) models are characterized by the frequency range where the insertion loss is greater than 20 dB and 40 dB in the stop band. These two values are arbitrary; they could easily have been chosen for

some other values. The purpose of selecting 20 dB and 44 dB is twofold. One is to provide the design engineer with a simple means to calculate the frequency selectivity of the filter. The second is to allow a quick calculation of the suitability of the filter in a particular situation. Since 20 dB or 40 dB represent sufficient loss requirements in many systems, these values were chosen. [51].

3.8.5 Cutoff Frequency

Cut-off frequency, f_{co} is the frequency at which the filter insertion loss is equal to 3dB. It is a very convenient point for expressing the pass band and stop band boundary points. In addition, it allows a convenient means to normalize the frequency response of a filter. For example, if the frequency of a low-pass filter (LPF) response were divided by f_{co} then the resulting response would be “normalized” to f_{co} . The normalized response allows the design engineer to quickly specify the filter needed to meet his system requirements [51].

3.8.6 Slow Wave

Electromagnetic waves having the velocity lower than the velocity of light in free space are called slow waves. Periodic perturbation in the ground plane provides periodic discontinuity. Slow wave structures (SWS) are promising candidates for compact designs [66].

3.8.7 Surface Waves

Surface waves can be illustrated in several different ways. In optics, they are called surface plasmons. They also exist at radio frequencies, where they are simply called surface currents. One way to derive their properties is to solve for waves that decay exponentially away from a dielectric interface. We find that such waves only exist on materials with a non-positive dielectric constant, such as metals. The same waves can be found by starting from the viewpoint that a material can be assigned effective surface impedance. In the case of a metal, the surface impedance is determined by the skin depth. It is found that the skin depth is equivalent to the surface wave penetration depth, and thus, surface waves are nothing more than ordinary surface currents, which are well understood at radio frequencies [67].

3.9 Periodic Structures

An infinite transmission line or waveguide periodically loaded with reactive elements is an example of a periodic structure. As shown in Fig.3.9, periodic structures can take various forms, depending on the transmission line media being used. Often the loading elements are formed as discontinuities in the line itself, but in any case they can be modeled as lumped reactance in shunt (or series) on a transmission line, as shown in Fig. 3.4. Periodic structures support slow-wave propagation (slower than the phase velocity of the unloaded line), and have passband and stopband characteristics similar to those of filters; they find application in traveling-wave tubes, masers, phase shifters, and antennas [51].

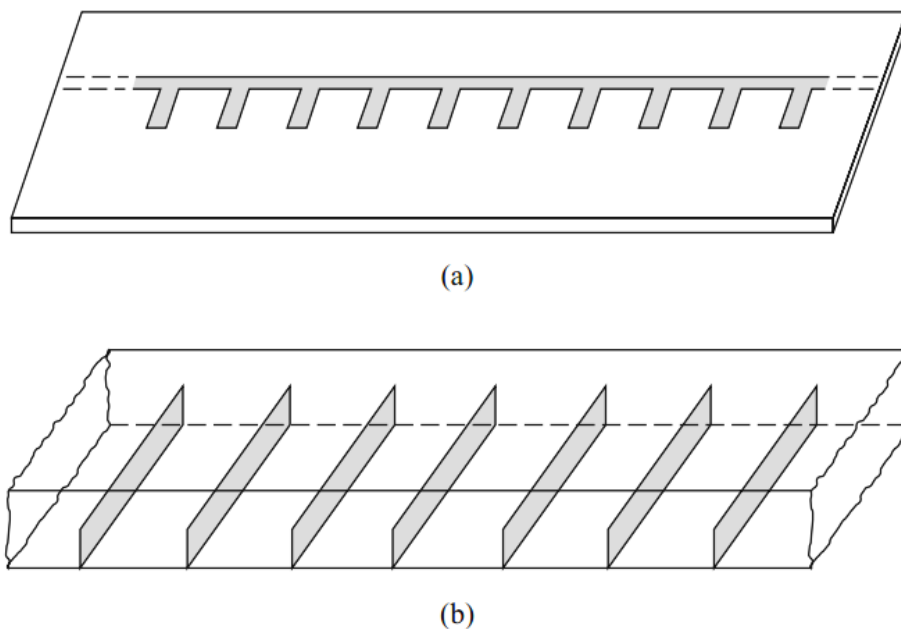


Fig. 3.9: Periodic structures. (a) Periodic stubs on a microstrip line. (b) Periodic diaphragms in a waveguide.

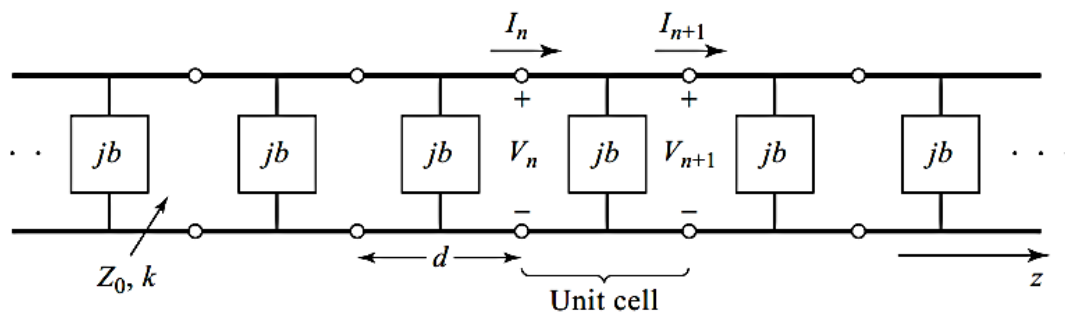


Fig. 3.10: Equivalent circuit of a periodically loaded transmission line. The unloaded line has characteristic impedance Z_0 and propagation constant k .

3.9.1 Capacitively Loaded Transmission Line Circuit Analysis

A simple capacitively loaded transmission line can be analyzed to conceive the idea on periodic structures. The velocity of EM wave in a physically smooth transmission line can be written as

$$V_P = \frac{1}{\sqrt{LC}} = \frac{1}{\sqrt{\mu_0 \epsilon_0 \epsilon_r}} \quad (3.30)$$

Where,

V_P is the phase velocity of EM wave.

L is the series inductance per unit length.

C is the shunt capacitance per unit length.

ϵ_r is the dielectric constant of the medium surrounding the conductor.

ϵ_0 and μ_0 are free-space values of the permittivity and permeability respectively.

From equation (3.30) it is seen that with the value of the dielectric constant (ϵ_r), the phase velocity of EM waves reduces. One problem arises on this simplest way of reducing the phase velocity. If the value of dielectric constant is increased then the higher-order mode of wave propagates. To avoid this propagation, the cross sectional dimensions of the line must be reduced accordingly. This is the limitation of increasing the value of dielectric constant to get the reduced value of the phase velocity of EM waves [51].

We know $LC = \mu_0 \epsilon$ for dielectric media. So any attempt of increasing the value of C to reduce the phase velocity is restricted here. Because if the value of C is increased the value of L will be automatically reduced to maintain the relation, $LC = \mu_0 \epsilon$ in a physically smooth transmission line. Under this circumstance, the restriction of a physically smooth transmission line can be relaxed instead of an electrical smooth line. An effective increase in the shunt capacitance per unit length (C) can be achieved without disturbing the value of inductance per unit length (L) by loading lumped shunt capacitance at periodic intervals where the spacing between the loaded shunt capacitance are small compared with the wavelength. At this stage, though the line is not physically smooth but it will be an electrically smooth line. Under this condition the capacitance will be increased which can be observed from the following equation of the phase velocity.

$$V_P = \frac{1}{\sqrt{(C + C_0/d)L}} = \frac{\omega}{\beta} \quad (3.31)$$

Where C_0/d is the loaded lumped capacitance per unit length and C_0 is the capacitance loaded per interval d .

There are many ways of obtaining periodic structures. One of the simplest ways is to load a thin diaphragm at regular intervals in a coaxial transmission line. The diaphragm may be machined as the integral part of the center conductor. The fringing electric field in the vicinity of the diaphragm increases the local storage of the electric energy and hence giving more extra shunt capacitance [51].

3.9.2 Circuit Analysis of a Periodic Structure

A transmission line can be considered as the combination of finite unit cell of the structure. Fig. 3.11(a) is the equivalent circuit of a basic unit cell of a capacitively loaded coaxial line and Fig. 3.11(b) is the complete transmission line composed of basic unit cell.

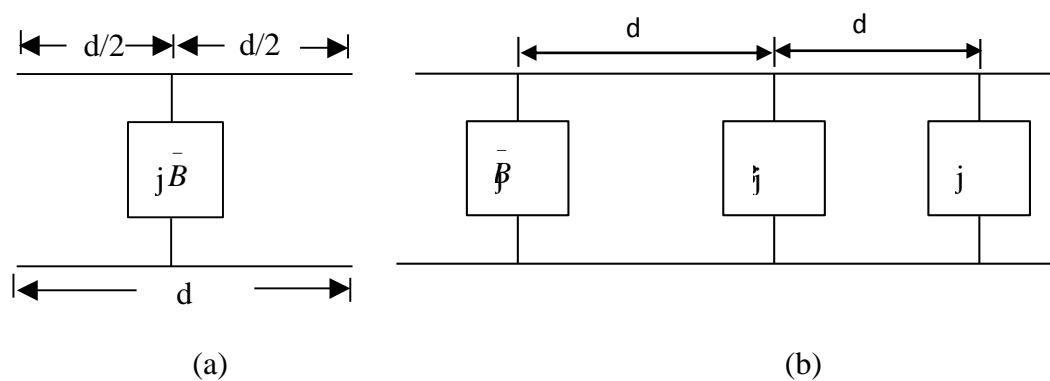


Fig. 3.11: (a) Equivalent circuit model of a unit cell, (b) a transmission line cascaded by unit cells. The unit cell may be divided into three parts as a transmission line of length $d/2$ on either side of normalized susceptance B [51].

3.9.3 Analysis of Infinite Periodic Structures

We first consider the propagation characteristics of the infinite loaded line shown in Fig. 3.10. Each unit cell of this line consists of a length, d , of transmission line with a shunt susceptance across the midpoint of the line; the susceptance, b , is normalized to the characteristic impedance, Z_0 . If we consider the infinite line as being composed of a

cascade of identical two-port networks, we can relate the voltages and currents on either side of the n^{th} unit cell using the ABCD matrix:

$$\begin{bmatrix} V_n \\ I_n \end{bmatrix} = \begin{bmatrix} A & B \\ C & D \end{bmatrix} \begin{bmatrix} V_{n+1} \\ I_{n+1} \end{bmatrix} \quad (3.32)$$

Where A, B, C and D are the matrix parameters for a cascade of a transmission line section of length $d/2$, a shunt susceptance b , and another transmission line section of length $d/2$. The reader can verify that $AD - BC = 1$, as required for reciprocal networks [51].

For a wave propagating in the $+z$ direction, we must have

$$\begin{aligned} V(z) &= V(0)e^{-\gamma z} \\ I(z) &= I(0)e^{-\gamma z} \end{aligned} \quad (3.33)$$

For a phase reference at $z = 0$. Since the structure is infinitely long, the voltage and current at the n^{th} terminals can differ from the voltage and current at the $n + 1$ terminals only by the propagation factor, $e^{-\gamma d}$. Thus,

$$\begin{aligned} V_{n+1} &= V_n e^{-\gamma d} \\ I_{n+1} &= I_n e^{-\gamma d} \end{aligned} \quad (3.34)$$

Using this result in (3.32) gives the following:

$$\begin{bmatrix} V_n \\ I_n \end{bmatrix} = \begin{bmatrix} A & B \\ C & D \end{bmatrix} \begin{bmatrix} V_{n+1} \\ I_{n+1} \end{bmatrix} = \begin{bmatrix} V_{n+1} e^{\gamma d} \\ I_{n+1} e^{\gamma d} \end{bmatrix} \quad (3.35)$$

For a nontrivial solution, the determinant of the above matrix must vanish:

$$AD + e^{2\gamma d} - (A + D)e^{\gamma d} - BC = 0 \quad (3.36)$$

since $AD - BC = 1$,

$$\begin{aligned} 1 + e^{2\gamma d} - (A + D)e^{\gamma d} &= 0 \\ e^{-\gamma d} + e^{\gamma d} &= A + D \\ \cosh \gamma d &= \frac{A + D}{2} = \cos \theta - \frac{b}{2} \sin \theta \end{aligned} \quad (3.37)$$

Now, if $\gamma = \alpha + j\beta$, we have that

$$\cosh \gamma d = \cosh \alpha d \cosh \beta d + j \sinh \alpha d \sinh \beta d = \cos \theta - \frac{b}{2} \sin \theta \quad (3.38)$$

Since the right-hand side of (3.38) is purely real, we must have either $\alpha = 0$ or $\beta = 0$.

Explanation:

Case 1: $\alpha = 0$, $\beta \neq 0$. This case corresponds to a nonattenuated propagating wave on the periodic structure, and defines the passband of the structure. Equation (3.38) reduces to

$$\cosh \beta d = \cos \theta - \frac{b}{2} \sin \theta \quad (3.39a)$$

which can be solved for β if the magnitude of the right-hand side is less than or equal to unity. Note that there are an infinite number of values of β that can satisfy (3.39a).

Case 2: $\alpha \neq 0$, $\beta = 0, \pi$. In this case the wave does not propagate, but is attenuated along the line; this defines the stopband of the structure. Because the line is lossless, power is not dissipated, but is reflected back to the input of the line. The magnitude of (3.38) reduces to

$$\cosh \alpha d = \left| \cos \theta - \frac{b}{2} \sin \theta \right| \geq 1 \quad (3.39b)$$

which has only one solution ($\alpha > 0$) for positively traveling waves; $\alpha < 0$ applies for negatively traveling waves. If $\cos \theta - (b/2) \sin \theta \leq -1$, (3.37b) is obtained from (3.38) by letting $\beta = \pi$; then all the lumped loads on the line are $\lambda/2$ apart, yielding an input impedance the same as if $\beta = 0$.

Thus, depending on the frequency and normalized susceptance values, the periodically loaded line will exhibit either passbands or stopbands, and so can be considered as a type of filter. It is important to note that the voltage and current waves defined in (3.33) and (3.35) are meaningful only when measured at the terminals of the unit cells, and do not apply to voltages and currents that may exist at points within a unit cell. These waves are similar to the elastic waves (Bloch waves) that propagate through periodic crystal lattices [51].

3.10 Conventional Filter Design

There are two methods whose have been following for making the conventional designs. They are named as the image parameter method and the insertion loss method. Those will

be briefly described one by one. Then the implementation of the microstrip filter will be described.

3.10.1 Filter Design by the Image Parameter Method

The image parameter method of filter design involves the specification of passband and stopband characteristics for a cascade of simple two-port networks, and so is related in concept to the periodic structures. The method is relatively simple but has the disadvantage that an arbitrary frequency response cannot be incorporated into the design. This is in contrast to the insertion loss method, which is the subject of the following section. Nevertheless, the image parameter method is useful for simple filters, and it provides a link between infinite periodic structures and practical filter design. The image parameter method also finds application in solid-state traveling-wave amplifier design [51].

❖ Image Impedances and Transfer Functions for Two-Port Networks

Consider the arbitrary two-port network shown in Fig. 3.12, where the network is specified by its ABCD parameters. Note that the reference direction for the current at port 2 has been chosen according to the convention for ABCD parameters. The image impedances, Z_{i1} and Z_{i2} , are defined for this network as follows:

Z_{i1} = input impedance at port 1 when port 2 is terminated with Z_{i2}

Z_{i2} = input impedance at port 2 when port 1 is terminated with Z_{i1}

Thus both ports are matched when terminated in their image impedances. We can derive expressions for the image impedances in terms of the ABCD parameters of the network.

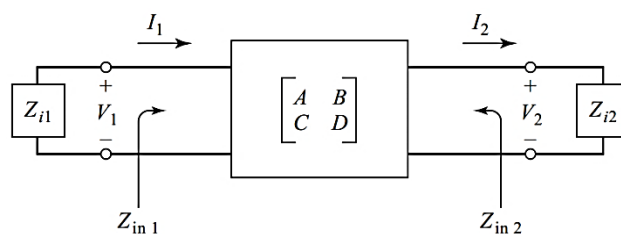


Fig. 3.12: A two-port network terminated in its image impedances.

The port voltages and currents are related as

$$V_1 = AV_2 + BI_2 \quad (3.40a)$$

$$I_1 = CV_2 + DI_2 \quad (3.40b)$$

The input impedance at port 1, with port 2 terminated in Z_{i2} , is

$$Z_{in1} = \frac{V_1}{I_1} = \frac{AV_2 + BI_2}{CV_2 + DI_2} = \frac{AZ_{i2} + B}{CZ_{i2} + D} \quad (3.41)$$

Since $V_2 = Z_{i2}I_2$ and $AD - BC = 1$ for a reciprocal network, here obtains

$$V_2 = DV_1 - BI_1 \quad (3.42a)$$

$$I_2 = -CV_1 + AI_1 \quad (3.42b)$$

Then the input impedance at port 2, with port 1 terminated in Z_{i1} , can be found as

$$Z_{in2} = \frac{-V_2}{I_2} = \frac{DV_1 - BI_1}{-CV_1 + AI_1} = \frac{DZ_{i1} + B}{CZ_{i1} + A} \quad (3.43)$$

since $V_1 = -Z_{i1}I_1$, $Z_{in1} = Z_{i1}$ and $Z_{in2} = Z_{i2}$ are desired.

So (3.41) and (3.43) give two equations for the image impedances:

$$Z_{i1} = \sqrt{\frac{AB}{CD}} \quad (3.44a)$$

$$Z_{i2} = \sqrt{\frac{BD}{AC}} \quad (3.44b)$$

If the network is symmetric, then $A = D$ and $Z_{i1} = Z_{i2}$ as expected. Now consider the voltage transfer function for a two-port network terminated in its image impedances. With reference to Fig. 3.13 the output voltage at port 2 can be expressed as

$$V_2 = DV_1 - BI_1 = \left(D - \frac{B}{Z_{i1}}\right)V_1 \quad (3.45)$$

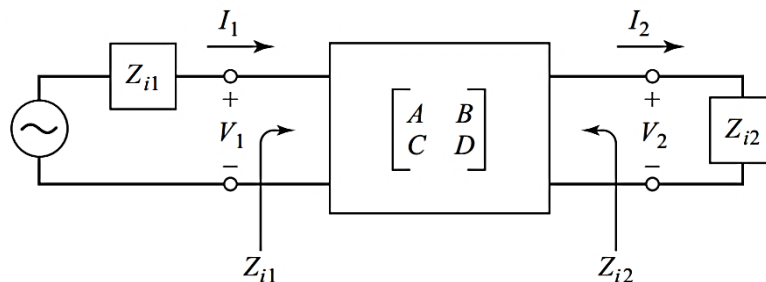


Fig. 3.13: A two-port network terminated in its image impedances and driven with a voltage generator.

(Since we now have $V_1 = I_1 Z_{i1}$), the voltage ratio is

$$\frac{V_2}{V_1} = \sqrt{\frac{D}{A}} (\sqrt{AD} - \sqrt{BC}) \quad (3.46a)$$

Similarly, the current ratio is,

$$\frac{I_2}{I_1} = \sqrt{\frac{A}{D}} (\sqrt{AD} - \sqrt{BC}) \quad (3.46b)$$

The factor $\sqrt{D/A}$ occurs in reciprocal positions in (3.46a) and (3.46b), and so can be interpreted as a transformer turns ratio. Apart from this factor, we can define a propagation factor for the network as

$$e^{-\gamma} = \sqrt{AD} - \sqrt{BC} \quad (3.47)$$

Where, $\gamma = \alpha + j\beta$

$$\begin{aligned} e^{\gamma} &= \sqrt{AD} + \sqrt{BC} \\ \cosh \gamma &= (e^{\gamma} + e^{-\gamma})/2 = \sqrt{AD} \end{aligned} \quad (3.48)$$

Two important types of two-port networks are the T and π circuits, which can be made in symmetric form [51].

❖ Constant-k Filter Sections

We can now develop low-pass and high-pass filter sections. First consider the T-network shown in Fig. 3.14. Intuitively, we can see that this is a low-pass filter network because the series inductors and shunt capacitor tend to block high-frequency signals while passing low frequency signals. Now, we have $Z_1 = j\omega L$ and $Z_2 = 1/j\omega C$, so the image impedance is

$$Z_{iT} = \sqrt{\frac{L}{C}} \sqrt{1 - \frac{\omega^2 LC}{4}} \quad (3.49)$$

If we define a cutoff frequency, ω_c , as

$$\omega_c = \frac{2}{\sqrt{LC}} \quad (3.50)$$

and a nominal characteristic impedance, R_0 , as

$$R_0 = \sqrt{\frac{L}{C}} = k \quad (3.51)$$

$$Z_{iT} = R_0 \sqrt{1 - \frac{\omega^2}{\omega_c^2}} \quad (3.52)$$

Then $Z_{iT} = R_0$ for $\omega = 0$

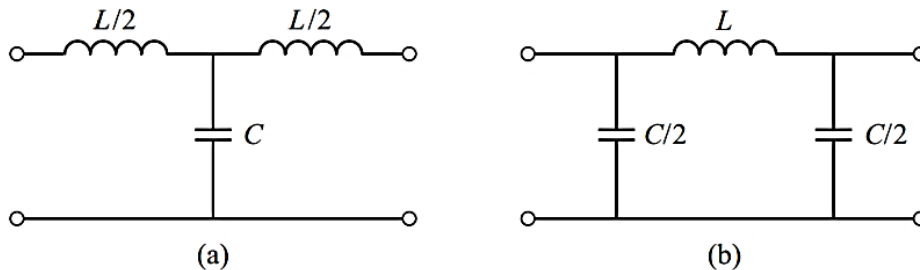


Fig. 3.14: Low-pass constant- k filter sections in T and π forms. (a) T-section. (b) π - section.

The propagation factor is,

$$e^\gamma = 1 - \frac{2\omega^2}{\omega_c^2} + \frac{2\omega}{\omega_c} \sqrt{\frac{\omega^2}{\omega_c^2} - 1} \quad (3.53)$$

Now consider two frequency regions:

1. For $\omega < \omega_c$: This is the passband of the filter section. Equation (3.52) shows that Z_{iT} is real and equation for e^γ shows that γ is imaginary, since $\omega^2/\omega_c^2 - 1$ is negative and $|e^\gamma|=1$:

$$|e^\gamma|^2 = \left(1 - \frac{2\omega^2}{\omega_c^2}\right)^2 + \frac{4\omega^2}{\omega_c^2} \left(1 - \frac{\omega^2}{\omega_c^2}\right) = 1$$

2. For $\omega > \omega_c$: This is the stopband of the filter section. Equation (3.52) shows that Z_{iT} is imaginary, and equation (3.53) shows that e^γ is real and $-1 < e^\gamma < 0$ (as seen from the limits as $\omega \rightarrow \omega_c$ and $\omega \rightarrow \infty$). The attenuation rate for $\omega \gg \omega_c$ is 40 dB/decade. Typical phase and attenuation constants are sketched in Fig. 3.15. Observe that the attenuation, α , is zero or relatively small near the cutoff frequency, although $\alpha \rightarrow \infty$ as

For the low-pass π -network of Fig. 3.15, we have that $Z_1 = j\omega L$ and $Z_2 = 1/j\omega C$, so the propagation factor is the same as that for the low-pass T-network. The cutoff frequency, ω_c , and nominal characteristic impedance, R_0 , are the same as the corresponding quantities

for the T-network. At $\omega = 0$ $Z_{iT} = Z_{i\pi} = R_0$, where $Z_{i\pi}$ is the image impedance of the low-pass π -network, but Z_{iT} and $Z_{i\pi}$ are generally not equal at other frequencies [51].

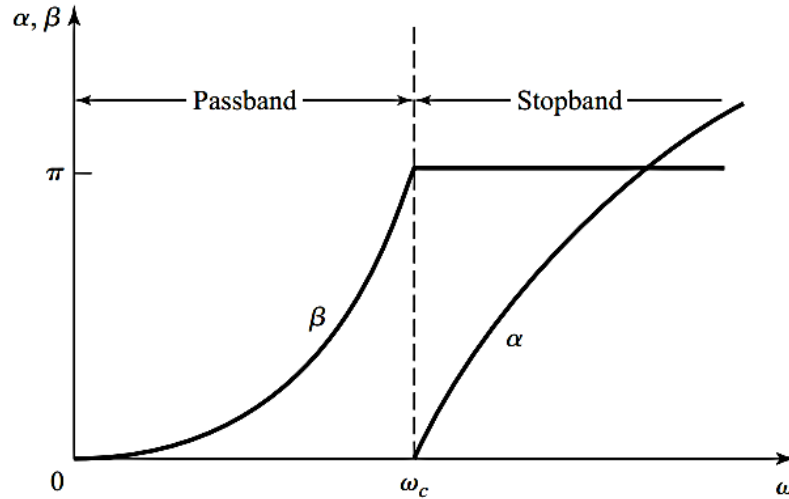


Fig. 3.15: Typical passband and stopband characteristics of the low-pass constant- k sections of Fig. 3.6.

High-pass constant- k sections are shown in Fig. 3.16; we see that the positions of the inductors and capacitors are reversed from those in the low-pass prototype. The design equations are easily shown to be

$$R_0 = \sqrt{\frac{L}{C}} \quad \text{and,} \quad \omega_c = \frac{1}{2\sqrt{LC}}$$

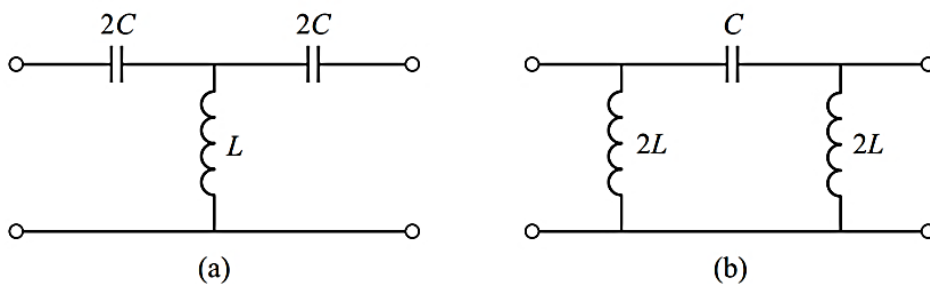


Fig. 3.16: High-pass constant- k filter sections in T and π forms. (a) T-section. (b) π - section.

❖ **m -Derived Filter Sections**

As shown in Fig. 3.17 the impedances Z_1 and Z_2 in a constant- k T-section are replaced with Z_1' and Z_2' .

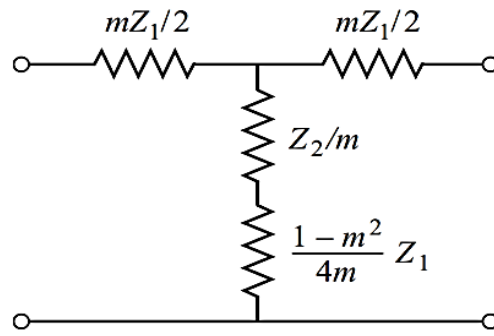


Fig. 3.17: Development of an m -derived filter section from a constant- k section.

The replaced equation is,

$$Z'_1 = mZ_1 \quad (3.54)$$

Then it has chosen Z_2 to obtain the same value of Z_{iT} as for the constant- k section. It shows the following equation

$$Z_{iT} = \sqrt{mZ_1Z'_2 + \frac{m^2Z_1^2}{4}} \quad (3.55)$$

And solution for Z'_2 gives,

$$Z'_2 = \frac{Z_2}{m} + \frac{Z_1}{4m} - \frac{mZ_1}{4} = \frac{Z_2}{m} + \frac{(1-m^2)}{4m}Z_1 \quad (3.56)$$

For a low-pass filter, we have $Z_1 = j\omega L$ and $Z_2 = 1/j\omega C$. Then (3.54) and (3.55) give the m -derived components as

$$Z'_1 = j\omega Lm \quad (3.57a)$$

$$Z'_2 = \frac{1}{j\omega Cm} + \frac{(1-m^2)}{4m}j\omega L \quad (3.57b)$$

which results in the circuit of Fig. 3.18. Now consider the propagation factor for the

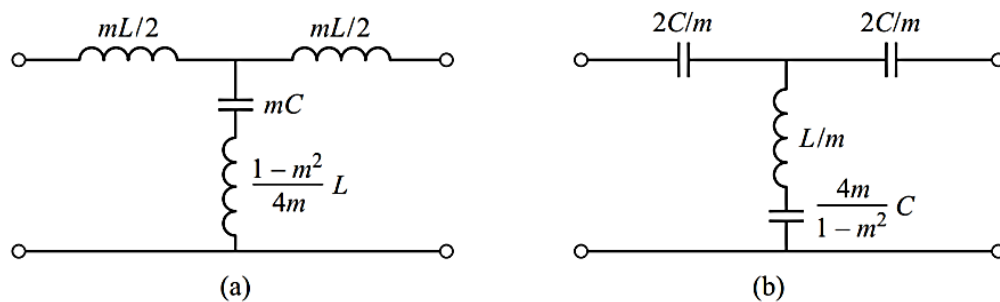


Fig. 3.18: m -Derived filter sections (a) Low-pass T-section (b) High-pass T-section.

$$e^\gamma = 1 + \frac{Z'_1}{Z'_2} + \sqrt{\frac{Z'_1}{Z'_2} \left(1 + \frac{Z'_1}{4Z'_2} \right)} \quad (3.58)$$

If we restrict $0 < m < 1$, then these results show that e^γ is real and $|e^\gamma| > 1$ for $\omega > \omega_c$. Thus the stopband begins at $\omega = \omega_c$, as for the constant- k section. However, when $\omega = \omega_\infty$, where

$$\omega_\infty = \frac{\omega_c}{\sqrt{1 - m^2}} \quad (3.59)$$

The denominators vanish and e^γ becomes infinite, implying infinite attenuation. Physically, this pole in the attenuation characteristic is caused by the resonance of the series LC resonator in the shunt arm of the T; this is easily verified by showing that the resonant frequency of this LC resonator is ω_∞ . Note that the equation of ω_∞ indicates that $\omega_\infty > \omega_c$, so infinite attenuation occurs after the cutoff frequency, ω_c , as illustrated in Fig. 3.19. The position of the pole at ω_∞ can be controlled with the value of m [51].

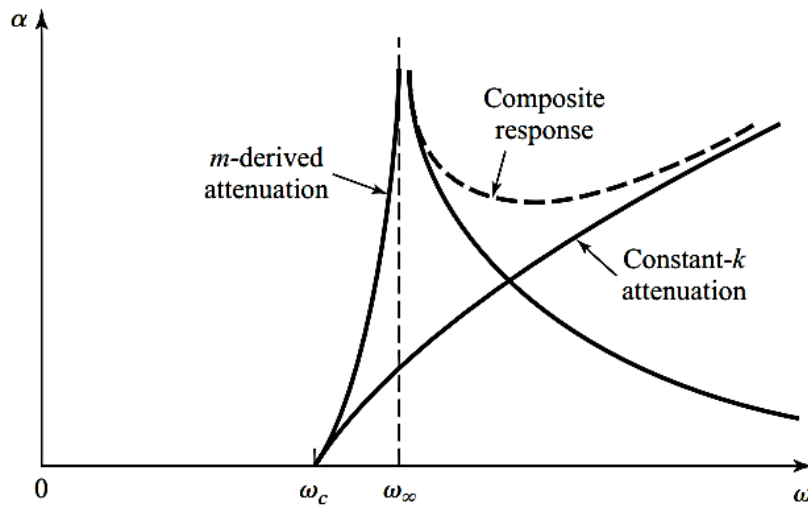


Fig. 3.19: Typical attenuation responses for constant- k , m -derived, and composite filters.

❖ Composite Filters

By combining in cascade the constant- k , m -derived sharp cutoff and the m -derived matching sections we can realize a filter with the desired attenuation and matching properties.

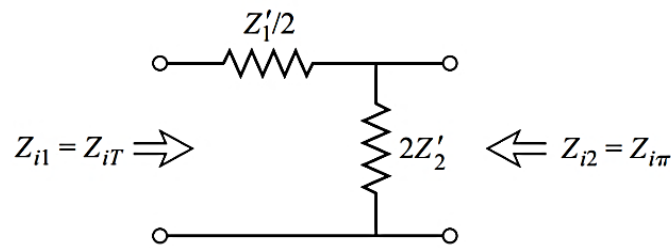


Fig. 3.20: A bisected π -section used to match $Z_{i\pi}$ to Z_{iT}

This type of design is called a composite filter, and is shown in Fig. 3.21. The sharp-cutoff section, with $m < 0.6$, places an attenuation pole near the cutoff frequency to provide a sharp attenuation response; the constant- k section provides high attenuation further in to the stopband. The bisected- π sections at the ends of the filter match the nominal source and load impedance, R_0 , to the internal image impedances, Z_{iT} , of the constant- k and m -derived sections.

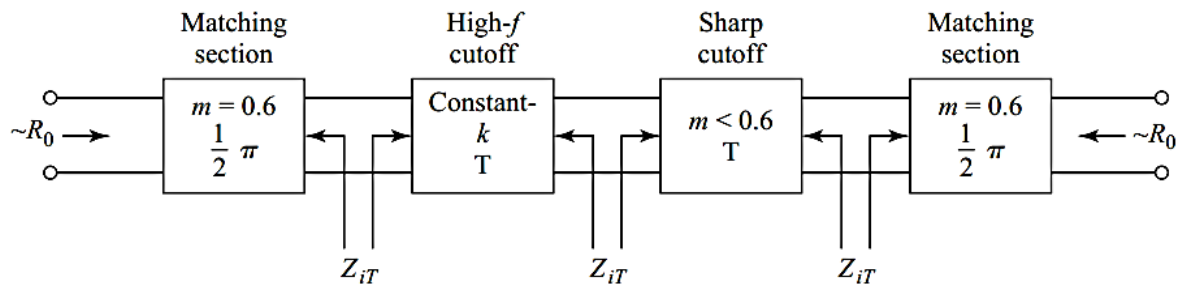


Fig. 3.21: The final four-stage composite filter [51].

3.10.2 Filter Design by the Insertion Loss Method

The image parameter method of the previous section may yield a usable filter response for some applications, but there is no methodical way of improving the design. The insertion loss method, however, allows a high degree of control over the passband and stop-band amplitude and phase characteristics, with a systematic way to synthesize a desired response. The necessary design trade-offs can be evaluated to best meet the application requirements. If, for example, a minimum insertion loss is most important, a binomial response could be used; a Chebyshev response would satisfy a requirement for the sharpest cutoff. If it is possible to sacrifice the attenuation rate, a better phase response can be obtained by using a linear phase filter design. In addition, in all cases, the insertion loss method allows filter performance to be improved in a straightforward manner, at the

expense of a higher order filter. For the filter prototypes to be discussed below, the order of the filter is equal to the number of reactive elements [51].

In the insertion loss method a filter response is defined by its insertion loss, or power loss ratio, P_{LR} :

$$P_{LR} = \frac{\text{Power available from the source}}{\text{Power delivered to load}} = \frac{P_{inc}}{P_{load}} = \frac{1}{1 - |\Gamma(\omega)|^2}$$

Observe that this quantity is the reciprocal of $|S_{12}|^2$ if both load and source are matched.

The insertion loss (IL) in dB is

$$IL = 10 \log P_{LR}$$

$$P_{LR} = 1 + \frac{M(\omega^2)}{N(\omega^2)}$$

where M and N are real polynomials in ω^2 . The practical filter responses are described below.

❖ Maximally flat

This characteristic is also called the binomial or Butterworth response, and is optimum in the sense that it provides the flattest possible passband response for a given filter complexity, or order. For a low-pass filter, it is specified by

$$P_{LR} = 1 + k^2 \left(\frac{\omega}{\omega_c} \right)^{2N}$$

where N is the order of the filter and ω_c is the cutoff frequency. The passband extends from $\omega=0$ to $\omega=\omega_c$; at the band edge the power loss ratio is $1 + k^2$. If we choose this as the -3 dB point, as is common, we have $k=1$, which we will assume from now on. For $\omega > \omega_c$, the attenuation increases monotonically with frequency, as shown in Fig. 3.22. For $\omega \gg \omega_c$, $P_{LR} \cong k^2 (\omega/\omega_c)^{2N}$, which shows that the insertion loss increases at the rate of 20N dB/decade. Like the binomial response for multi section quarter-wave matching transformers, the first $(2N - 1)$ derivatives of the equation of P_{LR} are zero at $\omega = 0$.

❖ Equal ripple

If a Chebyshev polynomial is used to specify the insertion loss of an Nth-order low-pass filter as

$$P_{LR} = 1 + k^2 T_N^2 \left(\frac{\omega}{\omega_c} \right)$$

then a sharper cutoff will result, although the passband response will have ripples of amplitude $1 + k^2$, as shown in Fig. 3.22, since $T_N(x)$ oscillates between ± 1 for $|x|^2$. Thus, k^2 determines the passband ripple level. For large x , $T_N(x) \cong \frac{1}{2}(2x)^{2N}$, so for $\omega \gg \omega_c$ the insertion loss becomes

$$P_{LR} \cong \frac{k^2}{4} \left(\frac{2\omega}{\omega_c} \right)^{2N}$$

which also increases at the rate of $20N$ dB/decade.

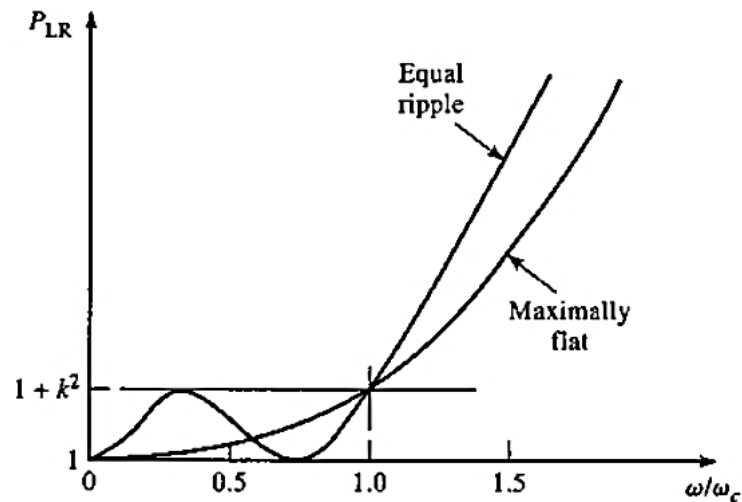


Fig. 3.22: Maximally flat and equal-ripple low-pass filter responses ($N = 3$).

❖ Elliptic function

The maximally flat and equal-ripple responses both have monotonically increasing attenuation in the stopband. In many applications it is adequate to specify a minimum stopband attenuation, in which case a better cutoff rate can be obtained. Such filters are

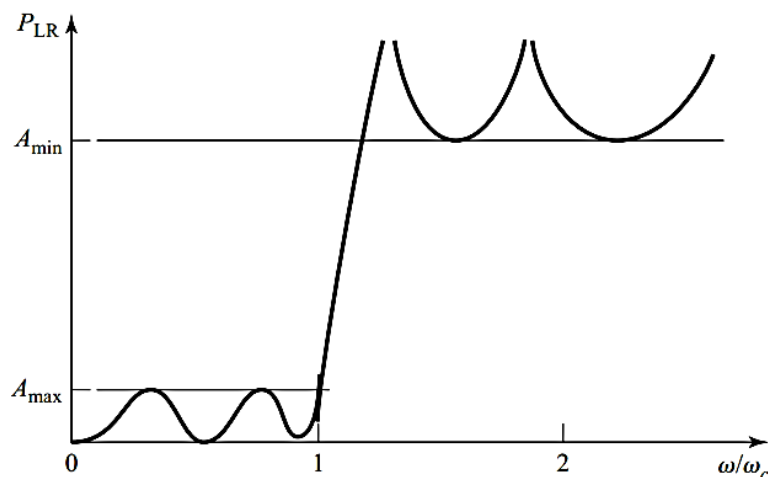


Fig. 3.23: Elliptic function lowpass filter response.

called elliptic function filters, and they have equal-ripple responses in the pass band as well as in the stopband, as shown in Fig. 3.23. The maximum attenuation in the pass-band, A_{\max} , can be specified, as well as the minimum attenuation in the stopband, A_{\min} . Elliptic function filters are difficult to synthesize, so we will not consider them further [51].

❖ Linear phase

The above filters specify the amplitude response, but in some applications it is important to have a linear phase response in the passband to avoid signal distortion. Since a sharp-cutoff response is generally incompatible with a good phase response, the phase response of a filter must be deliberately synthesized, usually resulting in an inferior attenuation characteristic. A linear phase characteristic can be achieved with the following phase response:

$$\phi(\omega) = A\omega \left[1 + p \left(\frac{\omega}{\omega_c} \right)^{2N} \right]$$

Where $\phi(\omega)$ is the phase of the voltage transfer function of the filter, and p is a constant. A related quantity is the group delay, defined as

$$\tau_d = \frac{d\phi}{d\omega} = \left[1 + p(2N + 1) \left(\frac{\omega}{\omega_c} \right)^{2N} \right]$$

Which shows that the group delay for a linear phase filter is a maximally flat function.

More general filter specifications can be obtained, but the above cases are the most common. We will next discuss the design of low-pass filter prototypes that are normalized in terms of impedance and frequency; this normalization simplifies the design of filters for arbitrary frequency, impedance, and type (low-pass, high-pass, bandpass, or bandstop). The low-pass prototypes are then scaled to the desired frequency and impedance, and the lumped-element components replaced with distributed circuit elements for implementation at microwave frequencies [51]. This design process is illustrated in Fig. 3.24.

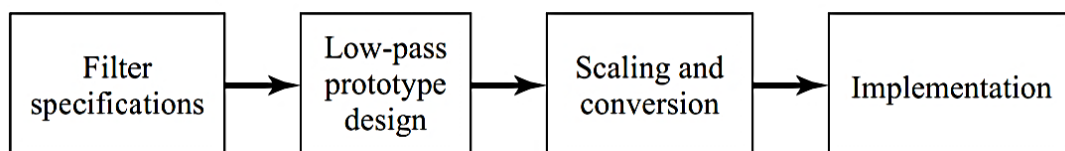


Fig. 3.24: The process of filter design by the insertion loss method.

3.10.3 Filter Implementation

The lumped-element filter designs generally work well at low frequencies, but two problems arise at higher RF and microwave frequencies. First, lumped-element inductors and capacitors are generally available only for a limited range of values, and can be difficult to implement at microwave frequencies. Distributed elements, such as open-circuited or short-circuited transmission line stubs, are often used to approximate ideal lumped elements. In addition, at microwave frequencies the distances between filter components is not negligible. The first problem is treated with Richards' transformation, which can be used to convert lumped elements to transmission line sections. Kuroda's identities can then be used to physically separate filter elements by using transmission line sections. Because such additional transmission line sections do not affect the filter response, this type of design is called redundant filter synthesis. It is possible to design microwave filters that take advantage of these sections to improve the filter response; such non-redundant synthesis does not have a lumped-element counterpart [51].

❖ Richards' Transformation

This is the first step to make lumped element into RF element. This transformation converts inductor and capacitor element into stubs. The working principle is described below,

The transformation,

$$\Omega = \tan \beta l = \tan \left(\frac{\omega l}{v_p} \right) \quad (3.60)$$

maps the ω plane to the Ω plane, which repeats with a period of $\omega l/v_p = 2\pi$. This transformation was introduced by P. Richards [68] to synthesize an LC network using open- and short-circuited transmission line stubs. Thus, if we replace the frequency variable ω with Ω , we can write the reactance of an inductor as

$$jX_L = j\Omega L = jL \tan \beta l \quad (3.61)$$

and the susceptance of a capacitor as

$$jB_C = j\Omega C = jC \tan \beta l \quad (3.62)$$

These results indicate that an inductor can be replaced with a short-circuited stub of length β and characteristic impedance L , while a capacitor can be replaced with an open-circuited stub of length β and characteristic impedance $1/C$. An unity filter impedance is assumed.

Cutoff occurs at unity frequency for a low-pass filter prototype; to obtain the same cutoff frequency for the Richards'-transformed filter, (3.60) shows that

$$\Omega = 1 = \tan \beta l$$

which gives a stub length of $l = \lambda/8$, where λ is the wavelength of the line at the cutoff frequency, ω_c . At the frequency $\omega_0 = 2\omega_c$, the lines will be $\lambda/4$ long, and an attenuation pole will occur. At frequencies away from ω_c , the impedances of the stubs will no longer match the original lumped-element impedances, and the filter response will differ from the desired prototype response. In addition, the response will be periodic in frequency, repeating every $4\omega_c$.

In principle, then, Richards' transformation allows the inductors and capacitors of a lumped-element filter to be replaced with short-circuited and open-circuited transmission line stubs, as illustrated in Fig. 3.25. Since the electrical lengths of all the stubs are the same ($\lambda/8$ at ω_c), these lines are called *commensurate* lines [51].

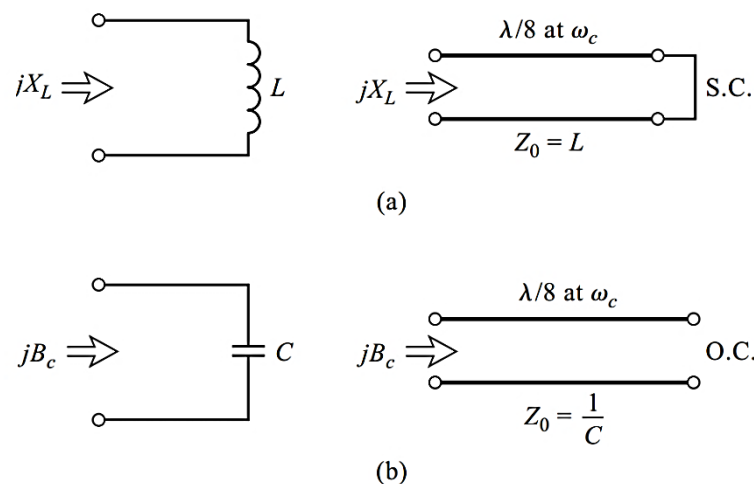


Fig. 3.25: Richards' transformation. (a) For an inductor to a short-circuited stub. (b) For a capacitor to an open-circuited stub.

❖ Kuroda's Identities

The four Kuroda identities use redundant transmission line sections to achieve a more practical microwave filter implementation by performing any of the following operations:

- Physically separate transmission line stubs
- Transform series stubs into shunt stubs, or vice versa
- Change impractical characteristic impedances into more realizable values

The additional transmission line sections are called unit elements and are $\lambda/8$ long at ω_c ; the unit elements are thus commensurate with the stubs used to implement the inductors and capacitors of the prototype design. The four Kuroda identities are illustrated in Fig. 3.26, where each box represents a unit element, or transmission line, of the indicated characteristic impedance and length ($\lambda/8$ at ω_c). The inductors and capacitors represent short-circuit and open-circuit stubs, respectively [51].

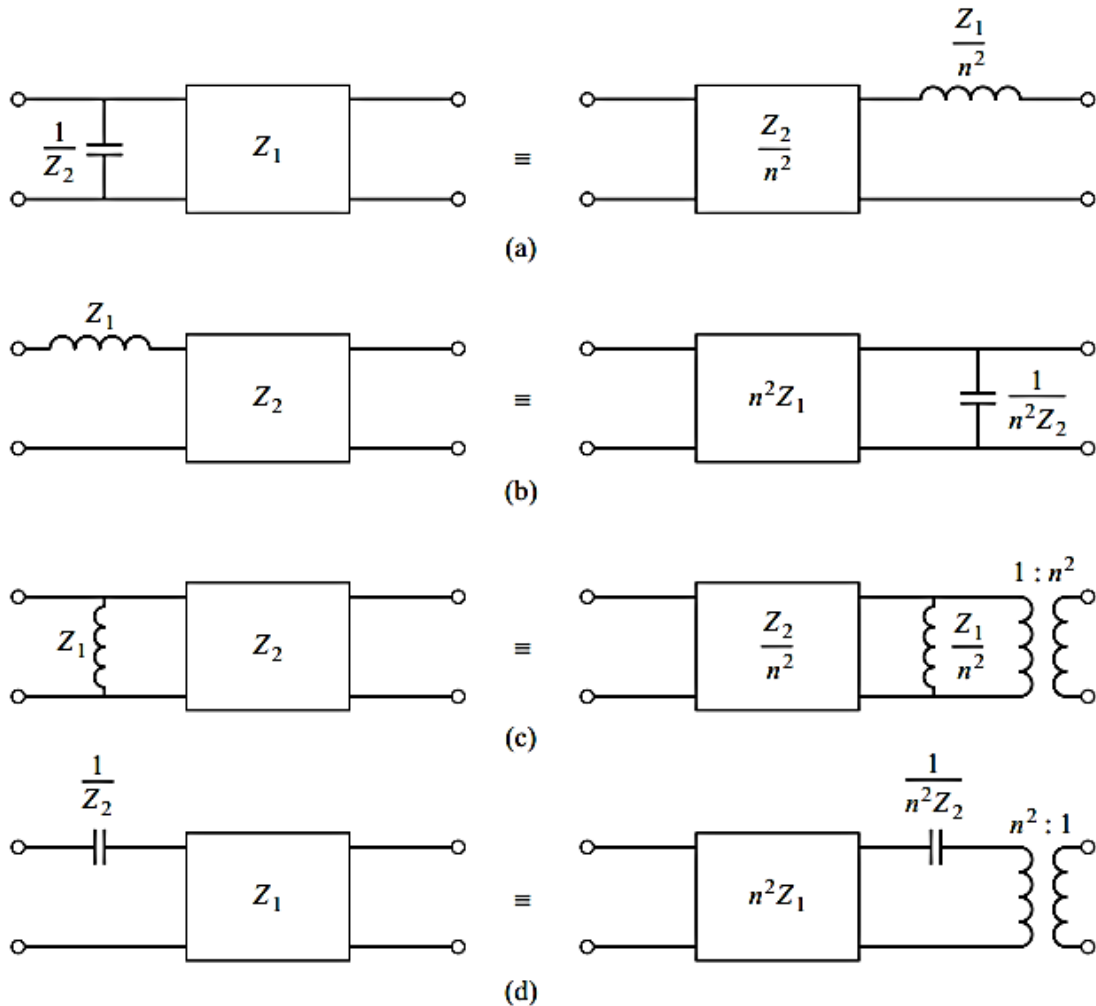


Fig. 3.26: The Four Kuroda Identities ($n^2 = 1 + Z_2/Z_1$)

3.11 Coupled Line Filter

The parallel coupled transmission lines can be used to construct many types of filters. Fabrication of multisection bandpass or bandstop coupled line filters is particularly easy in microstrip or stripline form for bandwidths less than about 20%. Wider bandwidth filters generally require very tightly coupled lines, which are difficult to fabricate. We will first

study the filter characteristics of a single quarter-wave coupled line section, and then show how these sections can be used to design a bandpass filter [69].

A parallel coupled line section is shown in Fig. 3.27a, with port voltage and current definitions. We will derive the open-circuit impedance matrix for this four-port network by considering the superposition of even- and odd-mode excitations [70], which are shown in Fig. 3.27b. Thus, the current sources i_1 and i_3 drive the line in the even mode, while i_2 and i_4 drive the line in the odd mode. By superposition, we see that the total port currents, I_i , can be expressed in terms of the even and odd mode currents as

$$I_1 = i_1 + i_2 \quad (3.63a)$$

$$I_2 = i_1 - i_2 \quad (3.63b)$$

$$I_3 = i_3 - i_4 \quad (3.63c)$$

$$I_4 = i_3 + i_4 \quad (3.63d)$$

First consider the line as being driven in the even mode by the i_1 current sources. If the other ports are open-circuited, the impedance seen at port 1 or 2 is

$$Z_{in}^e = -j Z_{0e} \cot \beta \ell \quad (3.64)$$

The voltage on either conductor can be expressed as

$$\begin{aligned} v_a^1(z) = v_b^1(z) &= V_e^+ [e^{-j\beta(z-\ell)} + e^{j\beta(z-\ell)}] \\ &= 2V_e^+ \cos \beta(\ell - z) \end{aligned} \quad (3.65)$$

so the voltage at port 1 or 2 is

$$v_a^1(0) = v_b^1(0) = 2V_e^+ \cos \beta \ell = i_1 Z_m^e \quad (3.66)$$

This result and (3.63) can be used to rewrite (3.64) in terms of i_1 as

$$Z_{in}^e = -j Z_{0e} \frac{\cos \beta(\ell - z)}{\sin \beta \ell} i_1 \quad (3.67)$$

The voltage on either conductor can be expressed as

$$v_a^2(z) = -v_b^2(z) = V_o^+ [e^{-j\beta(z-\ell)} + e^{j\beta(z-\ell)}] = 2V_o^+ \cos \beta(\ell - z) \quad (3.70)$$

Then the voltage at port 1 or port 2 is

$$v_a^2(0) = -v_b^2(0) = 2V_o^+ \cos \beta \ell = i_2 Z_{in}^o$$

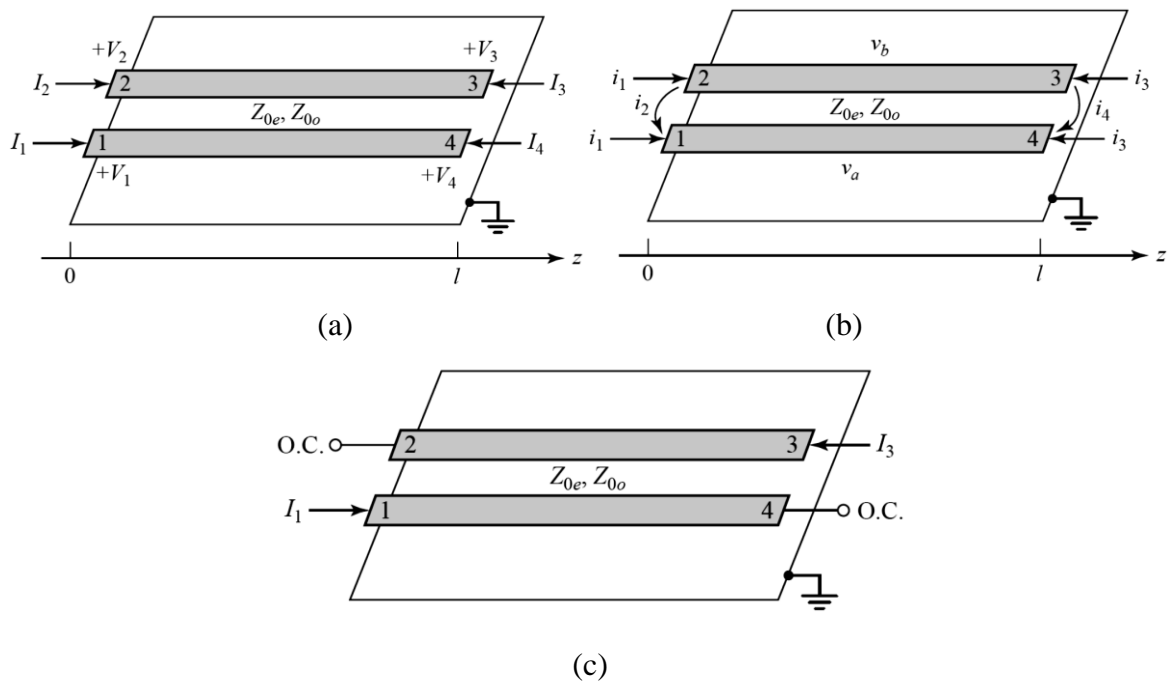


Fig 3.27: Definitions pertaining to a coupled line filter section. (a) A parallel coupled line section with port voltage and current definitions. (b) A parallel coupled line section with even- and odd-mode current sources. (c) A two-port coupled line section having a bandpass response [51].

This result and (3.69) can be used to rewrite (3.70) in terms of i_2 as

$$v_a^2(z) = -v_b^2(z) = -jZ_{0o} \frac{\cos\beta(\ell - z)}{\sin\beta\ell} i_2 \quad (3.71)$$

Similarly, the voltages due to current i_4 driving the line in the odd mode are

$$v_a^4(z) = -v_b^4(z) = -jZ_{0o} \frac{\cos\beta z}{\sin\beta\ell} i_4 \quad (3.72)$$

The total voltage at port 1 is

$$\begin{aligned} V_1 &= v_a^1(0) + v_a^2(0) + v_a^3(0) + v_a^4(0) \\ &= -j(Z_{0e}i_1 + Z_{0o}i_2) \cot\theta - j(Z_{0e}i_3 + Z_{0o}i_4) \csc\theta \end{aligned} \quad (3.73)$$

Where the results of (3.70), (3.71), (3.72), and (3.73) were used, and $\theta = \beta\ell$. Next, we solve (3.63) for the i_j in terms of the I_s :

$$i_1 = \frac{1}{2}(I_1 + I_2) \quad (3.74a)$$

$$i_2 = \frac{1}{2}(I_1 - I_2) \quad (3.74b)$$

$$i_3 = \frac{1}{2}(I_3 + I_4) \quad (3.74c)$$

$$i_4 = \frac{1}{2}(I_4 - I_3) \quad (3.74d)$$

and use these results in (3.73):

$$\begin{aligned} V_1 &= \frac{-j}{2} (Z_{0e}I_1 + Z_{0e}I_2 + Z_{0o}I_1 + Z_{0o}I_2) \cot \theta \\ &= \frac{-j}{2} (Z_{0e}I_3 + Z_{0e}I_4 + Z_{0o}I_4 - Z_{0o}I_3) \csc \theta \end{aligned} \quad (3.75)$$

This result yields the top row of the open-circuit impedance matrix $[Z]$ that describes the coupled line section. From symmetry, all other matrix elements can be found once the first row is known. The matrix elements are then

$$Z_{11} = Z_{22} = Z_{33} = Z_{44} = \frac{-j}{2} (Z_{0e} + Z_{0o}) \cot \theta \quad (3.76a)$$

$$Z_{12} = Z_{21} = Z_{34} = Z_{43} = \frac{-j}{2} (Z_{0e} - Z_{0o}) \cot \theta \quad (3.76b)$$

$$Z_{13} = Z_{31} = Z_{24} = Z_{42} = \frac{-j}{2} (Z_{0e} - Z_{0o}) \csc \theta \quad (3.76c)$$

$$Z_{14} = Z_{41} = Z_{23} = Z_{32} = \frac{-j}{2} (Z_{0e} + Z_{0o}) \csc \theta \quad (3.76d)$$

A two-port network can be formed from a coupled line section by terminating two of the four ports with either open or short circuits, or by connecting two ends [51].

3.12 Design of Coupled Line Bandpass Filter

Narrowband bandpass filters can be made with cascaded coupled line sections of the form shown in Fig. 3.27c. To derive the design equations for filters of this type, we first show that a single coupled line section can be approximately modeled by the equivalent circuit shown in Fig. 3.28. We will do this by calculating the image impedance and propagation constant of the equivalent circuit and showing that they are approximately equal to those of the coupled line section for $\theta = \pi/2$, which will correspond to the center frequency of the bandpass response.

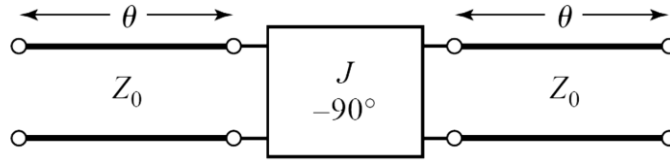


Fig 3.28: Equivalent circuit of the coupled line section of Fig. 3.27c.

The ABCD parameters of the equivalent circuit is

$$\begin{aligned}
 \begin{bmatrix} A & B \\ C & D \end{bmatrix} &= \begin{bmatrix} \cos \theta & jZ_0 \sin \theta \\ \frac{j \sin \theta}{Z_0} & \cos \theta \end{bmatrix} \begin{bmatrix} 0 & -\frac{j}{J} \\ -jJ & 0 \end{bmatrix} \begin{bmatrix} \cos \theta & jZ_0 \sin \theta \\ \frac{j \sin \theta}{Z_0} & \cos \theta \end{bmatrix} \\
 &= \begin{bmatrix} \left(JZ_0 + \frac{1}{JZ_0}\right) \sin \theta \cos \theta & j\left(JZ_0^2 \sin^2 \theta - \frac{\cos^2 \theta}{j}\right) \\ j\left(\frac{1}{JZ_0^2} \sin^2 \theta - J \cos^2 \theta\right) & \left(JZ_0 + \frac{1}{JZ_0}\right) \sin \theta \cos \theta \end{bmatrix} \quad (3.77)
 \end{aligned}$$

The ABCD parameters of the admittance inverter were obtained by considering it as a quarter-wave length of transmission of characteristic impedance, $1/J$. The image impedance of the equivalent circuit is

$$Z_i = \sqrt{\frac{B}{C}} = \sqrt{\frac{JZ_0^2 \sin^2 \theta - \left(\frac{1}{J}\right) \cos^2 \theta}{\left(\frac{1}{JZ_0^2}\right) \sin^2 \theta - J \cos^2 \theta}} \quad (3.78)$$

$$Z_i = JZ_0^2$$

which reduces to the following value at the center frequency, $\theta = \pi/2$:

the propagation constant is

$$\cos \beta = A = \left(JZ_0 + \frac{1}{JZ_0}\right) \sin \theta \cos \theta$$

So the image impedance and propagation constant should be

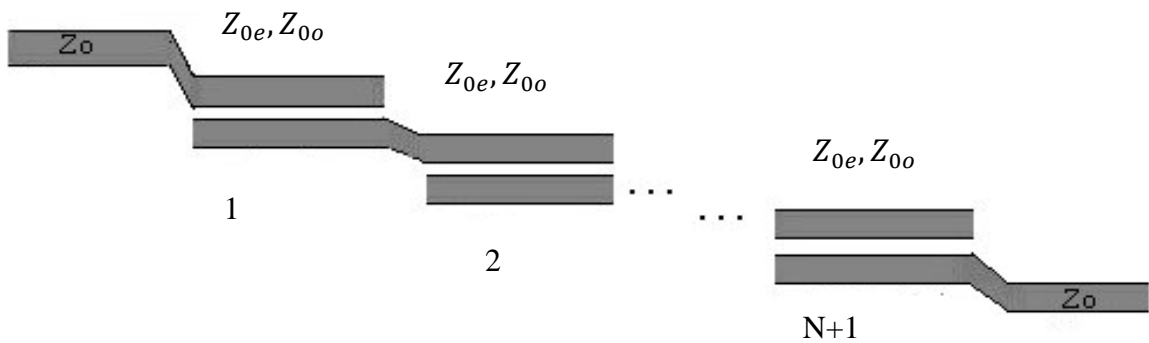
$$\begin{aligned}
 \frac{1}{2}(Z_{0e} - Z_{0o}) &= JZ_0^2 \\
 \frac{Z_{0e} + Z_{0o}}{Z_{0e} - Z_{0o}} &= JZ_0 + \frac{1}{JZ_0}
 \end{aligned}$$

where we have assumed $\sin \theta \approx 1$ for θ near $\pi/2$. These equations can be solved for the even- and odd-mode line impedances to give

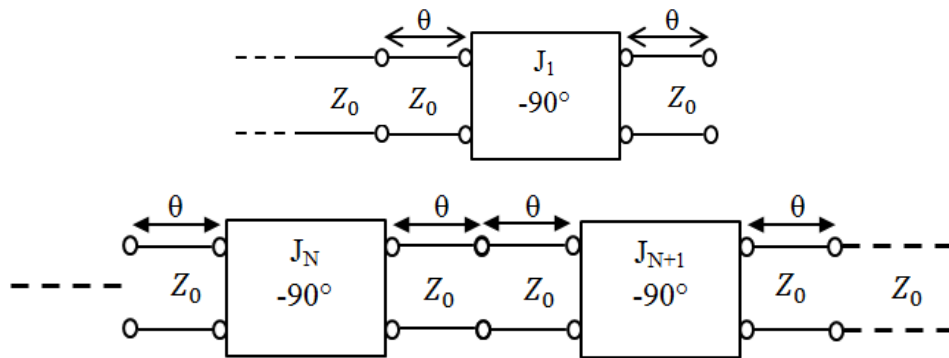
$$Z_{0e} = Z_0[1 + JZ_0 + (JZ_0)^2] \quad (3.79a)$$

$$Z_{0o} = Z_0[1 - JZ_0 + (JZ_0)^2] \quad (3.79b)$$

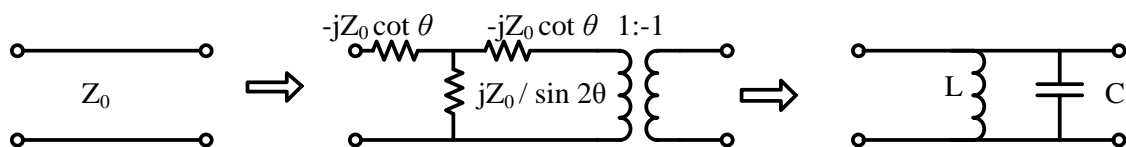
Now consider a bandpass filter composed of a cascade of $N + 1$ coupled line sections, as shown in Fig. 3.29a. The sections are numbered from left to right, with the load on the right, but the filter can be reversed without affecting the response. Since each coupled line section has an equivalent circuit of the form shown in Fig. 3.28, the equivalent circuit of the cascade is as shown in Fig. 3.29b. Between any two consecutive inverters we have a transmission line section that is effectively 2θ in length. This line is approximately $\lambda/2$ long in the vicinity of the bandpass region of the filter, and has an approximate equivalent circuit that consists of a shunt parallel LC resonator, as in Fig. 3.29c.



(a)



(b)



(c)

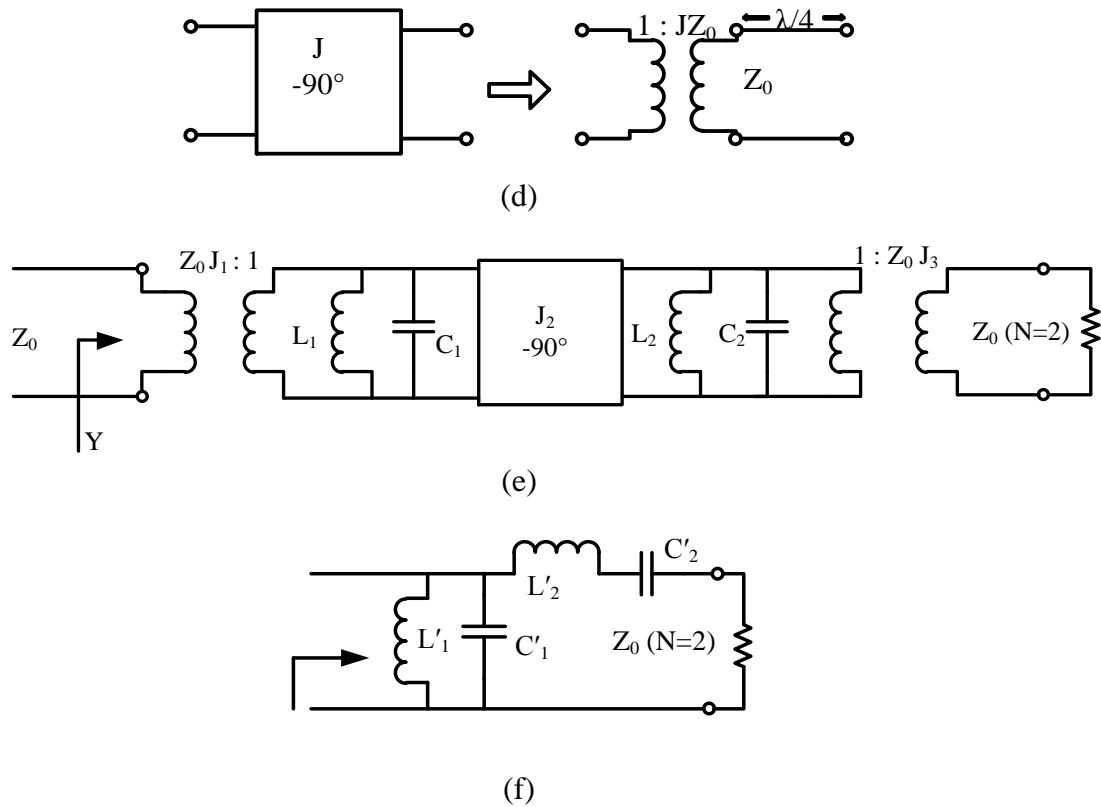


Fig. 3.29: Development of an equivalent circuit for derivation of design equations for a coupled line bandpass filter. (a) Layout of an $(N + 1)$ -section coupled line bandpass filter. (b) Using the equivalent circuit of Fig. 3.28 for each coupled line section. (c) Equivalent circuit for transmission lines of length 2θ . (d) Equivalent circuit of the admittance inverters. (e) Using results of (c) and (d) for the $N = 2$ case. (f) Lumped-element circuit for a bandpass filter for $N = 2$ [51].

The first step in establishing this equivalence is to find the parameters for the T-equivalent and ideal transformer circuit of Fig. 3.29c (an exact equivalent). The ABCD matrix for this circuit can be calculated for a T-circuit and an ideal transformer:

$$\begin{bmatrix} A & B \\ C & D \end{bmatrix} = \begin{bmatrix} Z_{11} & Z_{11}^2 - Z_{12}^2 \\ Z_{12} & Z_{12} \\ 1 & Z_{11} \\ Z_{12} & Z_{12} \end{bmatrix} \begin{bmatrix} -1 & 0 \\ 0 & -1 \end{bmatrix} = \begin{bmatrix} -Z_{11} & Z_{12}^2 - Z_{11}^2 \\ Z_{12} & Z_{12} \\ -1 & -Z_{11} \\ Z_{12} & Z_{12} \end{bmatrix} \quad (3.80)$$

Equating this result to the ABCD parameters for a transmission line of length 2θ and characteristic impedance Z_0 gives the parameters of the equivalent circuit as

$$Z_{12} = \frac{-1}{C} = \frac{jZ_0}{\sin 2\theta} \quad (3.81a)$$

$$Z_{11} = Z_{22} = -Z_{12}A = -jZ_0 \cot 2\theta \quad (3.81b)$$

Then the series arm impedance is

$$Z_{11} - Z_{12} = -jZ_0 \frac{\cos 2\theta + 1}{\sin 2\theta} = -jZ_0 \cot \theta \quad (3.82)$$

The 1: -1 transformer provides a 180° phase shift, which cannot be obtained with the T-network alone; since this does not affect the amplitude response of the filter, it can be discarded. For $\theta \sim \pi/2$ the series arm impedances of (3.82) are near zero and can also be ignored. The shunt impedance Z_{12} , however, looks like the impedance of a parallel resonant circuit for $\theta \sim \pi/2$. If we let $\omega = \omega_0 + \Delta\omega$, where $\theta = \pi/2$ at the center frequency ω_0 , then we have $2\theta = \beta\ell = \omega\ell/v_p = (\omega_0 + \Delta\omega) \pi/\omega_0 = \pi(1 + \Delta\omega/\omega_0)$, so (3.81a) can be written for small $\Delta\omega$ as

$$Z_{12} = \frac{jZ_0}{\sin\pi(1 + \Delta\omega/\omega_0)} \simeq \frac{-jZ_0\omega_0}{\pi(\omega - \omega_0)} \quad (3.83)$$

the impedance near resonance of a parallel LC circuit is

$$Z = \frac{-jL\omega_0^2}{2(\omega - \omega_0)} \quad (3.84)$$

with $\omega_0^2 = 1/LC$. Equating this to (3.84) gives the equivalent inductor and capacitor values as

$$L = \frac{2Z_0}{\pi\omega_0} \quad (3.85a)$$

$$C = \frac{1}{\omega_0^2 L} = \frac{\pi}{2Z_0\omega_0} \quad (3.85b)$$

The lines of length θ on either end of the filter are matched to Z_0 and so can be ignored. The end inverters, J_1 and J_{N+1} , can each be represented as a transformer followed by a $\lambda/4$ section of line, as shown in Fig. 3.29d. The ABCD matrix of a transformer with a turns ratio N in cascade with a quarter-wave line is

$$\begin{bmatrix} A & B \\ C & D \end{bmatrix} = \begin{bmatrix} 1 & 0 \\ N & N \end{bmatrix} \begin{bmatrix} 0 & -jZ_0 \\ -j & 0 \end{bmatrix} = \begin{bmatrix} 0 & \frac{-jZ_0}{N} \\ \frac{-jN}{Z_0} & 0 \end{bmatrix} \quad (3.86)$$

Comparing this to the ABCD matrix of an admittance inverter shows that the necessary turns ratio is $N = JZ_0$. The $\lambda/4$ line merely produces a phase shift and so can be ignored.

Using these results for the interior and end sections allows the circuit of Fig. 3.29b to be transformed into the circuit of Fig. 3.29e, which is specialized to the $N = 2$ case. We see that each pair of coupled line sections leads to an equivalent shunt LC resonator, and an admittance inverter occurs between each pair of LC resonators. Next, we show that the admittance inverters have the effect of transforming a shunt LC resonator into a series LC resonator, leading to the final equivalent circuit of Fig. 3.29f (shown for $N = 2$). This will then allow the admittance inverter constants, J_n , to be determined from the element values of a low-pass prototype. We will demonstrate this for the $N = 2$ case.

With reference to Fig. 3.29e, the admittance just to the right of the J_2 inverter is

$$j\omega C_2 + \frac{1}{j\omega L_2} + Z_0 J_3^2 = j \sqrt{\frac{C_2}{L_2}} \left(\frac{\omega}{\omega_0} - \frac{\omega_0}{\omega} \right) + Z_0 J_3^2$$

since the transformer scales the load admittance by the square of the turns ratio. Then the admittance seen at the input of the filter is

$$\begin{aligned} Y &= \frac{1}{J_1^2 Z_0^2} \left\{ j\omega C_1 + \frac{1}{j\omega L_1} + \frac{J_2^2}{j\sqrt{C_2/L_2} [(\omega/\omega_0) - (\omega_0/\omega)] + Z_0 J_3^2} \right\} \\ &= \frac{1}{J_1^2 Z_0^2} \left\{ j \sqrt{\frac{C_1}{L_1}} \left(\frac{\omega}{\omega_0} - \frac{\omega_0}{\omega} \right) + \frac{J_2^2}{j\sqrt{C_2/L_2} [(\omega/\omega_0) - (\omega_0/\omega)] + Z_0 J_3^2} \right\} \end{aligned} \quad (3.87)$$

These results also use the fact, from (3.85), that $L_n C_n = 1/\omega_0^2$ for all LC resonators.

Now the admittance seen looking into the circuit of Fig. 3.29f is

$$\begin{aligned} Y &= j\omega C'_1 + \frac{1}{j\omega L'_1} + \frac{1}{j\omega L'_2 + \frac{1}{j\omega C'_2} + Z_0} \\ &= j \sqrt{\frac{C'_1}{L'_1}} \left(\frac{\omega}{\omega_0} - \frac{\omega_0}{\omega} \right) + \frac{1}{j\sqrt{\omega L'_2 + 1/j\omega C'_2} + Z_0} \end{aligned} \quad (3.88)$$

which is identical in form to (3.87). Thus, the two circuits will be equivalent if the following conditions are met:

$$\frac{1}{J_1^2 Z_0^2} \sqrt{\frac{C_1}{L_1}} = \sqrt{\frac{C'_1}{L'_1}} \quad (3.89a)$$

$$\frac{J_1^2 Z_0^2}{J_2^2} \sqrt{\frac{C_2}{L_2}} = \sqrt{\frac{C'_2}{L'_2}} \quad (3.89b)$$

$$\frac{J_1^2 Z_0^3 J_3^2}{J_2^2} = Z_0 \quad (3.89c)$$

We know L_n and C_n from (3.85); L_n and C_n are determined from the element values of a lumped-element low-pass prototype that has been impedance scaled and frequency transformed to a bandpass filter. Now the impedance scaling formulas allows the L_n and C_n values to be written as

$$L'_1 = \frac{\Delta Z_0}{\omega_0 g_1} \quad (3.90a)$$

$$C'_1 = \frac{g_1}{\Delta Z_0 \omega_0} \quad (3.90b)$$

$$L'_2 = \frac{g_2 Z_0}{\Delta \omega_0} \quad (3.90c)$$

$$C'_2 = \frac{\Delta}{\omega_0 g_2 Z_0} \quad (3.90d)$$

where $\Delta = (\omega_2 - \omega_1)/\omega_0$ is the fractional bandwidth of the filter. Then (3.89) can be solved for the inverter constants with the following results (for $N = 2$):

$$J_1 Z_0 = \left(\frac{C_1 L'_1}{L_1 C'_1} \right)^{1/4} = \sqrt{\frac{\pi \Delta}{2 g_1}} \quad (3.91a)$$

$$J_2 Z_0 = J_1 Z_0^2 \left(\frac{C_2 C'_2}{L_2 L'_2} \right)^{1/4} = \frac{\pi \Delta}{2 \sqrt{g_1 g_2}} \quad (3.91b)$$

$$J_3 Z_0 = \frac{J_2}{J_1} \sqrt{\frac{\pi \Delta}{2 g_2}} \quad (3.91c)$$

After the J_n are found, Z_{0e} and Z_{0o} for each coupled line section can be calculated from (3.91) [51].

The above results were derived for the special case of $N = 2$ (three coupled line sections), but more general results can be derived for any number of sections, and for the case where $Z_L \neq Z_0$ (or $g_{N+1} \neq 1$, as in the case of an equal-ripple response with N even). Thus, the design equations for a bandpass filter with $N + 1$ coupled line sections are

$$Z_0 J_1 = \sqrt{\frac{\pi \Delta}{2g_1}}, \quad (3.92a)$$

$$Z_0 J_n = \frac{\pi \Delta}{2\sqrt{g_{n-1}g_n}} \quad \text{for } n = 2, 3, \dots, N, \quad (3.92b)$$

$$Z_0 J_{N+1} = \sqrt{\frac{\pi \Delta}{2g_N g_{N+1}}} \quad (3.92c)$$

Now we can calculate the admittance inverter constants, J_n with the help of these equations. Finally, the even- and odd-mode characteristic impedances can be found from (3.79).

3.13 Conclusions

In this chapter, the theory of the conventional filter and how the bandpass filter could be calculated were investigated. We have investigated on simple two port network and from there how to obtain simple filter. Then we have investigated on coupled line filter and we have obtained how couple lined can be used as bandpass filter. Then we have investigated on coupled line bandpass filter and found that how much critical they are for designing and calculating it.

Our main purpose of this thesis is to design new bandpass filter using electromagnetic bandgap structure to reduce the complexity of the calculations and design procedure. The design of bandpass filter using electromagnetic bandgap structure is chosen for simplify the designs and the procedures and optimize the amplitude response.

Chapter IV

Electromagnetic Bandgap Structure (EBGS)

4.1 Introduction

Electromagnetic band gap structures (EBGS) are periodic structures in which propagation of energy in certain bands of frequencies is prohibited. EBGS can be achieved by using metallic, dielectric, ferromagnetic or ferroelectric implants. Dielectric EBGS have been used in microstrip circuits. A number of studies have been carried out in EBG for microwave application, for example, by drilling a periodic pattern in the dielectric substrate, etching the periodic pattern in the ground plane or using sinusoidal variation of the characteristic impedance. They have wide band-pass and band-stop properties at microwave and millimeter-wave frequencies. For this characteristic they offer tremendous applications in active and passive devices. These applications are seen in filter designs, gratings, frequency selective surfaces (FSS), photonic crystals and photonic band gaps (PBG) etc. We classify them under the broad terminology of “Electromagnetic Band Gap (EBG)” structures. In the open microwave literature EBGS is also known as photonic bandgap structure (PBGS) or Defected ground structure (DGS). The perturbation in the ground plane of a structure is widely known as PBGS / EBGS / DGS. Generally speaking, electromagnetic band gap structures are defined as artificial periodic (or sometimes non-periodic) objects that prevent/assist the propagation of electromagnetic waves in a specified band of frequency for all incident angles and all polarization states. EBGS may be formed in the ground plane or over the substrate [55].

4.1.1 Classification of EBG Structures

The EBGS configuration is categorized as shown in Fig. 4.1. On the basis of dimension, PBG structures may be divided into 1-D, 2-D and 3-D PBGSs. Planar PBG structures and

their applications to antennas has been reported in [41]. Following are the descriptions of different PBG structures.

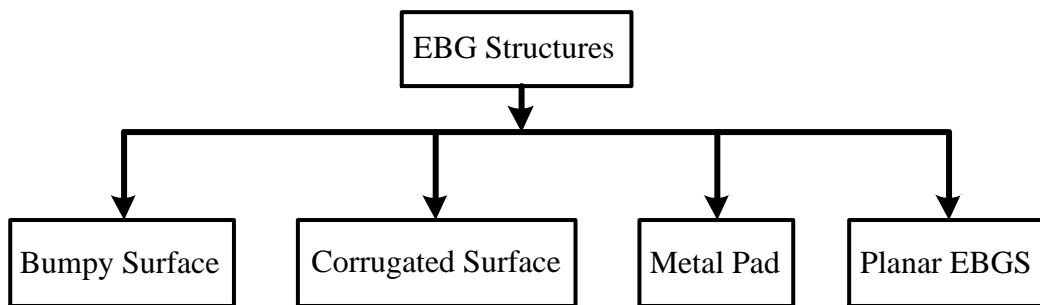


Fig. 4.1: Different EBG structures

❖ Bumpy Surface

Several configurations have been reported in the literature. The first structure is made by drilling a periodic pattern of holes in the substrate or etching a periodic pattern of circles in the ground plane. A bumpy metal sheet [32], [37] has a narrow surface wave band-gap. Electric field wraps around the bumps at the upper edge of the band gap and the electric field also extends across the bumps at the lower edge of the band-gap, hence a slow wave structure is formed. Bumpy surface is shown in Fig. 4.2.

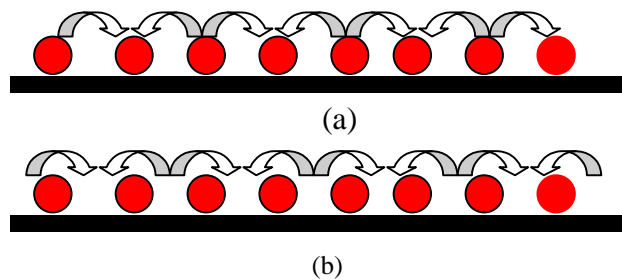


Fig. 4.2: Bumpy metal sheet: (a) electric field extends across the bumps and (b) electric field wraps around the bumps.

❖ Corrugated Surface

A corrugated surface [38]-[39] is a metal slab into which a series of vertical slots are cut. The slots are narrow so that many of them fit within one wavelength across the slab. Each slot can be regarded as a parallel plate transmission line, running down into the slab, and shorted at the bottom. If the slots are one quarter-wavelength deep, then the short circuit at

the bottom is transformed by the length of the slots into an open circuit at the top end. Thus the impedance at the top end is very high. In this situation the surface impedance is capacitive and transverse magnetic (TM) surface waves are forbidden. Furthermore, a plane wave polarized with the electric field perpendicular to the ridges will appear to be reflected with no phase reversal. Corrugated surface is shown in Fig. 4.3.

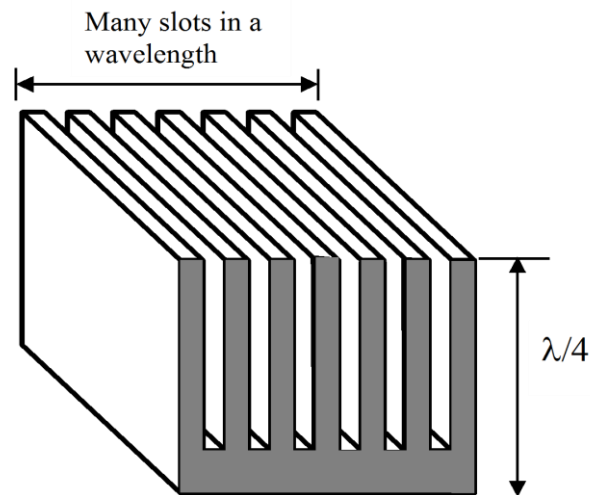


Fig. 4.3: Corrugated metal surface

❖ Metal Pad or High-Impedance Surface

A more effective and compact approach, compared to the corrugated surfaces, which makes use of a triangular or square lattice of metal pads connected to ground with vias, has been recently proposed and applied in [71] to enhance the gain of planar antennas.

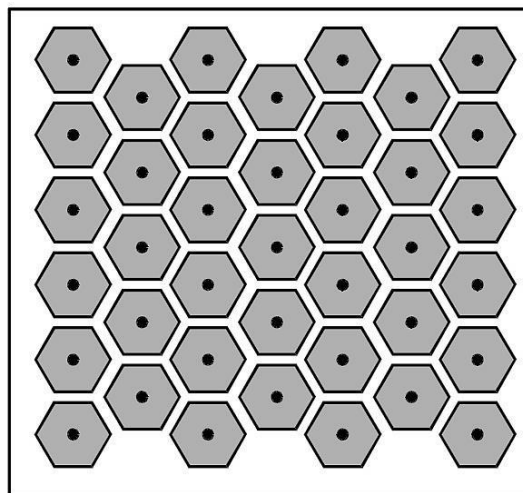


Fig. 4.4: Periodic metal connected to ground with via holes to yield high-impedance surface.

These structures are the first realization of planar compact electromagnetic crystals with a complete stop-band in the microwave range. This type of structure with a triangular lattice of hexagonal metal plates and square vias to ground is shown in Fig. 4.4.

❖ Planar PBG Structures

The planar periodic PBG structures are normally etched in the ground plane. They may be of different forms on the basis of lattice structures. The lattice structure may be square, triangular, rectangular and honeycomb etc. The shape of the unit cell may also be square, rectangular, circular, triangular and sinusoidal etc. Researchers are continuing to develop different PBG structures to obtain better performance.

Uni-planar compact photonic Bandgap structure (UC-PBGS) [72] is shown in Fig. 4.5. Planar slow wave structures and low-leaky conductor backed coplanar waveguides (CPW) using UC-PBGS have been recently presented. Vias are not used in a UC-PBGS.

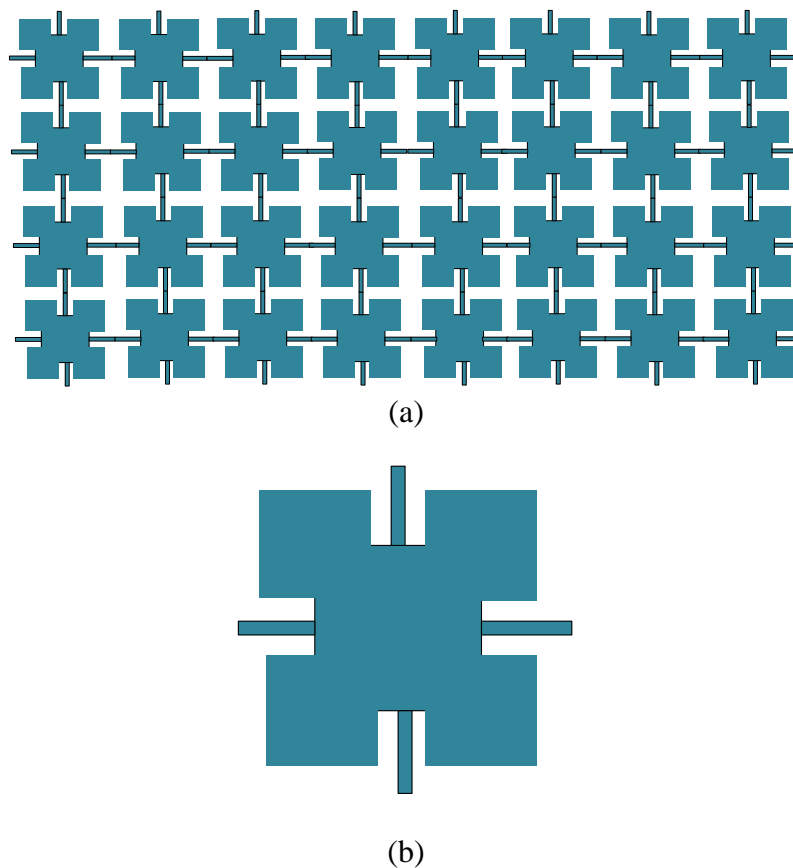


Fig. 4.5: (a) UC-PBG structure (b) Unit cell.

Advantages of this crystal are; simple, low-cost configuration and compatibility with MMIC photolithography. The UC-PBG structure, shown in Fig. 4.5, is a two-dimensional periodic lattice pattern on a dielectric substrate. The unit cell of the PBG lattice consists of square pads and narrow branches having inductive property, which is further, enhanced by the insets. The PBG structure forms a distributed LC network with a specific resonant frequency. At this frequency the periodic loading becomes an open circuit and an equivalent magnetic surface is created. Very recently a new simplified UC-PBGS in the form of square metal pads connected with thin lines has been proposed [73].

Few pictures are shown in this section to give a clear understanding about the lattice structures and shapes. Fig. 4.6 is a three dimensional view of a PBG engineered substrate. In the ground plane, uniform circular patterned PBG structures have been etched to realize an artificial (Photonic crystal) PC. This type of perturbation is truly responsible to generate unique characteristics. They provide stopband and passband that have many useful applications in microwave engineering. The radius of the circular slot is 'r' and the inter-

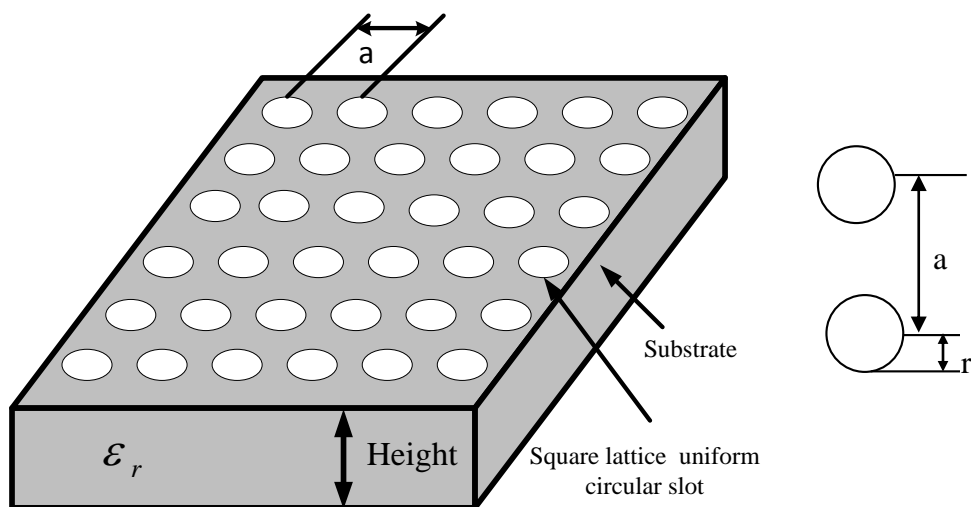


Fig. 4.6: Three-dimensional view of a substrate perturbed by uniform circular slots.

element distance is 'a'. One of the important factors in PBG structure design is known as filling factor (FF). In case of uniform circular slots, the FF is r/a that can be understood from the Fig. 4.6. If the slots are square having their sides to be 'b' then FF is b/a . Lattice structures and shapes influence the performance of the structures [23]. The substrate being

perturbed by triangular slots is shown in Fig. 4.7. In this figure, though the slots are triangular but their lattice structure is square having same distance along x and y direction.

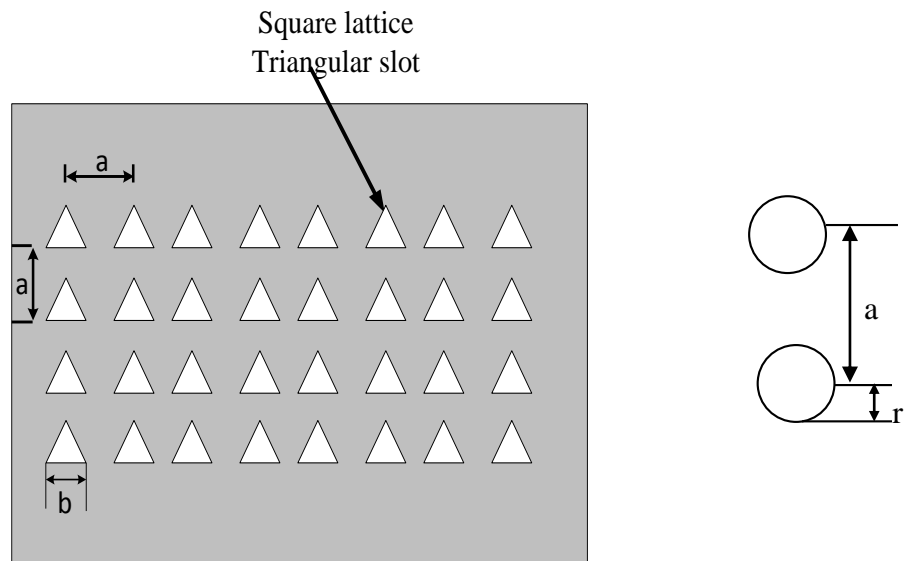


Fig. 4.7: Triangular slots with square lattice.

If the triangle is equilateral then FF for this structure is b/a as shown in Fig. 4.7; where 'b' is the length of the arm of the triangle and 'a' is the inter-cell separation. The substrate perturbed by square slots is shown in Fig. 4.8. It can be seen from the figure that the square is having the length of all sides of 'b' with inter-element spacing of 'a'. In this case the FF is also b/a .

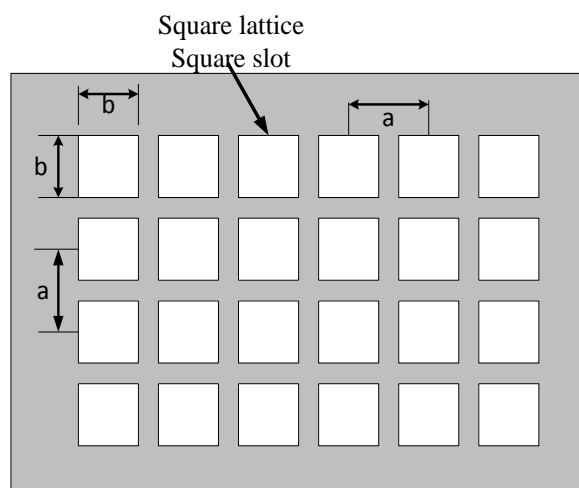


Fig. 4.8: The geometry of 2-D square slots having square lattice structure.

The uniform circular slots with different lattice structure are shown in below. It can be

same as Fig. 4.6. The only difference is their dimensions. Fig. 4.6 is 3-D while Fig. 4.9 is 2-D. The circular slots with triangular lattice arrangement are shown in Fig. 4.10. From this figure, it can be seen that their grids are in triangular form. But the period along the x direction is 'a' and along the y direction the slots rows maintain the same distance equal to period 'a'. It is suggested that triangular lattice can suppress the surface wave significantly. It is also encouraged to use non-equilateral triangular lattice for significant suppression of surface waves [74].

The lattice may be rectangular having different periods in x and y direction. This layout is more useful when PBGSs are required to design for dual band operations. Such geometry is proposed in VSAT antennas [40]. In VSAT antennas the dual band operations are needed for transmitting and receiving purposes.

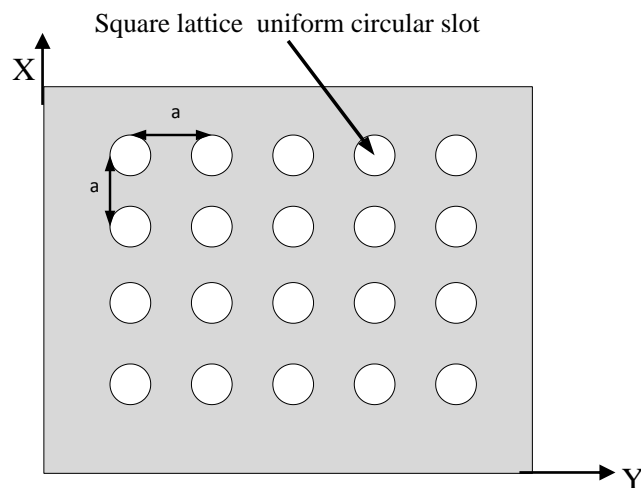


Fig. 4.9: 2-D geometry of a substrate having uniform circular slots with square lattice.

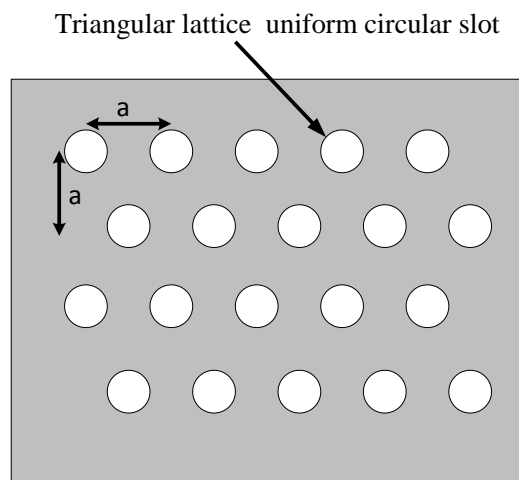


Fig. 4.10: Uniform circular slots with triangular lattice arrangement.

Normally conventional microstrip patch antenna operates at a single frequency. The PBGSs are designed at the operating frequency. So in case of single frequency the lattice structures may be square or triangular. But in dual band operations the frequencies determine different periods resulting in a rectangular lattice. Such geometry with rectangular lattice is shown in Fig. 4.11.

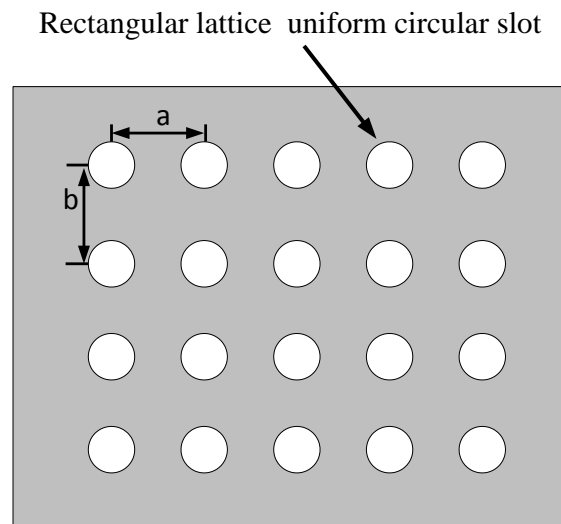


Fig. 4.11: Uniform circular slots with rectangular lattice.

4.1.2 Types of EBG Structures On The Basis of Dimensions

EBG structures are periodic in nature, which may be realized by drilling, cuffing, and etching on the metal or dielectric substrates. They may be formed in the ground plane or over the substrate. On the basis of dimensions EBG structures are categorized as one dimensional (1-D), two dimensional (2-D), and three dimensional (3-D) periodic structures that satisfies Bragg's conditions, i.e., inter-cell separation (period) is close to half guided wavelength ($\lambda_g/2$). They are capable of forbidding electromagnetic propagation in either all or selected directions [75] [76].

❖ 3-D EBG Crystals

In the beginning a 3D EBG was designed only. A successful attempt to obtain a 3D periodic dielectric structure was made in Iowa State University (ISU) [71]. It was called the woodpile structure as shown in the figure 4.8. Three dimensional EBG crystals have

periodicity along all the three dimensions and the remarkable feature is that these systems can have complete band gaps, therefore, that propagation states are not allowed in any direction [72]. Although, a perfect 3-D EBG structure is required to block all waves in all directions, but then these structures are difficult to fabricate and integrate. From the literature, we learned that 2-D EBG could be even more valuable. 2-D EBG structures are easy to fabricate and are capable of maintaining a similar control on the wave propagation in the structure as the 3-D structure.

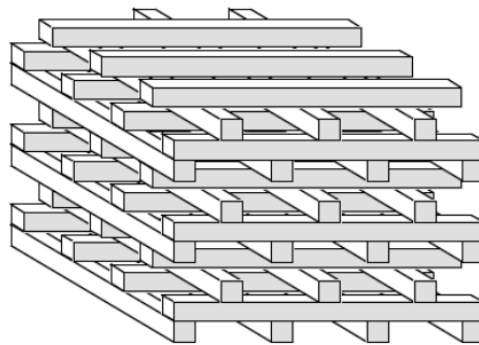


Fig. 4.12: Three dimensional EBG structure [71]

❖ 2-D EBG Crystals

These crystals have periodicity in two dimensions and are homogeneous along the third direction, or we can say that, all variations happen in the two dimensions, whereas everything is constant along the third dimension, thereby propagation is allowed along one axis of the crystal [71]. These 2-D EBG structures have substantial advantages in terms of compactness, stability, and fabrication, which make them more attractive for microwave devices [72]. One of the greatest advances in the development of these 2-D EBG structures in microwave range has been their implementation in microstrip technology.

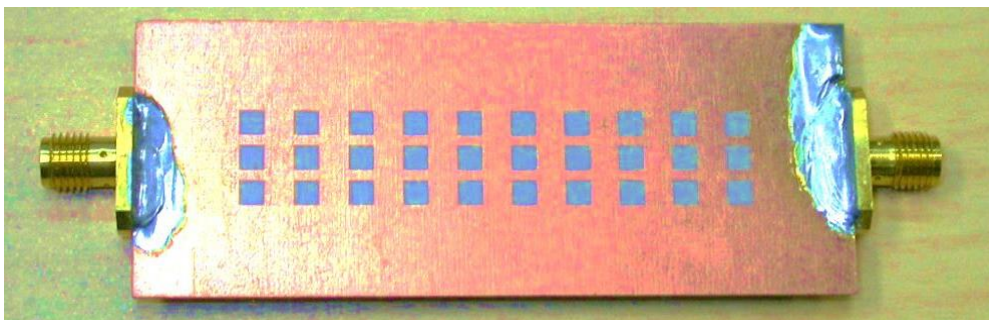


Fig. 4.13 Two dimensional EBG structure [63].

❖ 1-D EBG Crystals

One dimensional EBG structures can also be implemented in microstrip technology. 1-D EBG structures have periodicity of two different media along one direction only. These basic crystals exhibit three important phenomena: photonic band gaps, localized modes, and surface states. However, as the index contrast is only along one direction, the band gaps and bound states are limited to that direction. Nevertheless, these simple structures show most of the features of 2-D and 3-D EBG crystals [77].

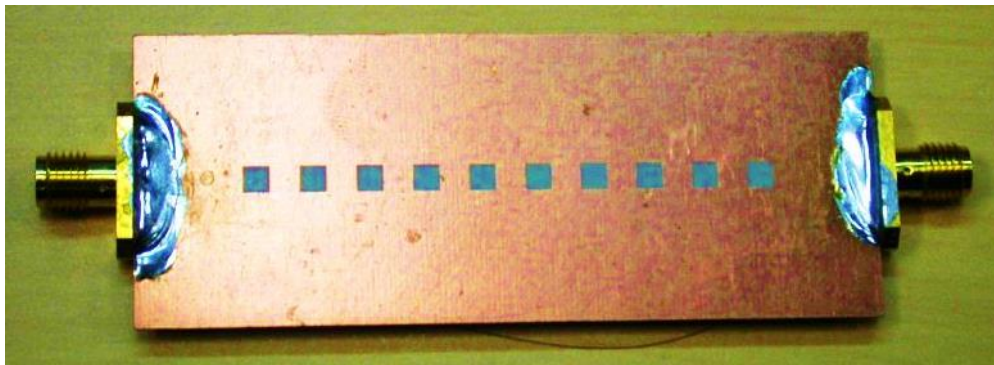


Fig. 4.14 One dimensional EBG structure [55].

4.2 Microstrip Lines

The Microstrip line is a one type of electrical transmission line which belongs to parallel plate Transmission line and can be fabricated using printed circuit board technology. It is used to convey microwave-frequency signals. It consists of a single ground plane and an open strip conductor separated by a dielectric substrate. Microwave components such as antennas, couplers, resonators, filters, power dividers, filters phase shifters, etc. can be formed from microstrip structure.

4.2.1 Microstrip Structure

The general structure of a microstrip structure is illustrated in Figure 4.15. A conducting strip (microstrip line) with a width W and a thickness t is on the top of a dielectric substrate that has a relative dielectric constant ϵ_r and a thickness h , and the bottom of the substrate is a ground (conducting) plane.

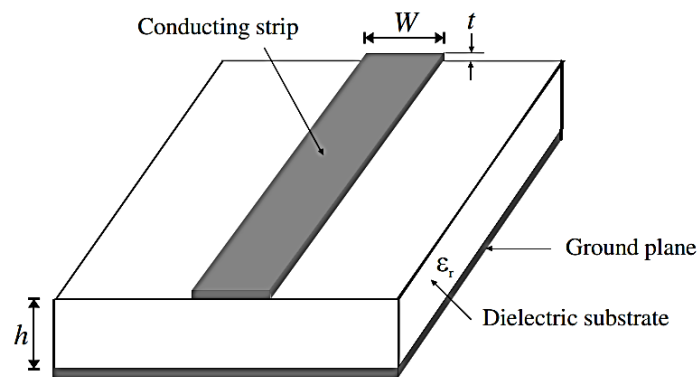


Fig. 4.15: General microstrip structure.

4.2.2 Waves in Microstrips Line

The fields in the microstrip extend within two media air above and dielectric below so that the structure is inhomogeneous. Due to this inhomogeneous nature, the microstrip does not support a pure TEM wave. This is because that a pure TEM wave has only transverse components, and its propagation velocity depends only on the material properties, namely the permittivity ϵ and the permeability μ . However, with the presence of the two guided-wave media (the dielectric substrate and the air), the waves in a microstrip line will have no vanished longitudinal components of electric and magnetic fields, and their propagation velocities will depend not only on the material properties, but also on the physical dimensions of the microstrip.

4.2.3 Microstrip Lines

The microstrip belongs to the group of parallel plate transmission line consist of a single ground plane and an open strip conductor separated by a dielectric substrate. Figure 4.16 shows the most commonly used microstrip transmission line for microwave integrated circuits. This line is the major component for making a filter. The electromagnetic field in the microstrip line is not confined only to the dielectric because of the fringing; the effective relative permittivity ϵ_{eff} is less than the relative permittivity ϵ_r of the substrate. The electromagnetic waves in microstrip propagate in TEM (transverse electric magnetic) mode, which is characterized by electric and magnetic field that exists only in the plane perpendicular to the axis of the propagation.

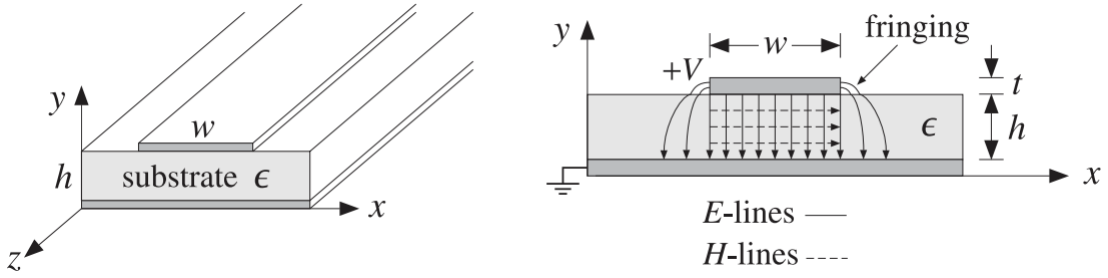


Fig. 4.16: A microstrip transmission line.

Practical microstrip lines, shown in Figure 4.16, have width-to-height ratios w/h that are not necessarily much greater than unity, and can vary over the interval $0.1 < w/h < 10$. Typical heights h are of the order of millimeters.

Fringing effects cannot be ignored completely and the simple assumptions about the fields of the parallel plate line are not valid. For example, assuming a propagating wave in the z -direction with z, t dependence of $e^{j\omega t - j\beta z}$ with a common β in the dielectric and air, the longitudinal-transverse decomposition gives:

$$\nabla_T \times E_Z \times \hat{z} - j\beta \hat{z} \times E_T = -j\omega \mu H_T$$

In particular, we have for the x -component:

$$\partial_y E_Z + j\beta E_y = -j\omega \mu H_x$$

The boundary conditions require that the components H_x and $D_y = \epsilon E_y$ continuous across the dielectric-air interface (at $y = h$). This gives the interface conditions:

$$\begin{aligned} \partial_y E_Z^{air} + j\beta E_y^{air} &= \partial_y E_Z^{diel} + j\beta E_y^{diel} \\ \epsilon_0 E_y^{air} &= \epsilon E_y^{diel} \end{aligned}$$

Combining the two conditions, we obtain:

$$\partial_y (E_Z^{diel} - E_Z^{air}) = j\beta \frac{\epsilon - \epsilon_0}{\epsilon} E_y^{air} = j\beta \frac{\epsilon - \epsilon_0}{\epsilon} E_y^{diel} \quad (4.1)$$

Because E_y is non-zero on either side of the interface, it follows that the left-hand side of Eq. (4.1) cannot be zero and the wave cannot be assumed to be strictly TEM. However, E_y is small in both the air and the dielectric in the fringing regions (to the left and right of the upper conductor). This gives rise to the so-called *quasi-TEM approximation* in which the

fields are assumed to be approximately TEM and the effect of the deviation from TEM is taken into account by empirical formulas for the line impedance and velocity factor.

In particular, the air-dielectric interface is replaced by an effective dielectric, filling uniformly the entire space, and in which there would be a TEM propagating mode. If we denote by ϵ_{eff} the relative permittivity of the effective dielectric, the wavelength and velocity factor of the line will be given in terms of their free-space values λ_0, c_0 :

$$\lambda = \frac{\lambda_0}{\sqrt{\epsilon_{eff}}}, \quad c = \frac{c_0}{\sqrt{\epsilon_{eff}}} \quad (4.2)$$

There exist many empirical formulas for the characteristic impedance of the line and the effective dielectric constant. Hammerstad and Jensen's are some of the most accurate ones:

$$\epsilon_{eff} = \frac{\epsilon_r + 1}{2} + \frac{\epsilon_r - 1}{2} \left(1 + \frac{10}{u}\right)^{-ab}, \quad u = \frac{w}{h} \quad (4.3)$$

Where, $\epsilon_r = \epsilon/\epsilon_0$ is the relative permittivity of the dielectric and the quantities a, b are defined by:

$$a = 1 + \frac{1}{49} \ln \left[\frac{u^4 + \left(\frac{u}{52}\right)^2}{u^4 + 0.432} \right] + \frac{1}{18.7} \ln \left[1 + \left(\frac{u}{18.1}\right)^3 \right]$$

$$b = 0.564 \left(\frac{\epsilon_r - 0.9}{\epsilon_r + 3} \right)^{0.053}$$

The accuracy of these formulas is better than 0.01% for $u < 1$ and 0.03% for $u < 1000$. Similarly, the characteristic impedance is given by the empirical formula:

$$Z = \frac{\eta_0}{2\pi\sqrt{\epsilon_{eff}}} \ln \left[\frac{f(u)}{u} + \sqrt{1 + \frac{4}{u^2}} \right] \quad (4.4)$$

Where, $\eta_0 = \sqrt{\mu_0/\epsilon_0}$ and the function f (u) is defined by:

$$f(u) = 6 + (2\pi - 6) \exp \left[- \left(\frac{30.666}{u} \right)^{0.7528} \right]$$

The accuracy is better than 0.2% for $0.1 \leq u \leq 100$ and $\epsilon_r < 128$. In the limit of large ratio w/h or $u \rightarrow \infty$, Equations (4.3) and (4.4) tend to those of the parallel plate line of the

previous section:

$$\epsilon_{eff} \rightarrow \epsilon_r, \quad Z \rightarrow \frac{\eta_0}{\sqrt{\epsilon_r}} \frac{h}{w} = \eta \frac{h}{w}$$

Some typical substrate dielectric materials used in microstrip lines are alumina, a ceramic form of Al_2O_3 with $\epsilon_r = 9.8$, and RT-Duroid, a Teflon composite material with $\epsilon_r = 2.2$. Practical values of the width-to-height ratios are in the range $0.1 \leq w/h \leq 10$ and practical values of characteristic impedances are between 10–200 ohm but in this literature I have used transmission line of 50 ohm characteristic impedance and Taconic substrate with $\epsilon_r = 2.45$. Fig. 4.17 shows the dependence of Z and ϵ_{eff} on w/h for the two cases of $\epsilon_r = 2.2$ and $\epsilon_r = 9.8$.

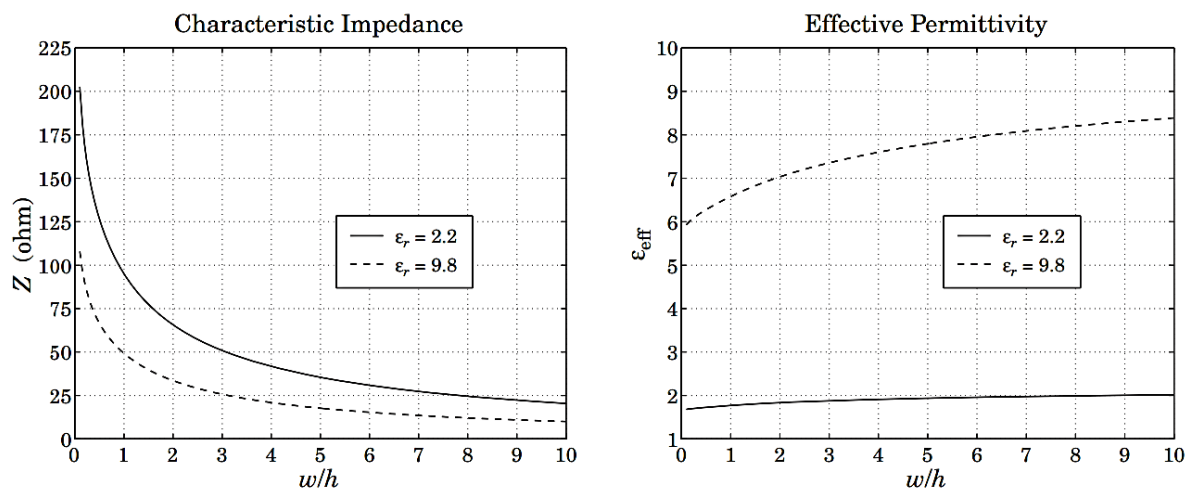


Fig. 4.17: Characteristic impedance and effective permittivity of microstrip line.

4.3 Analysis methods for EBG structures

To analyze unique features of EBG structures, various methods have been implemented. These methods can be put into three categories:

- (1) Lumped element model,
- (2) Periodic transmission line method, and
- (3) Full wave numerical methods.

The lumped element model is the simplest one that describes the EBG structure as an LC resonant circuit [67], as shown in Figure 4.18. The values of the inductance L and capacitance C are determined by the EBG geometry and its resonance behavior is used to

explain the band gap feature of the EBG structure. This model is simple to understand, but the results are not very accurate because of the simplified approximation of L and C .

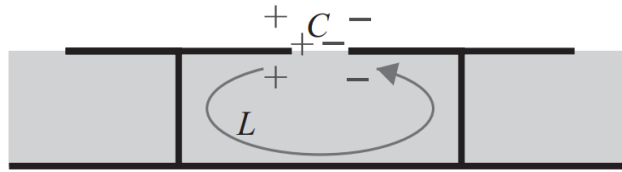


Fig. 4.18: Lumped LC model for EBG analysis.

The periodic transmission line method is another popularly used technique to analyze EBG structures [51]. Figure 4.19 depicts a transmission line model of EBG structures, where Z_P is the impedance for each periodic element and X_C is the coupling capacitor. The

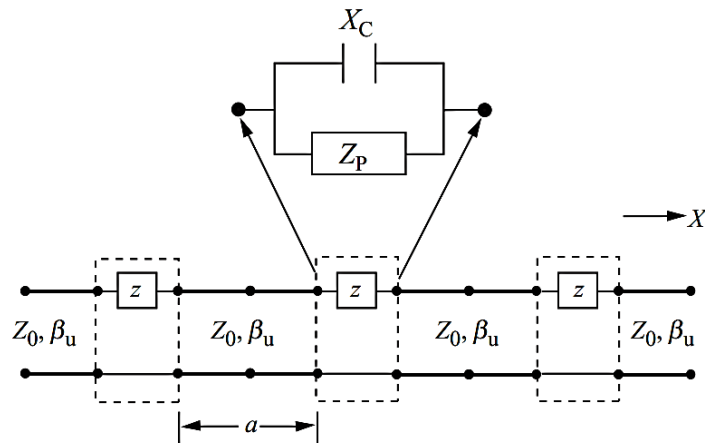


Fig. 4.19: Periodic transmission line method for EBG analysis [51].

Floquet periodic boundary condition is considered in this approach. After analyzing the cascaded transmission line, the dispersion curve can be readily obtained, which provides more information than the lumped element method. The surface wave modes, leaky wave modes, left- and right-hand regions, and band gaps can be easily identified from the curve. However, a difficulty in this method is how to accurately obtain the equivalent Z_P and X_C values for the EBG structures.

4.4 Defected Ground Structure

Defected ground structure (DGS) is an etched periodic or non-periodic cascade configuration defect in ground of a planar transmission line (e.g. microstrip, coplanar and

conductor backed coplanar waveguide) which disturbs the shield current distribution in the ground plane cause of the defect in the ground. This disturbance will change the characteristics of the transmission line such as line capacitance and inductance. In a word, any defect etched in the ground plane of the microstrip can give rise to increasing effective capacitance and inductance [2].

4.4.1 Uniform PBG (UPBG) Configurations Applied To Microstrip Lines

In modern microwave devices, microstrip transmission lines are most common. Therefore, in the following sections, the investigation is concentrated into only on PBG assisted microstrip transmission line. To derive the characteristic performance of PBG assisted lines it is more logical to use scattering parameters (S-parameters) instead of showing K- β diagram. S-parameters are universally accepted format of device characterizations. Moreover, commercially available software tool Zealand IE3D will be used to design and to extract S-parameters for all designs due to the flexibility of Zealand IE3D. Zealand IE3D is a method of moment (MOM) based full-wave analysis tool, hence very accurate.

The perturbation in the ground plane of any microstrip transmission line in the form of PBGS creates stopband that is useful for suppression of surface waves, leakage, and spurious transmission and to improve the performance of antennas, filter and other microwave devices and components. The stopband characteristic is highly influenced by the shape, size and the period of the PBGSs located on the ground plane. Therefore, it is useful to see the performance of the standard 50-ohm microstrip transmission line on PBGSs. The lines will be investigated to see the performance of three rows of uniform PBG structure as [22]. In this section, uniform circular and square patterned PBGS will be investigated. It is well known that the EM field is highly concentrated under the microstrip line. Under this consideration, one dimensional (1-D) uniform PBGS (one line) will be investigated and compared the result with 2-D structure (three lines). Finally 1-D PBGS will be used as two structures yield similar performances.

4.4.2 Dumbbell Shaped Defected Ground Structures (DGS)

The center frequency of the stopband of a PBG is approximately calculated by well-known

formula of Bragg's condition. Using this formula, the period for any stopband frequency can be determined. The theory of DGS is different from PBGS. At DGS, the dimensions of the dumbbell shaped slot (DGS unit cell) control the current paths on the ground plane hence the equivalent inductance and capacitance of the ground. Figure 4.20 shows the unit cell of a dumbbell shaped DGS. It is composed of two larger slots connected by a narrow vertical slot. The larger slot is a square patterned PBG element. On the other hand narrower vertical slot is a rectangular patterned PBG element.

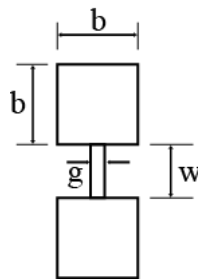


Fig. 4.20: Geometry of a unit cell of a dumbbell shape DGS. The arm length of a larger square patterned slot is 'b'. The vertical rectangular slot has width, w and gap g.

The unit cell is etched in the ground plane of a standard 50 ohm transmission line. In order to investigate the frequency characteristics of the unit DGS cell, few structures having different 'b' and 'g' are simulated. All simulation results in one-pole LPF characteristics, which is obvious. There are two frequency properties; one is pole location, another is the existence of cut-off frequencies. Employing DGS section increases the effective permittivity and hence effective inductance. The cut-off frequency is mainly dependent on the etched larger square patterned slot that depends on the value of 'b'. The pole location mainly depends on the gap distance 'g'. Two parameters 'b' and 'g' are studied to observe the frequency characteristics. The lumped LC equivalent model can be expressed as [78]:

$$C = \frac{\omega_c}{Z_0 g_1} \left[\frac{1}{\omega_0^2 - \omega_c^2} \right]$$

$$L = \frac{1}{4\pi^2 f_0 C}$$

Where, f_0 is the frequency of the attenuation pole, ω_c is the angular cutoff frequency, Z_0 is the characteristic impedance of the line, and g_1 is the admittance value of the Butterworth low pass filter response.

The equivalent circuit of dumbbell shaped DGS unit cell is shown in Figure 4.21.

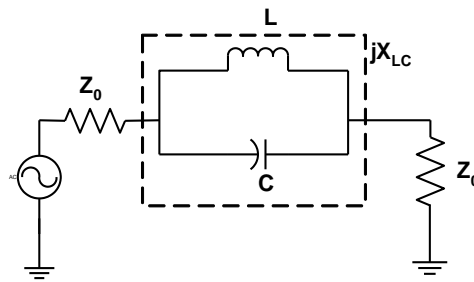


Fig. 4.21: The equivalent circuit of dumbbell shaped DGS unit.

4.5 Design of Microstrip Transmission Line over Uniform PBGS (uniform circular PBGS)

With the inclusion of PBGSs the dispersion characteristics of a transmission line change. At first a microstrip transmission line with unperturbed ground plane is designed that does not provide any stopband characteristics. Then the effect is observed on the dispersion characteristics in the form of scattering parameters matrices versus frequency by perturbing the ground plane with uniform circular PBGSs.

4.5.1 Designing Equation

In the PBG engineering it is a conventional rule to use Bragg's condition [19] to calculate the central stopband frequency provided by PBGSs. Under this condition, inter-cell separation (known as period) is approximately equal to half wavelength of the stopband central frequency. From the inter-cell separation, the size of the PBG element is calculated on the basis of Filing factor (FF).

The geometry of the design is patterned under 50 ohm transmission line are designed by using "Taconic Substrate" in which relative dielectric constant $\epsilon_r = 2.45$, Thickness, $h=31\text{mil}$ or 0.787mm . Using Personal Computer Aided Antenna Design 5.0 (PCAAD) software the values of transmission line width, $w = 0.2263\text{ cm}$ and effective dielectric constant, $\epsilon_{eff} = 2.068$ has been found.

We know that,

$$\lambda_0 = \frac{300 \text{ (mm)}}{f_c \text{ (GHz)}}$$

$$\lambda_g = \frac{\lambda_0}{\sqrt{\epsilon_{eff}}}$$

$$a = \frac{\lambda_g}{2}$$

For, $f_c = 10 \text{ GHz}$

$$\lambda_0 = \frac{300}{10} = 30 \text{ mm}$$

$$\lambda_g = \frac{\lambda_0}{\sqrt{\epsilon_{eff}}} = \frac{30}{2.068} = 20.86 \text{ mm}$$

Now,

$$a = \frac{\lambda_g}{2} = \frac{20.86}{2} = 10.43 \text{ mm}$$

Filing Factor, $FF = \frac{r}{a}$

Where, r = radius of circular PBGS, a = inter-element spacing.

The center frequency of the stopband is calculated approximately with the following expression:

$$\beta a = \pi$$

Where, a is the period of the PBG pattern, and β is the wave number in the dielectric slab and is defined by this expression:

$$\beta = \frac{2\pi f_0}{c} \sqrt{\epsilon_{eff}}$$

Where,

f_0 = the center frequency of the stopband

ϵ_{eff} = the effective relative permittivity of the dielectric slab

c = the speed of light in free space

4.5.2 Designs of Uniform Circular PBGSs

The following different microstrip transmission lines are designed. All the PBGSs are designed at the stopband central frequency of 10 GHz.

1. Standard 50-ohm transmission line: In this case there is no perturbation in the ground plane. A standard 50 ohm line is realized on Taconic substrate having width of 0.5957, dielectric constant of 10.2 and height of 25 mils.

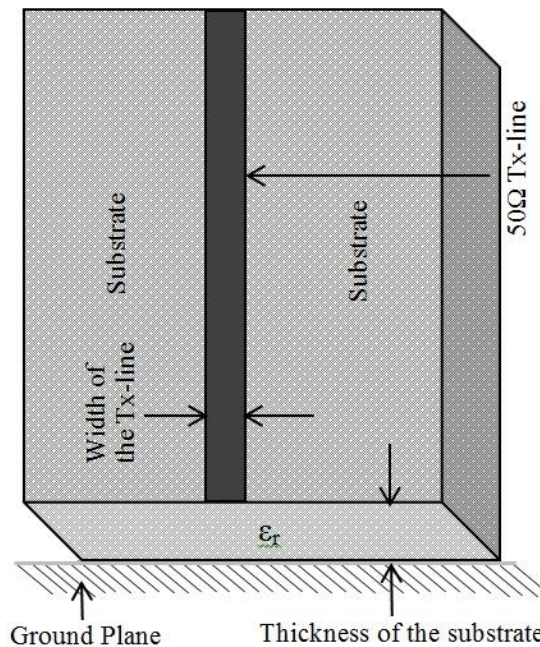


Fig. 4.22: Geometry of a standard 50Ω Tx-line

2. 2-D uniform circular elements in the ground plane: Here three PBG structures under 50 ohm transmission lines with FF of 0.125, 0.25 and 0.45 are designed to produce the same result of [23]. This design gives the idea of optimum value of FF to be 0.25. The geometry of a three rows (2-D) uniform hole patterned PBGSs in the ground plane of a 50 ohm transmission line is shown in Figure 4.23.

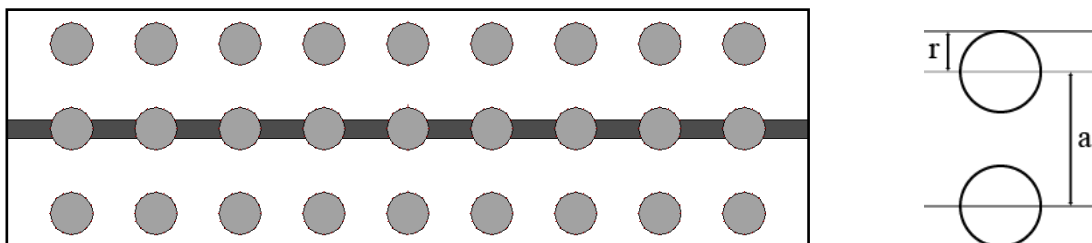


Fig. 4.23: (a) Geometry of a 50-ohm microstrip transmission line where 2-D (three lines) uniform circular PBGSs are etched in the ground plane. (b) The filling factor (FF) explanation ($FF = r/a$).

3. 1-D uniform circular PBGSs with FF of 0.25: This design will yield the performance to consider 1-D PBGSs that replace 2-D PBGSs. The geometry of 1-D uniform hole patterned PBGSs is shown in Figure 4.24. In this design only one row of PBG elements are etched in the ground plane just under the 50 ohm transmission line.

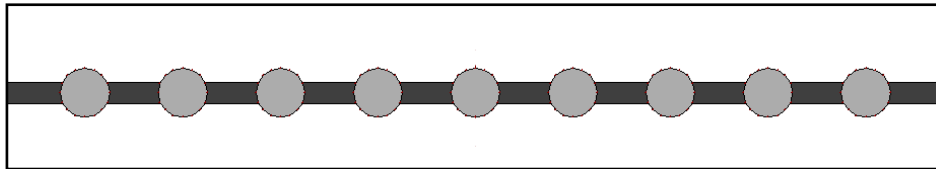


Fig. 4.24: Geometry of a standard 50-ohm transmission line with 1-D uniform circular PBGSs etched in the ground plane.

4.5.3 Designs of Uniform Square Patterned PBGSs

Uniform square patterned PBGSs will also be designed. Here three rows and one row PBGSs will be designed and their performances will be compared. It will be useful to replace three rows PBGSs by 1-D PBGSs. On the basis of the availability of the materials for the fabrications Taconic substrate with $\epsilon_r = 2.45$ and height (h) = 31 mils is used in the simulation.

1. 2-D Uniform Square Patterned PBGSs: The conventional uniform square patterned PBGSs are shown in Figure 4.25. Three lines of total 27 PBG elements are etched under the standard 50-ohm transmission line. The FF is taken to be 0.5.

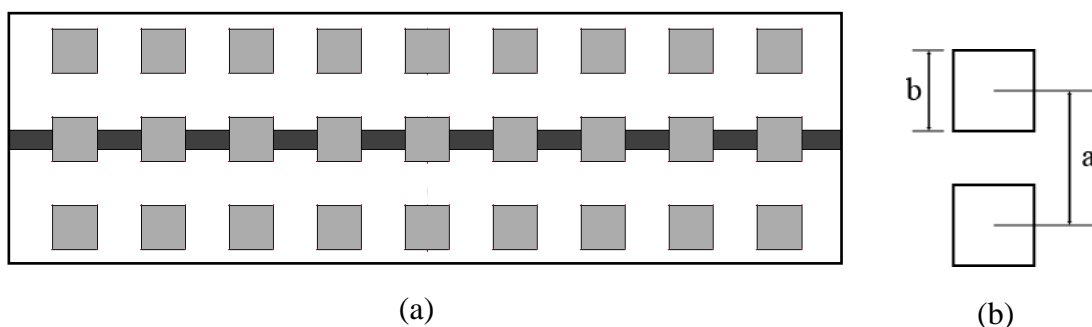


Fig. 4.25: 2-D (three lines) of square patterned PBGSs under standard 50 ohm transmission line. Substrates: $\epsilon_r = 2.45$ and height (h) = 31 mils and $\tan\delta = 0.002$. The inter-element spacing, $a = 10.43$ mm, element width and length, $b = 5.215$ mm.

2. 1-D square patterned PBGSs: The geometry of 1-D (one line) circular patterned PBGSs is shown in Fig. 4.26. Here only 9 PBG elements are etched in the ground plane.

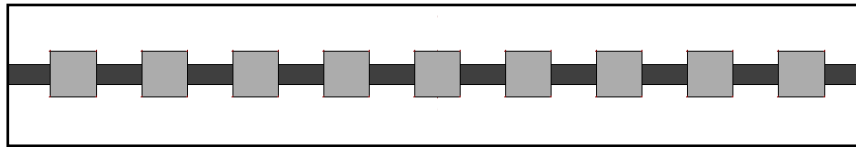


Fig. 4.26: 1-D square patterned periodic structures under standard 50-ohm transmission line. The substrate is Taconic having dielectric constant of 2.45 and height of 31 mils. The inter-element spacing, $a = 10.43$ mm, element width and length, $b = 5.215$ mm.

4.5.4 Designs of Dumbbell shaped Defected Ground Structures (DGSs)

Dumbbell shaped DGSs will also be designed. Here one row dumbbell shaped DGSs will be designed. On the basis of the availability of the materials for the fabrications Taconic substrate with $\epsilon_r = 2.45$ and height (h) = 31 mils is used in the simulation. The bigger slot dimension is 205×205 mil or (5.21×5.21 mm) and narrow slot dimension is 50×200 mil or (1.27×5.08 mm)

1-D Dumbbell shaped DGSs: The geometry of 1-D (one line) Dumbbell shaped DGSs is shown in Fig. 4.27. Here only 9 DGS elements are etched in the ground plane.

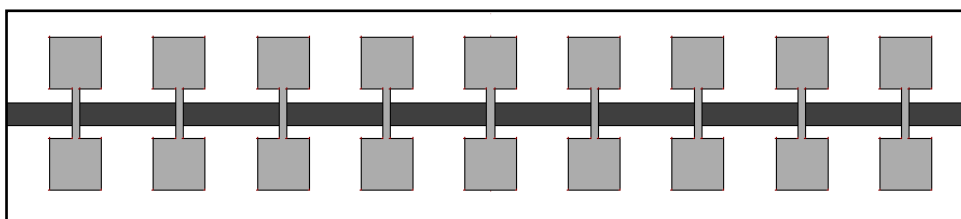


Fig. 4.27: 1-D Dumbbell shaped DGSs patterned periodic structures under standard 50-ohm transmission line. The substrate is Taconic having dielectric constant of 2.45 and height of 31 mils. The inter-element spacing, $a = 10.43$ mm, element width and length, $b = 5.215$ mm.

4.6 Simulated S-parameter Performances

An ideal transmission line as well as transmission lines having circular and square

patterned uniform PBGSs in the ground plane have been investigated. The performances have been analyzed of the lines in terms of 10 dB return loss bandwidth, 20 dB rejection bands, ripple heights in passband, the depth of the stopband and maximum value of return loss. The S-parameters of the designs have been investigated to conceive the idea of 1-D PBGSs in lieu of 2-D PBGSs, optimized FF and the influence of number of PBGSs on the dispersion characteristics of the microstrip transmission line. The Taconic substrate is used in the simulation for the ideal and uniform structured PBGSs.

1. Standard 50-ohm transmission line: The simulated S-parameters performances of an ideal transmission line are shown in Fig. 4.28. The insertion loss is approximately zero dB throughout the whole frequency range from 0 to 25 GHz.

It can be seen from the graph that the signal is being transmitted between two ports of transmission line with negligible loss. Therefore, within the whole range of frequencies (0-14 GHz) there is no stopband. The return loss performance of the ideal microstrip line over the whole frequency range is also excellent and >10 dB. Obviously the S-parameters performance shown in Figure 4.28 characterizes an ideal transmission line.

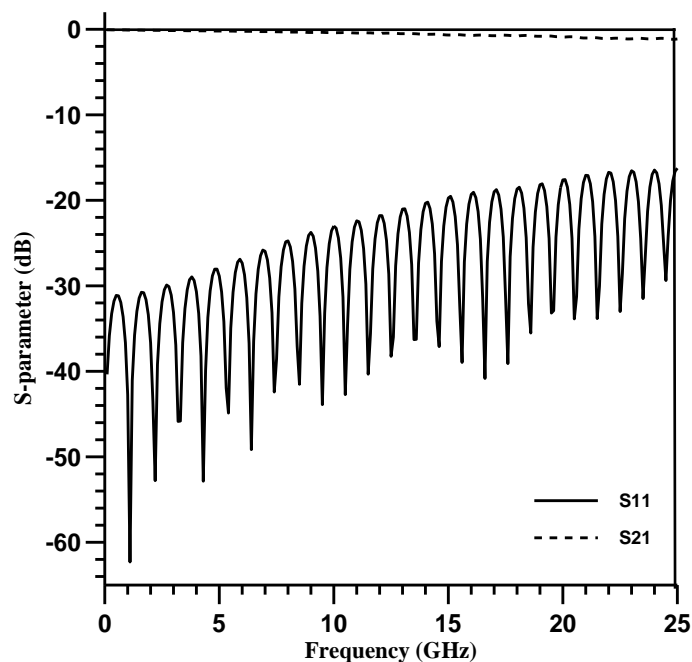


Fig. 4.28: IE3D simulated S-parameters versus frequency of an ideal 50-ohm transmission line. The substrate is Taconic having height of 31 mils and the dielectric constant is 2.45

2. The Transmission Line with 2-D (three lines) Uniform Circular PBGS: At first, small uniform and circular holes have been introduced in the ground plane to observe their effects on the performance of a standard 50 ohm transmission line. The radius of the uniform circular PBGSs are 2.6075 mm and the period is 10.43 mm. The S-parameters performance is shown in Fig. 4.29.

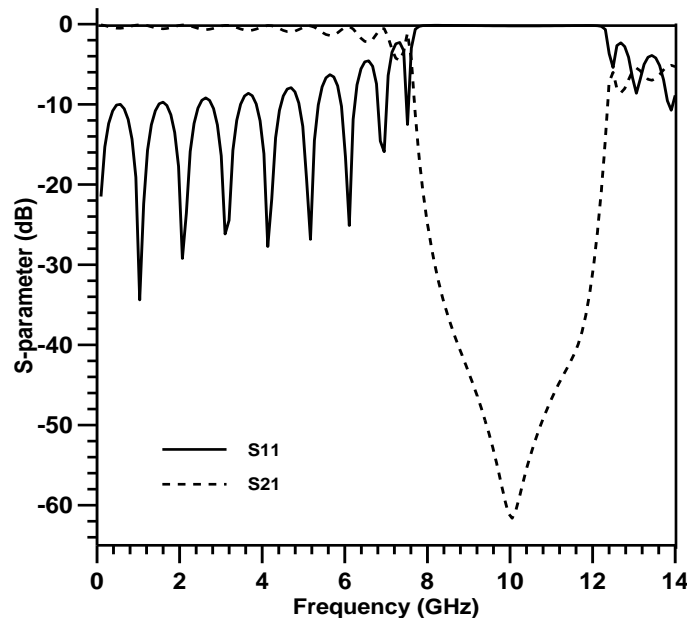


Fig. 4.29: Simulated S-parameter performances of a standard 50- ohm transmission line perturbed by 2-D (three lines) uniform circular PBGSs in the ground plane. The substrate is Taconic having height of 31 mils and dielectric constant of 2.45. The uniform circular PBGSs are of 2.6075 mm and the period is 10.43 mm (FF=0.25).

It can be seen from the figure that this design provides wider passband and deeper stopband. The 10 dB return loss bandwidth is found to be 6.31 GHz; the 20 dB rejection bandwidth is 4.35 GHz. The ripple height along the passband is negligible. But around cut-off frequencies ripples are observed. The center frequency is found to be shifted around 10.06 GHz, resulting in 1% frequency deviations from the design frequency. The maximum value of isolation is found to be -61.6 dB.

3. The Transmission Line with 1-D Uniform Circular PBGSs: It is mentioned that 0.25 is the optimum FF for Taconic with dielectric constant of 2.45 and height of 31 mils. Based on this value a microstrip transmission line with 1-D uniform circular PBGSs has also been investigated. The simulation result is shown in Fig. 4.30.

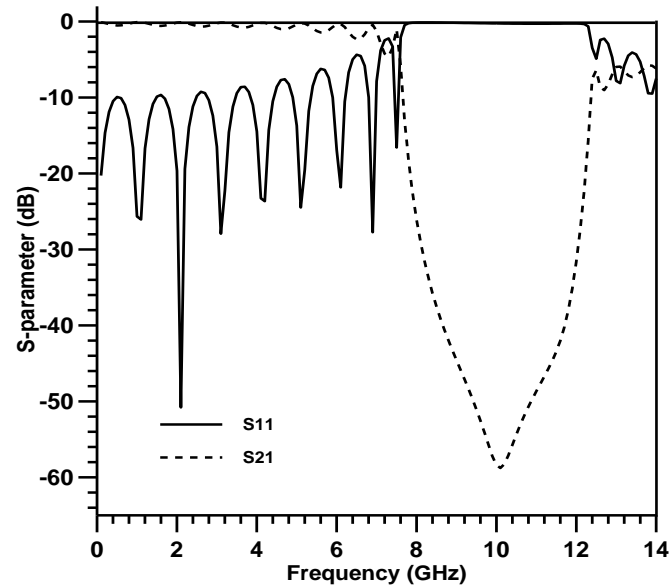


Fig. 4.30: Simulated S-parameter performances of a standard 50 ohm transmission line perturbed by 1-D (one line) uniform circular PBGSs in the ground plane.

From the Fig. 4.30, it can be seen that return loss performance, stopband characteristics and ripple height for this design is similar as 2-D design. A negligible difference in the value of maximum isolation is observed. In the case of three rows of uniform circular PBGSs the maximum isolation is found to be approximately -61.6 dB. On the other hand, one row of uniform circular PBGS provides approximately -61.46 dB

From this figures (Figure 4.29 and 4.30) it is very clear that 1-D PBGSs and 2-D PBGSs provide very similar performances.

4. The Transmission Line with 2-D Uniform rectangular PBGSs: The S-parameters performances of uniform square patterned PBGSs have also been analyzed. The simulated and measured S-parameters performances of three lines (2-D) uniform square patterned PBGSs are shown in Fig. 4.31.

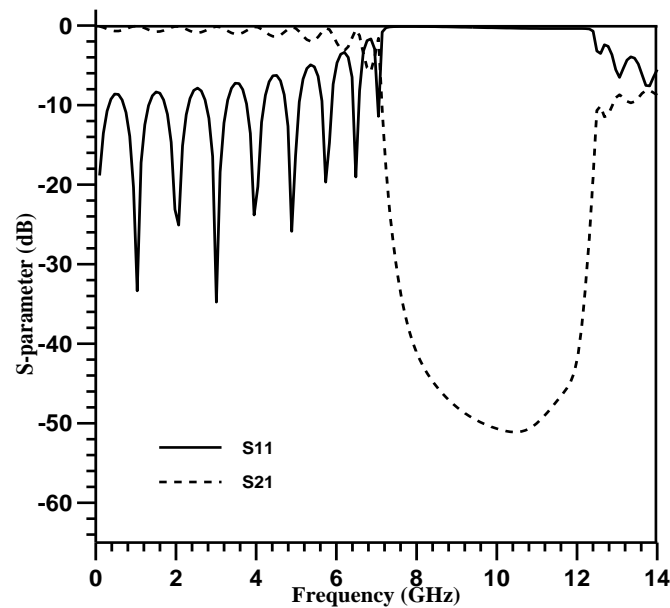


Fig. 4.31: S-parameters performances of three lines uniform square-patterned PBG structures. The substrate is Taconic having dielectric constant of 2.45 and height of 31 mils. The inter-element spacing is 10.43 mm and FF is 0.50.

At first, small uniform and rectangular holes have been introduced in the ground plane to observe their effects on the performance of a standard 50 ohm transmission line. The both length of the uniform rectangular PBGSs are 5.215 mm and the period is 10.43 mm.

It can be seen from the figure that this design provides wider passband and deeper stopband. The 20 dB rejection bandwidth is 5.12 GHz. The ripple height along the passband is negligible. But around cut-off frequencies ripples are observed. The center frequency is found to be shifted around 10.41 GHz, resulting in 4% frequency deviations from the design frequency. The maximum value of isolation is found to be 51.1 dB.

5. The Transmission Line with 1-D Uniform rectangular PBGSs: It is mentioned that 0.5 is the optimum FF for Taconic with dielectric constant of 2.45 and height of 31 mils. Based on this value a microstrip transmission line with 1-D uniform rectangular PBGSs has also been investigated. The simulation result is shown in Fig. 4.32.

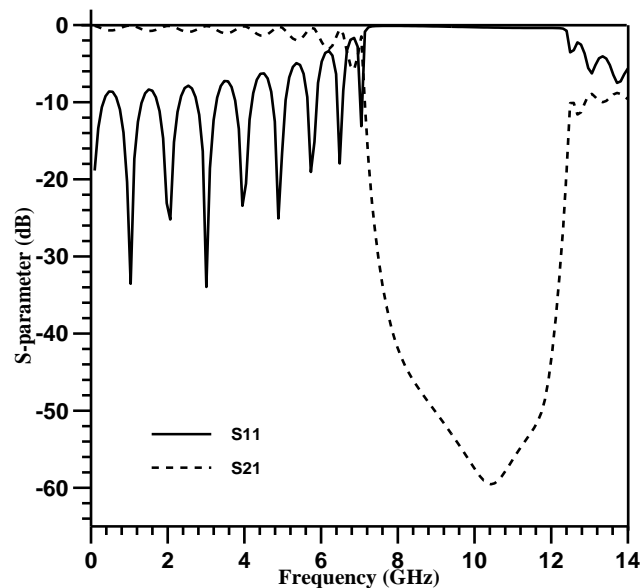


Fig. 4.32: Simulated S-parameter performances of a standard 50 ohm transmission line perturbed by 1-D (one line) uniform rectangular PBGSs in the ground plane.

From the Fig. 4.32, it can be seen that return loss performance, stopband characteristics and ripple height for this design is similar as 2-D design. A small difference in the value of maximum isolation is observed. In the case of three rows of uniform rectangular PBGSs the maximum isolation is found to be approximately -51.1 dB. On the other hand, one row of uniform rectangular PBGS provides approximately -59.5 dB.

6. The Transmission Line with 1-D Uniform Dumbbell shaped DGSs: It is mentioned that 0.5 is the optimum FF of the larger slot of DGS for Taconic with dielectric constant of 2.45 and height of 31 mils. Based on this value a microstrip transmission line with 1-D uniform Dumbbell shaped DGSs has been investigated. The simulation result is shown in Fig. 4.33.

It can be seen from the figure that this design provides wider passband and deeper stopband. The 20 dB rejection bandwidth is 3.66 GHz. The ripple height along the passband is not negligible in this time. The maximum value of isolation is found to be 41.1 dB. It looks like a low pass filter, but an observable harmonics is shown before 10 GHz frequency.

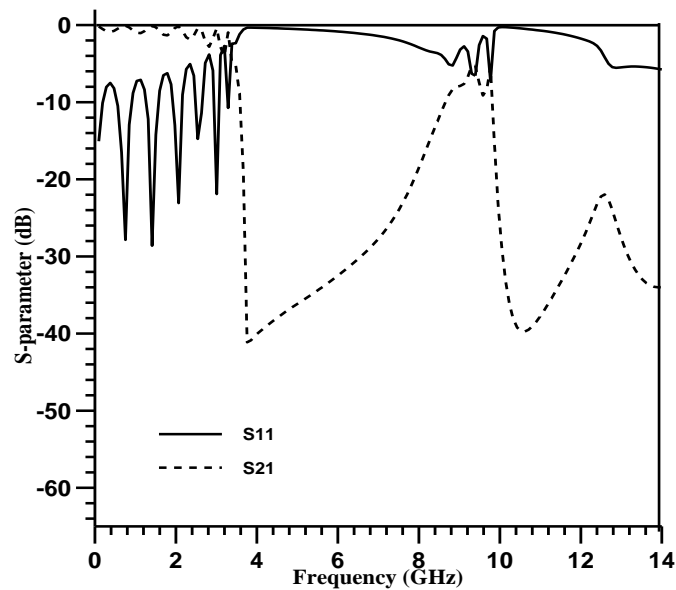


Fig. 4.33: S-parameters performances of three lines uniform Dumbbell shaped DGS structures. The substrate is Taconic having dielectric constant of 2.45 and height of 31 mils. The inter-element spacing is 10.43 mm and FF with respect to larger element is 0.50.

4.7 Conclusion

Firstly, the transmission line model has been presented. To understand the properties of PBGSs the theory of PBG structures and dumbbell shaped DGS structures has been presented in short extent. Since they are also periodic in nature all theories of periodic structures hold true for PBGSs.

Uniform circular, square shaped PBGSs and dumbbell shaped DGSs have been analyzed. All designs have been investigated with FF of 0.25 for circular PBGSs and 0.5 for both rectangular PBGSs and dumbbell shaped DGSs is considered to be the optimum value of FF. Three rows and one row uniform PBGSs are studied to replace 2-D PBG elements by 1-D PBG elements for both the shapes. Both the designs provide very similar performances. Throughout whole investigations, it is preferred to use 1-D PBGSs rather than 2-D PBGSs.

Chapter V

EBGS Assisted Bandpass Filter

5.1 Introduction

Microstrip BPF's are widely used in microwave integrated circuits [23]. Conventional parallel-coupled BPF's, however, present spurious pass bands of harmonic frequencies, which tend to degrade the performance of the overall RF system. Extra filters are usually required to suppress spurious transmissions and, as a consequence, the insertion loss will be increased. The advantages of the UC-PBG has been applied to construct a compact microstrip BPF with intrinsic spurious rejection [24]. But the structure is complex and requires larger space. For obtaining less space, better harmonic suppression linear and non-linear EBGSs could be applied. Since the stopband is intrinsic, extra filters are not required.

5.2 Compact EBG assisted Bandpass filter

Conventional parallel-coupled band pass filters (BPF) construction need complex and very long calculation of coupled line filter which is time consuming. Also in the s-parameter performances of conventional band pass filter spurious pass bands at harmonic frequencies are present. Extra filters are needed to suppress the spurious signals which increase the insertion loss and tend to degrade the performance of the overall RF system. For solving this problem T. It. Al [24] has come up with a new technique which is known as compact photonic bandgap structure. The theory of compact PBG has already explained in chapter 3.

It is reported [44] that the use of extra filters can be avoided by just applying PBG to obtain a compact microstrip BPF with intrinsic spurious rejection. The well-matched microstrip on the UC-PBG ground plane is suited as a low-loss transmission line.

Generated spurious pass bands at higher harmonics can be suppressed with the aid of PBGS as it provides a wide and deep stopband. The physical length of the filter circuit is reduced as well due to the slow-wave effect of the UC-PBG structure.

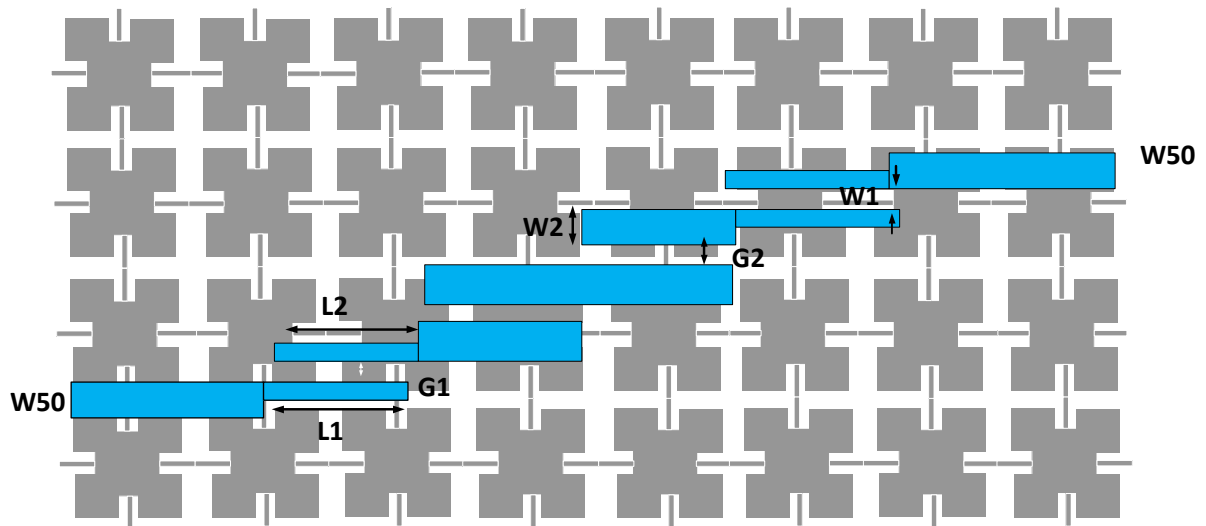


Fig. 5.1: The schematic of a microstrip BPF on the UC-PBG ground.

The reference [51] narrates the standard design procedures of the parallel-coupled BPF. The design specifications of the reference BPF are mentioned below [24]:

Center frequency = 6 GHz, $W1 = 17$ mils, $W2 = 21$ mils, $G1 = 8$ mils, $G2 = 28$ mils. The width of microstrip feed lines = 24 mils (corresponding to 50-ohm transmission line). Number of coupling sections = 4 (Four); a 0.5 dB equal-ripple response. The physical length of the coupled-line sections ($L1$ and $L2$) = 145 mils. This length is 20% shorter than that of a conventional quarter wavelength line.

In communication systems, harmonics cause intermodulation distortion. Traditional band-pass filters with half-wavelength resonators have inherently spurious passbands at harmonics; therefore, low-pass filters or band-stop filters must be used to suppress the harmonics. Also it is a coupled line BPF. Due to these coupled line harmonics are generated by coupling effect. At the frequency of 12 GHz and 17 GHz, transmission coefficients of a conventional BPF are seen to be -10 dB and -5 dB respectively. On the other hand, the UC-PBG assisted filter provides the spurious suppression of 30-40 -dB. Though the length of the microstrip resonator has been scaled accordingly to the slow-

wave factor, but the coupling gap remains same, which results the increased fractional bandwidth (21.6 %) at 6 GHz center frequency. Like conventional BPF the coupling coefficient can be optimized to improve the bandpass characteristics of the PBG assisted BPF. Including the effect of two SMA connectors, the minimum insertion loss of the PBG assisted filter is found to be 1.9 dB at 6.39 GHz. The s-parameter performance of the reference BPF and PBG assisted BPF reported in [24] is shown in below. It is seen that the measured transmission co-efficients

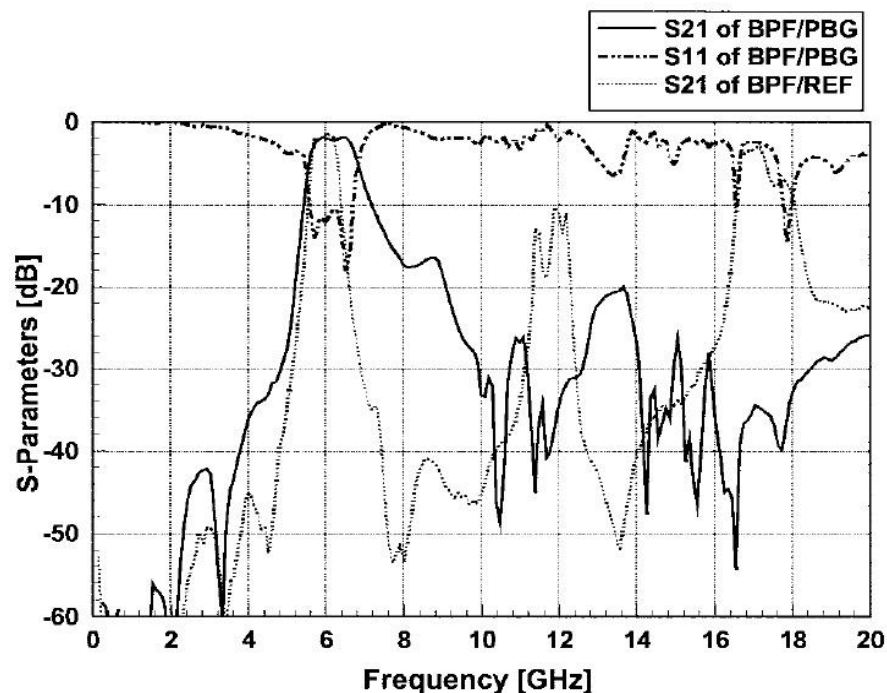


Fig. 5.2: Measured S-parameters of the PBG BPF. The S_{21} of a conventional BPF is also plotted for comparison (indicated by BPF/REF).

of a conventional BPF are 10 dB and 5 dB at 12 and 17 GHz, respectively. On the other hand, the experimental result of the BPF on a UC-PBG ground shows a 30 - 40 dB suppression of the spurious response. The minimum insertion loss of the PBG filter is 1.9 dB at 6.39 GHz, which includes the effect of two SMA connectors. The passband loss is comparable to that of a conventional BPF, as can be observed in Fig. 5.2.

5.3 Uniform PBGS assisted Bandpass filter

In modern microwave devices, microstrip transmission lines are commonplace. Therefore, in the following sections, the investigation is concentrated into only on PBG assisted band pass filter. To derive the characteristic performance of PBG assisted BPF it is more logical to use scattering parameters (S-parameters) instead of showing K- β diagram. S-parameters are universally accepted format of device characterizations. Moreover, commercially available software tool IE3D will be used to design and to extract S-parameters for all designs due to the flexibility of IE3D. IE3D is a method of moment (MOM) based full-wave analysis tool, hence very accurate.

The perturbation in the ground plane of any microstrip transmission line in the form of PBGS creates stopband that is useful for suppression of surface waves, leakage, and spurious transmission and to improve the performance of antennas, filter and other microwave devices and components. The stopband characteristic is highly influenced by the shape, size and the period of the PBGSs located on the ground plane. Therefore, it is useful to see the performance of the 4 section asymmetric coupled line BPF. The BPF will be investigated to see how PBGSs can reduce the higher order harmonics. In this section basic BPF, uniform circular pattern PBG assisted BPF and square patterned PBG assisted BPF will be investigated. It is well known that the EM field is highly concentrated under the microstrip line.

5.3.1 Reference Bandpass Filter

At first a coupled line BPF with an unperturbed ground plane is designed that has higher order harmonics in the stopband which can be observed on the dispersion characteristics in the form of scattering parameters matrices versus frequency.

❖ **Design of a Reference Bandpass Filter:** A 4 section parallel coupled line band pass filter is designed with unperturbed. The reference [51] narrates the standard design procedures of the parallel-coupled BPF. The requirements are [24]:

Relative di-electric constant, $\epsilon_r = 10.2$, center frequency = 7.5 GHz, $W1 = 17$ mils, $W2 = 21$ mils, $G1 = 8$ mils, $G2 = 28$ mils. The width of microstrip feed lines = 24 mils (corresponding to 50-ohm transmission line). Number of coupling sections = 4 (Four); a

0.5 dB equal-ripple response. The physical length of the coupled-line sections (L1 and L2) = 145 mils.

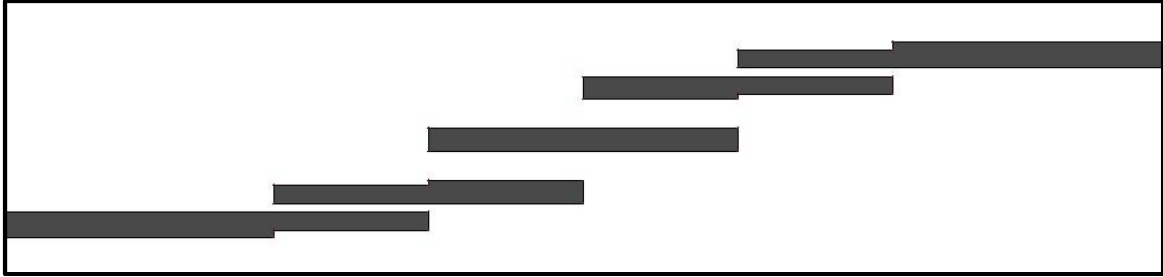


Fig. 5.3: Geometry of a reference 4 section parallel coupled line band pass filter with unperturbed on RT/Duroid 6010 substrate. Dielectric constant, $\epsilon_r = 10.2$, thickness, $h = 25$ mils, $\tan\delta = 0.0002$ and $W = 24$ mils.

❖ **Simulated Result of the Reference Bandpass Filter:** The S-parameters performance of an unperturbed 4 section parallel coupled line band pass filter is shown in Figure 5.4.

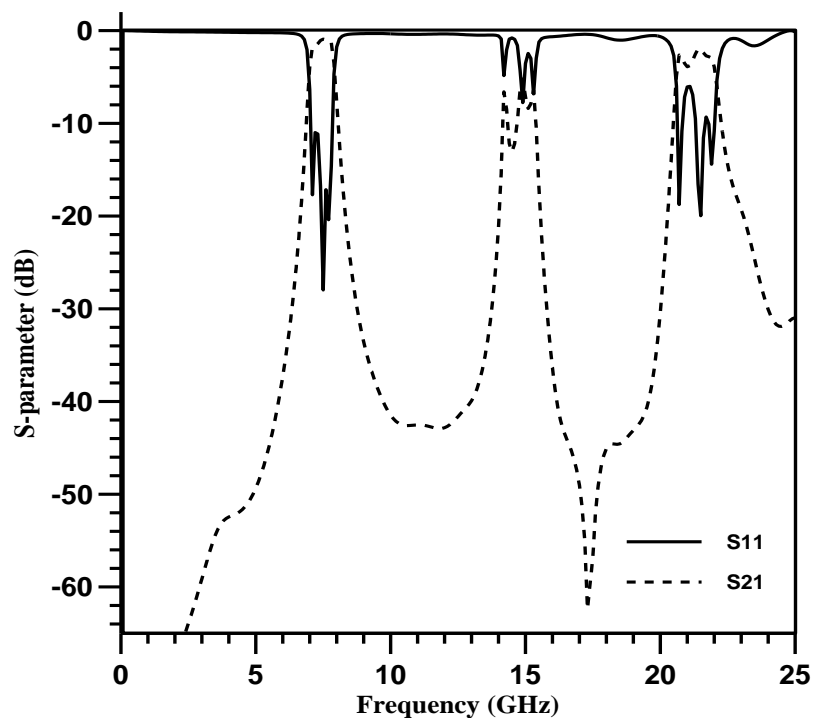


Fig. 5.4: S-parameters performance of an unperturbed 4 section parallel coupled line band pass filter according to Fig 5.3.

From the s-parameter performance, we could find the presence of 2nd and 3rd harmonics in the stopband. . At 7.5 GHz, which is the frequency of interest, the maximum value of

return loss is -27.96 dB and insertion loss is -0.9 dB. The reference unperturbed BPF has maximum peak insertion loss (IL) at 2nd harmonic (15GHz) and 3rd harmonic (22.5GHz) are -5.33 dB and -1.99 dB respectively. The maximum peak return loss (RL) at 2nd harmonic and 3rd harmonic are -7.41 dB and -19.58 dB respectively. The -3 dB bandwidth of this BPF is 833 MHz. The performance was also reported in [24] as shown in Fig 5.4. The average 3 dB insertion loss BW is 11.11%. The average 10 dB return loss BW is 10.86%.

5.3.2 Design of Uniform PBGS assisted Bandpass Filter

In the s-parameter performance of the reference BPF it is seen that the higher order harmonics are present in the stopband. This higher order harmonics will reduce the overall performance of the filter. In order to suppress the higher order harmonics we will design some circular pattern PBG assisted BPF and square patterned PBG assisted BPF.

❖ **Design 1: Uniform Circular (FF=.25) PBGS Transmission line assisted BPF:** The geometry of circular patterned PBGS assisted BPF is shown in Fig. 5.5. Here PBG elements are located under only the transmission line of the BPF. In this design there are 6 PBG elements and we have used optimized FF (0.25).

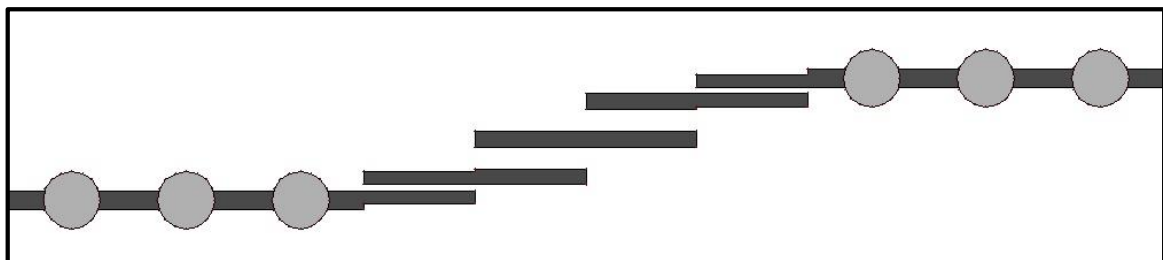


Fig. 5.5: Circular PBGSs (0.25 FF) assisted BPF under two extreme 50 ohm lines.

❖ **Design 2: Uniform Circular (FF=.25) PBGS all line assisted BPF:** The geometry of circular patterned PBGS assisted BPF is shown in Fig. 5.6. Here PBG elements are located under all lines of the BPF. In this design there are 13 PBG elements and we have used optimized FF (0.25)

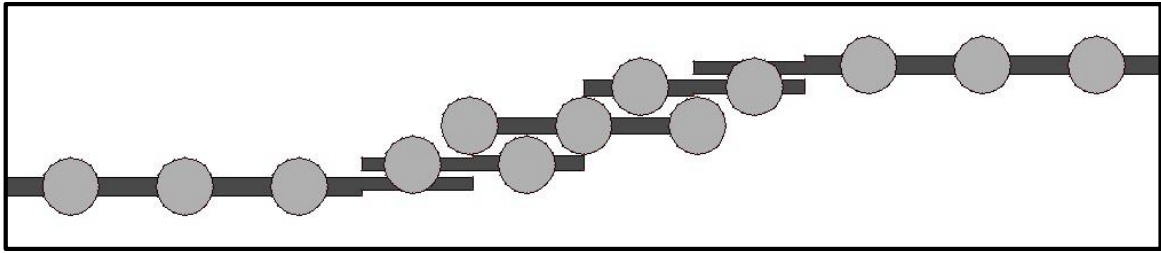


Fig. 5.6: Circular PBGSs (0.25 FF) under all lines assisted BPF.

❖ **Design 3: Circular PBGS (FF=.30) all line assisted BPF:** The geometry of circular patterned PBGS assisted BPF is shown in Fig. 5.7. Here PBG elements are located under all lines of the BPF. In this design there are 13 PBG elements and we have used 0.25FF.

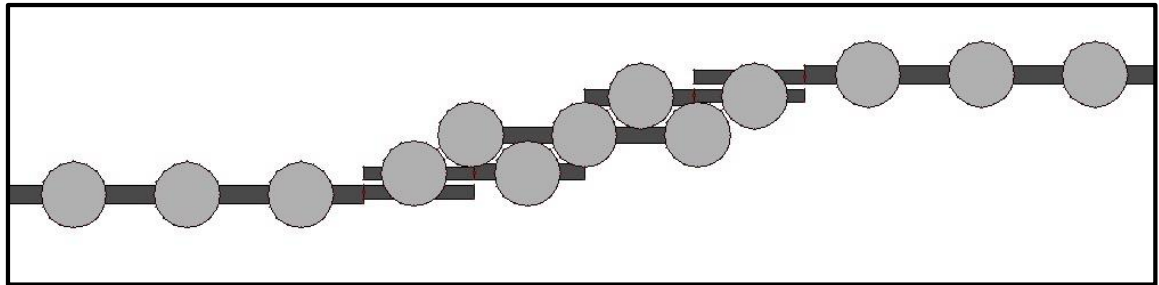


Fig. 5.7: Circular PBGSs (0.30 FF) under all lines assisted BPF.

❖ **Design 4: Square PBGS (FF=.40) all line assisted BPF:** The geometry of square patterned PBGS assisted BPF is shown in Fig. 5.8. Here PBG elements are located under all lines of the BPF. In this design there are 13 PBG elements and we have used 0.40FF.

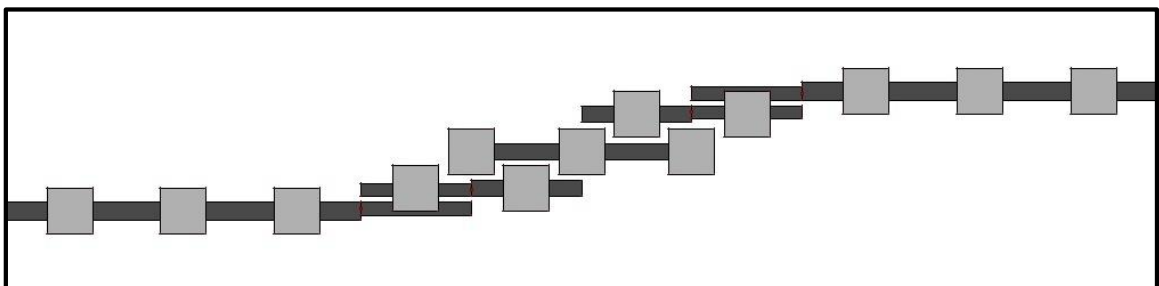


Fig. 5.8: Square PBGSs (0.25 FF) under all lines assisted BPF.

❖ **Design 5: Square PBGS (FF=.45) all line assisted BPF:** The geometry of square patterned PBGS assisted BPF is shown in Fig. 5.9. Here PBG elements are located under all lines of the BPF. In this design there are 13 PBG elements and we have used 0.45FF.

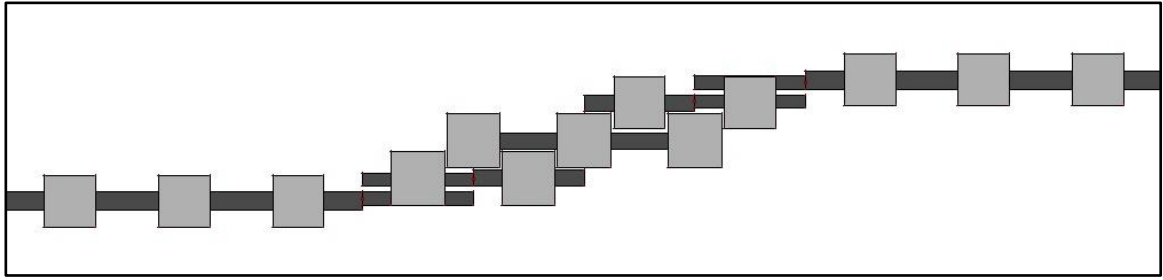


Fig. 5.9: Square PBGSs (0.45 FF) under all lines assisted BPF.

5.3.3 Performances of Uniform PBGS assisted Bandpass Filter

Theoretical results are produced for different geometries of uniform circular and square PBGS assisted BPF. To see the effect of uniform circular and square PBGS in harmonic suppression the performance of reference BPF is shown.

❖ Performance of BPF with uniform circular PBGSs under two extreme 50 ohm lines:

Thinking over the philosophy that the EM propagation takes place through the 50-ohm line first, uniform circular PBGSs are used under two 50-ohm lines only to see their effect

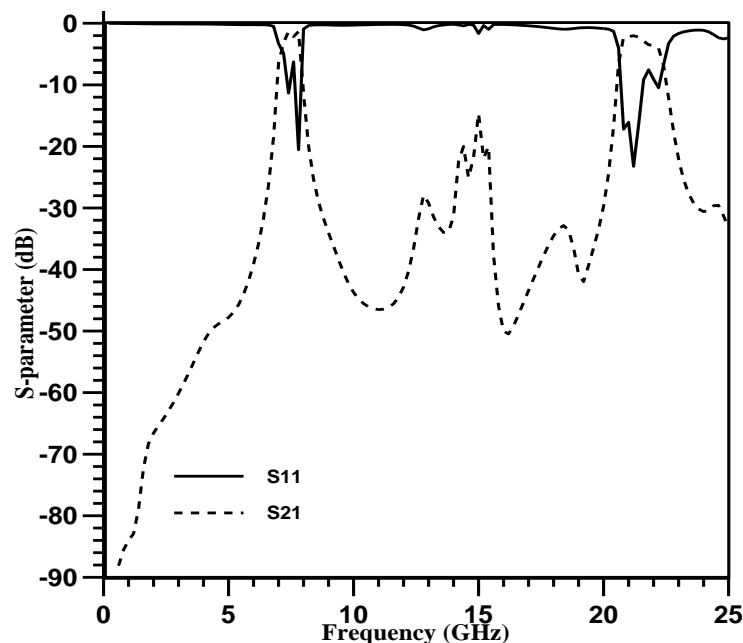


Fig. 5.10: S-parameters performances of a BPF where two 50-ohm lines are only perturbed with uniform circular PBGSs. Substrate is RT/Duroid having a dielectric constant of 10.2 and height of 0.635 mm.

in harmonic suppression. The simulated result is shown in Fig. 5.10. At 7.5 GHz (centre frequency), the maximum value of return loss is -19.73 dB and insertion loss is -1.21 dB. The perturbed BPF maximum peak insertion loss (IL) at 2nd harmonic and 3rd harmonic are -11.81 dB and -2.02 dB respectively. The maximum peak return loss (RL) at 2nd harmonic and 3rd harmonic are -2.64 dB and -22.98 dB respectively. The average 3 dB insertion loss BW and 10 dB return loss BW of fundamental frequency is 10.08% and 10.86% respectively. From the simulated result, it can be seen that the result is not promising at all. Rather the performance at 3rd harmonic frequencies are worse.

❖ **Performance of BPF with uniform circular (0.25FF) PBGSs under all the lines:**

Here PBGS is used just under all the lines. The design provides S-parameters performances as shown in Fig. 5.11. At 7.5 GHz (centre frequency), the maximum value of return loss is -25.4 dB and insertion loss is -0.71 dB. The perturbed BPF maximum peak insertion loss (IL) at 2nd harmonic and 3rd harmonic are -8.23 dB and -3.93 dB respectively. The maximum peak return loss (RL) at 2nd harmonic and 3rd harmonic are -8.25 dB and -11.52 dB respectively. The average 3 dB insertion loss BW and average 10 dB return loss BW of fundamental frequency is 14.82% and 13.98% respectively. So we can say that bandwidth enhancement is happened. At 22.5 GHz the bandwidth decreases. In this case an improvement in fundamental and third harmonic frequencies is achieved.

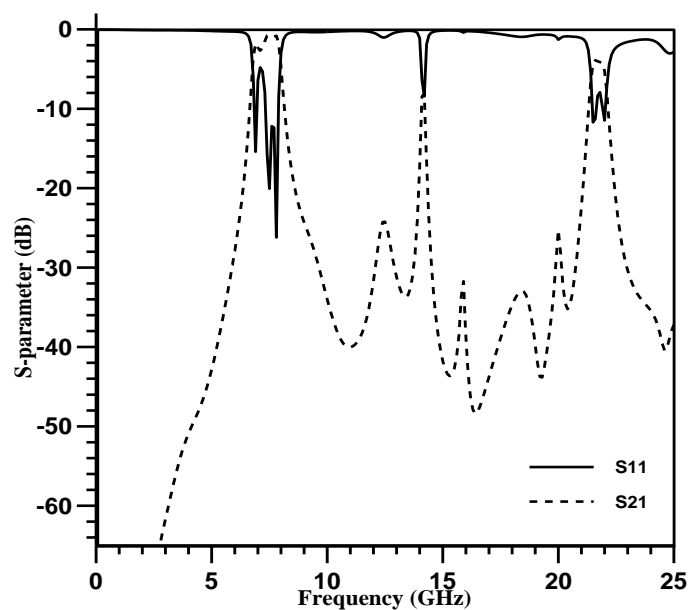


Fig. 5.11: S-parameters performances of a BPF when uniform circular PBGSs are situated under all the lines. Substrate is RT/Duroid having a dielectric constant of 10.2 and height of 0.635 mm.

❖ **Performance of BPF with uniform circular (0.30FF) PBGSs under all the lines:**

Here PBGS is used just under all the lines at 0.30 FF. The design provides S-parameter performances as shown in Fig. 5.13. At 7.5 GHz (centre frequency), the maximum value of return loss is -21.29 dB and insertion loss is -0.69 dB. The perturbed BPF maximum peak insertion loss (IL) at 2nd harmonic and 3rd harmonic are -15.95 dB and -8.63 dB respectively. The maximum peak return loss (RL) at 2nd harmonic and 3rd harmonic are -8.1 dB and -9.51 dB respectively. The average 3 dB insertion loss BW and average 10 dB return loss BW of fundamental frequency is 16.91% and 16.32% respectively. In this case an improvement in fundamental and third harmonic frequencies is achieved. Though this design can suppress the harmonics properly.

From above it is clearly understood that uniform circular patterned PBG elements can't suppress the higher order harmonics in the BPF. So we can investigate uniform square patterned PBG elements in the ground plane of BPF. From the s-parameter performances of the design we will conclude the results.

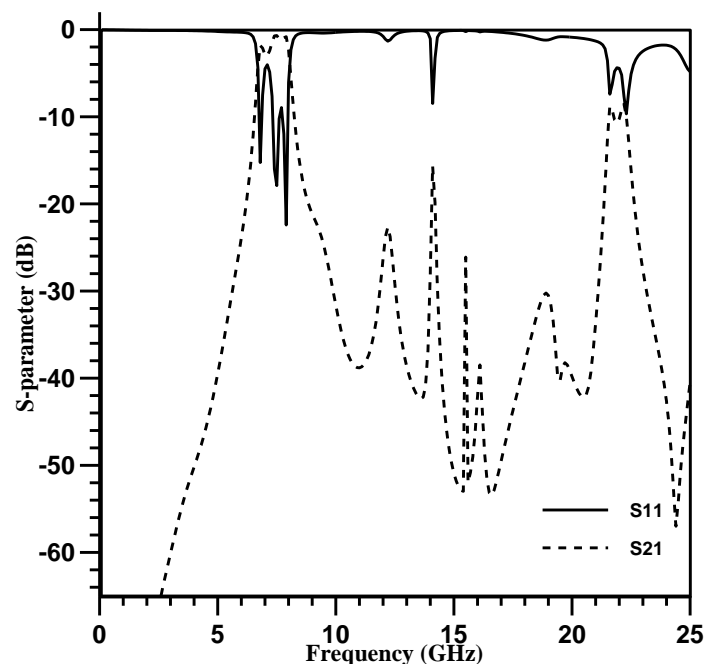


Fig. 5.12: S-parameters performances of a BPF when uniform circular at 0.30FF (design 3) PBGSs are situated under all the lines. Substrate is RT/Duroid having a dielectric constant of 10.2 and height of 0.635 mm.

❖ **Performance of BPF with uniform square (0.40FF) PBGSs under all the lines:**

Here square PBGS is used just under all the lines at 0.40 FF. The design (design 4) provides S-parameters performances as shown in Fig. 5.13. At 7.5 GHz, the maximum value of return loss is -20.33 dB and insertion loss is -0.78 dB. The perturbed BPF maximum peak insertion loss (IL) at 2nd harmonic and 3rd harmonic are -5.02 dB and -3.21 dB respectively. The maximum peak return loss (RL) at 2nd harmonic and 3rd harmonic are -15.27 dB and -16.21 dB respectively. The average 3 dB insertion loss BW and average 10 dB return loss BW of fundamental frequency is 13.44% and 13.24% respectively. The overall performance is worse than previous design.

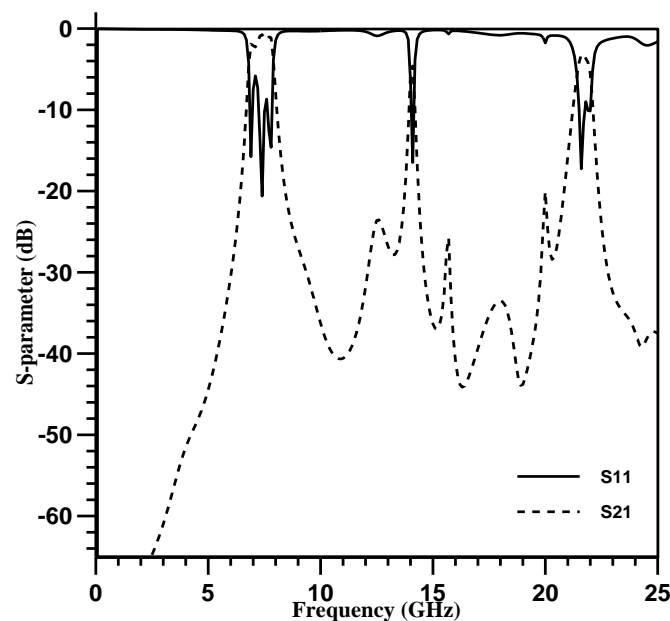


Fig. 5.13: S-parameters performances of a BPF when uniform square at 0.40FF PBGSs are situated under all the lines. Substrate is RT/Duroid having a dielectric constant of 10.2 and height of 0.635 mm.

Performance of BPF with uniform square (0.45FF) PBGSs under all the lines:

Here square PBGS is used just under all the lines at 0.45 FF. The design (design 5) provides S-parameters performances as shown in Fig. 5.14. At 7.5 GHz, the maximum peak insertion loss (IL) at 2nd harmonic and 3rd harmonic are -8.75 dB and -5.51 dB respectively. The maximum peak return loss (RL) at 2nd harmonic and 3rd harmonic are -8.58 dB and -12.50 dB respectively. The average 3 dB insertion loss BW and average 10 dB return loss BW of fundamental frequency is 15.52% and 14.73% respectively. Though the bandwidth has increased but still the over performance isn't satisfactory.

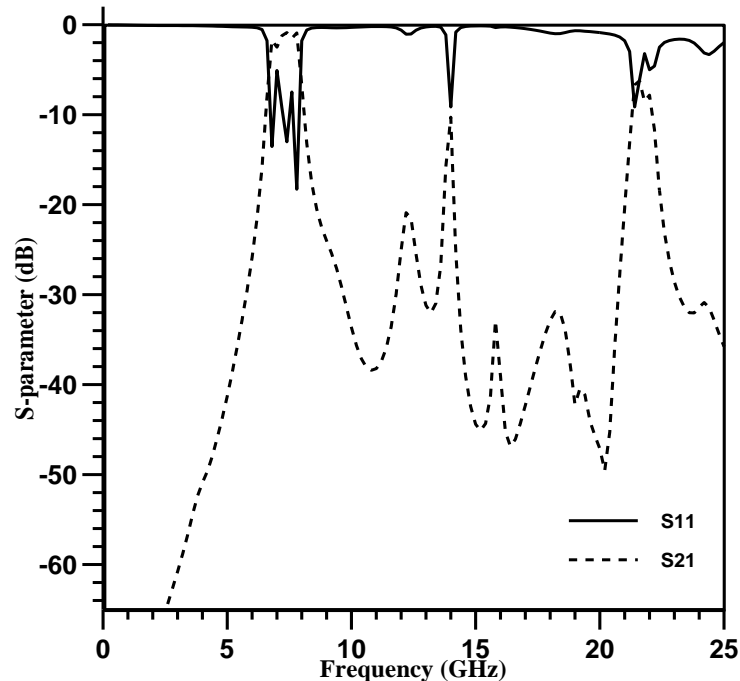


Fig. 5.14: S-parameters performances of a BPF when uniform square at $0.45FF$ PBGSs are situated under all the lines. Substrate is RT/Duroid having a dielectric constant of 10.2 and height of 0.635 mm.

The overall results of all circular and square patterned PBG elements have failed to completely suppress the higher order harmonics at different FF. So now we will investigate BPF by DGS and non-uniform design.

5.4 Uniform Dumbbell Shaped DGS assisted BPF for Harmonic Suppression

In this sub-section the novel idea is reported for simultaneous harmonic suppression of 2nd and 3rd order harmonics generated in a conventional BPF. It is already reported that the dumbbell shaped DGS can stem wider stopband [79-80]. Now this unique property is implemented into an asymmetric 4-section coupled line BPF to suppress the 2nd and 3rd order harmonics. 1-D EBGs (dumbbell shaped DGS) are proposed that are located just under standard 50-ohm lines. No DGS will be used under the coupled lines. This design is sufficient to suppress the 2nd and 3rd order harmonics. Few designs are investigated.

❖ **Dumbbell shaped DGS assisted BPF:** Here total 6 dumbbell shaped DGSs are used uniformly under two 50-ohm lines. Three dumbbell shaped DGSs will be located under each 50-ohm line. The larger square slot of dumbbell shaped DGS unit has the dimension

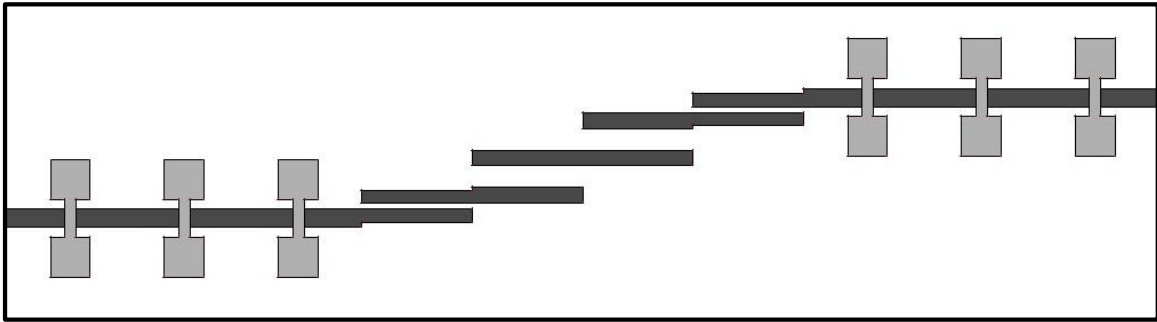


Fig. 5.15: Geometry of a dumbbell shaped DGS assisted BPF. 6 dumbbell shaped DGSs are used under two $50\ \Omega$ transmission line.

of 60×60 square mils and the vertical narrow slot has the dimension of 50×15 square mils. The geometry of a BPF with 6 dumbbell shaped DGSs in the ground plane is shown in Fig. 5.15. The dumbbell shaped DGSs are placed uniformly under the $50\ \Omega$ transmission line of the BPF.

❖ **Performance of dumbbell shaped DGS assisted BPF:** The theoretical investigations have been carried out to dumbbell shaped DGS assisted BPF to see the effective

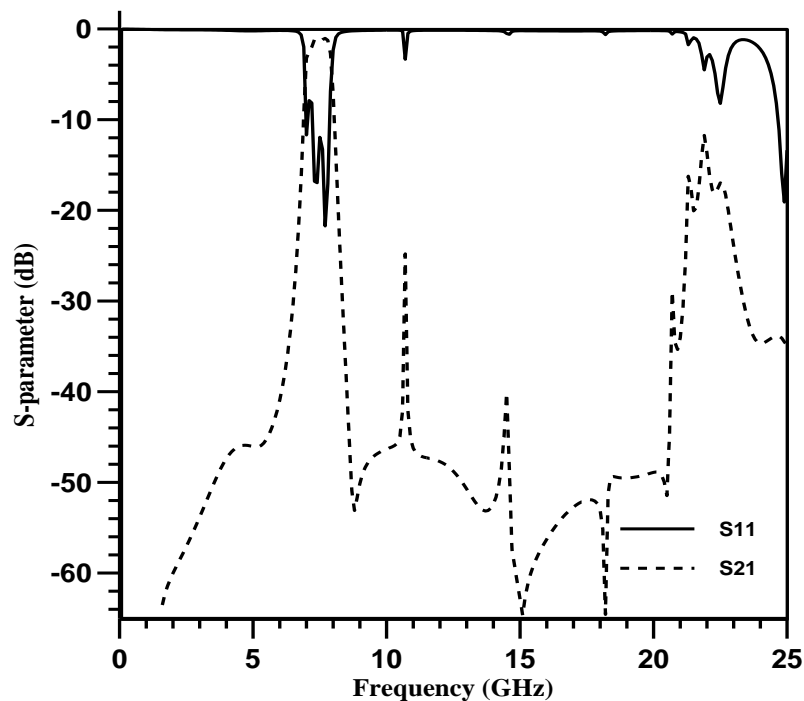


Fig. 5.16: S-parameters performances of a dumbbell shaped DGS assisted BPF having total 6 DGS (3+3) lying under two $50\ \Omega$ transmission lines.

suppression of 2nd (at 15 GHz) and 3rd (at 22.5 GHz) harmonics which is shown in Fig 5.16. At 7.5 GHz, the maximum value of return loss is -21.26 dB and insertion loss is -1.05 dB. The perturbed BPF maximum peak insertion loss (IL) at 2nd harmonic and 3rd harmonic are -40.30 dB and -11.7 dB respectively. The maximum peak return loss (RL) at 2nd harmonic and 3rd harmonic are -0.55 dB and -8.1 dB respectively. The average 3 dB insertion loss BW and average 10 dB return loss BW of fundamental frequency is 11.73% and 11.83% respectively. Though there is a spike of -28.02 dB before 2nd harmonic at 10.71 GHz, the overall performance improved significantly. This s-parameter performance showed that dumbbell shaped DGS can wider the stopband which is our expected result.

5.5 Non-Uniform Dumbbell Shaped DGS assisted Bandpass Filter for Harmonic Suppression

Nonlinear distribution in Electromagnetic Bandgap Structures (EBGSs) provides smoother transmission passband and dumbbell shaped defected ground structures (DGSs) provide wider stopband. In this section, we will combine these two distinct properties to investigate the improvement in S-parameters performance. The non-uniform distributions in the forms of Binomial and *Chebyshev* polynomials yield superior performances by suppressing passband ripples and producing distinct wide stopbands. Also the depth of passband return loss, selectivity and the ripples can be controlled with the side-lobe level index of *Chebyshev* polynomial. Using the non-uniform distribution of PBG patterns, both passband ripple and stop bandwidth problems are alleviated and the selectivity of the stopband of planar PBGSs increases.

5.5.1 Theory of Non-uniform 1-D Microstrip PBGSs

5.5.1.1 Binomial Distribution

Binomial distribution is the determination of the probability distribution for the discrete number of successes in an independent sequence of experiments. The coefficients of the polynomial are determined by the expression (5.1).

$$(1 + x)^{N-1} = 1 + (N - 1)x + \frac{(N - 1)(N - 2)}{2!}x^2 + \frac{(N - 1)(N - 2)(N - 3)}{3!}x^3 + \dots \dots \dots (5.1)$$

The positive coefficients of the series expansion for different values of N are expressed in terms of the Pascal’s triangle [51].

If the values of N represent the numbers of elements in an array, the coefficients of the expansion represent the relative amplitudes of the elements. Generally, this type of array suffers from the practical limitation of bandwidth and efficiency due to the abrupt change in amplitude tapering between adjacent elements. In this work the dimensions of the circular PBGSs are varied proportionally to the relative amplitudes of the polynomial.

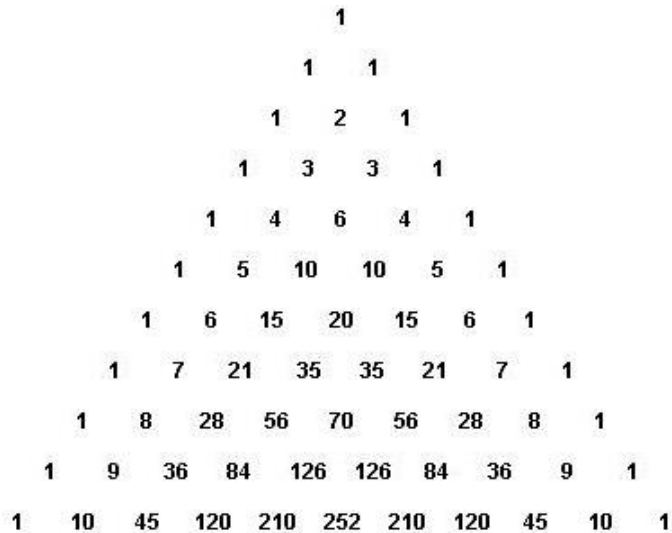


Figure 5.17: Pascal’s Triangle.

5.5.1.2 Chebyshev Distribution

Instead of maximally flat passband characteristics, an equally useful characteristic is one that may permit the transmission coefficient to vary with minute ripples over the stopband. This provides a considerable increase in bandwidth with respect to Binomial distribution. This equal-ripple characteristic is obtained by making the distribution according to Chebyshev polynomial. The basic properties of the polynomials [51] are expressed as follows:

$$T_m(z) = 2zT_{m-1}(z) - T_{m-2}(z) \tag{5.2}$$

Where $T_m(z)$ is expressed as:

$$T_m(z) = \cos[m \cos^{-1}(z)] \text{ for } |z| \leq 1 \quad (5.3)$$

The coefficients of the polynomial are determined for any prescribed side lobe level. The amplitudes of 10 element PBGSs according to *Chebyshev* equations are determined as follows:

$$0.36 \quad 0.49 \quad 0.71 \quad 0.78 \quad 1 \quad 1 \quad 0.78 \quad 0.71 \quad 0.49 \quad 0.36$$

The amplitude 1 is for the two center elements of the 10-element array and the rest elements follow suit. For PBG design the elements are varied proportionally to the relative amplitudes, respectively.

5.5.2 Binomially Distributed Dumbbell Shaped DGS assisted Bandpass Filter

In this design, we have used binomially distributed dumbbell shaped DGSs assisted BPF. In this design the relative amplitude of the dumbbell shaped PBG elements are varied proportionally. We have taken six (6) EBG elements in our designs by using the coefficient of the Pascal's triangle. Here are the co-efficient of the Pascal's triangle:

$$n = 6 \quad \quad \quad 1 \quad 5 \quad 10 \quad 10 \quad 5 \quad 1$$

The proportional amplitude co-efficients of (P) are as follows:

$$P3 = 0.10 \quad P2 = 0.50 \quad P1 = 1 \quad P1 = 1 \quad P2 = 0.50 \quad P3 = 0.10$$

These values are calculated from Pascal's triangle for $n = 6$.

Though the relative amplitude of the dumbbell shaped DGS elements are varied in accordance with binomial distribution, but the connected narrower slots are kept constant. The larger square slot of dumbbell shaped DGS unit has the dimension of 52×52 square mils and the vertical narrow slot has the dimension of 50×15 square mils. The design is shown in Fig. 5.18.

The s-parameter performance of this design is shown in Fig. 5.18. From the s-parameter performance, it can be seen that at 7.5 GHz the maximum RL is -20 dB and the IL is -1.4 dB. The perturbed BPF maximum peak insertion loss (IL) at 2nd harmonic and 3rd harmonic are -27.25 dB and -28.82 dB respectively. The maximum peak return loss (RL) at 2nd harmonic and 3rd harmonic are -7.81 dB and -2.47 dB respectively. The average 3

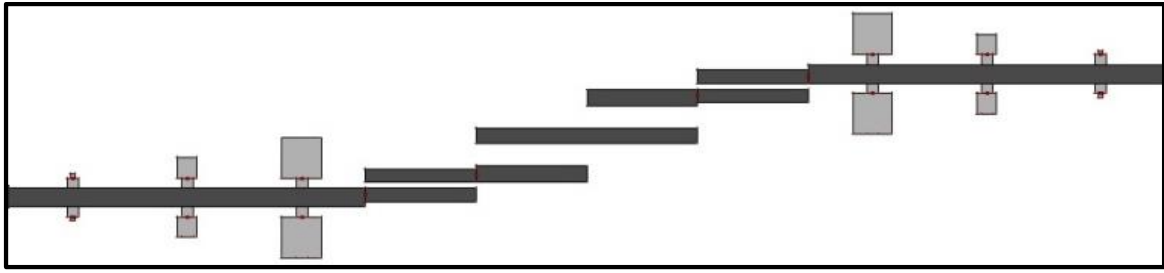


Fig. 5.18: Geometry of a binomially distributed dumbbell shaped DGS assisted BPF. 6 dumbbell shaped DGSs are used under two 50Ω transmission line.

dB insertion loss BW and average 10 dB return loss BW of fundamental frequency is 7.37% and 6.89% respectively. In this case significant improvements in 3rd harmonic frequencies are achieved. So from the above discussion it has seen that this design is capable of suppressing both 2nd and 3rd harmonics simultaneously.

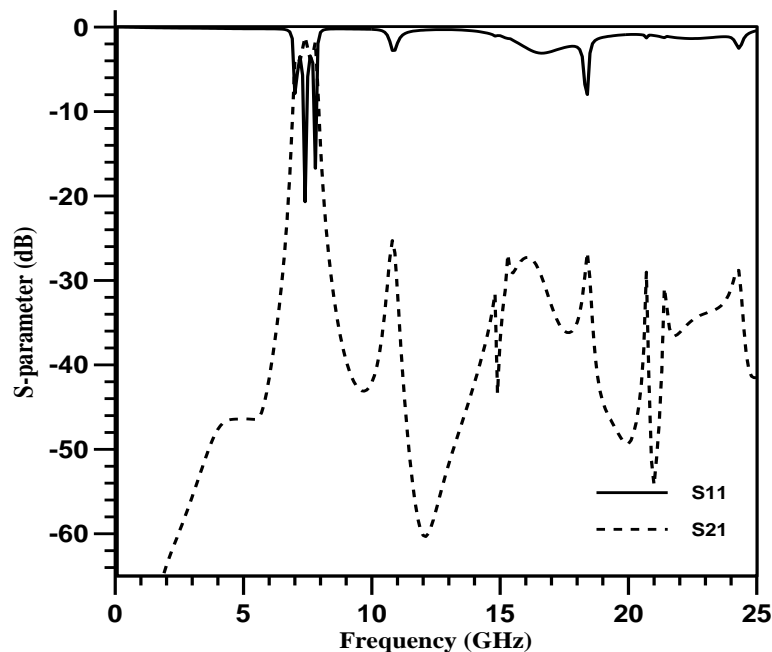


Fig. 5.19: Simulated s-parameter performances of a band pass filter perturbed by binomially distributed dumbbell shaped DGS in the ground plane. The substrate is RT/Duroid having height of 25 mils and dielectric constant of 10.2

5.5.3 Chebyshev Distributed Dumbbell Shaped DGS assisted Bandpass Filter

In this design, we have used chebyshev distribution on dumbbell shaped DGSs assisted BPF. In this design the relative width of the dumbbell shaped PBG elements are varied

proportionally. We have taken ten (10) EBG elements in our designs by using the co-efficient of Chebyshev polynomial. Here are the co-efficient of the Chebyshev polynomial:

0.36 0.49 0.71 0.78 1 1 0.78 0.71 0.49 0.36

Though the relative width of the dumbbell shaped DGS elements (both bigger slot and narrow slot) are varied in accordance with chebyshev distribution, but the length of both bigger slot and narrow slots are kept constant. The larger square slot of dumbbell shaped DGS unit has the dimension of 60×60 square mils and the vertical narrow slot has the dimension of 50×15 square mils. The design is shown in Fig. 5.20.

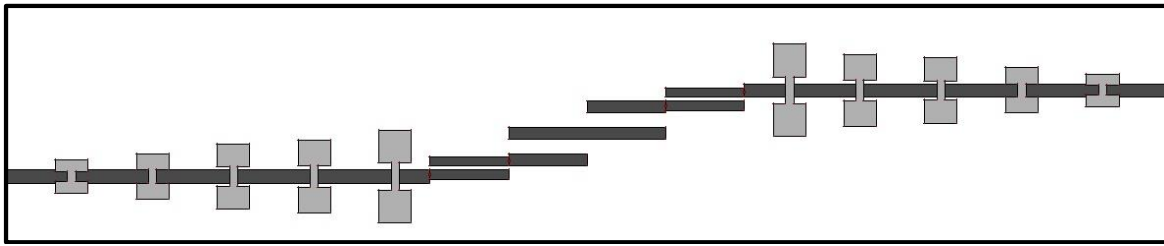


Fig. 5.20: Geometry of a chebyshev distributed dumbbell shaped DGS assisted BPF. 10 dumbbell shaped DGSs are used under two 50Ω transmission line.

The s-parameter performance of this design is shown in Fig. 5.21. At 7.5 GHz, the maximum value of return loss is -16.7 dB and insertion loss is -1.22 dB. The perturbed BPF maximum peak insertion loss (IL) at 2nd harmonic and 3rd harmonic are -33.47 dB and -38.41 dB respectively. The maximum peak return loss (RL) at 2nd harmonic and 3rd harmonic are -5.41 dB and -1.1 dB respectively. The average 3 dB insertion loss BW and average 10 dB return loss BW of fundamental frequency is 7.23% and 6.67% respectively.

In this case significant improvements in stopband are achieved. Though -5 dB spike IL is present in the stopband but from s-parameter performance the overall performance is remarkable. It has seen that this design is capable of suppressing both 2nd and 3rd harmonics simultaneously.

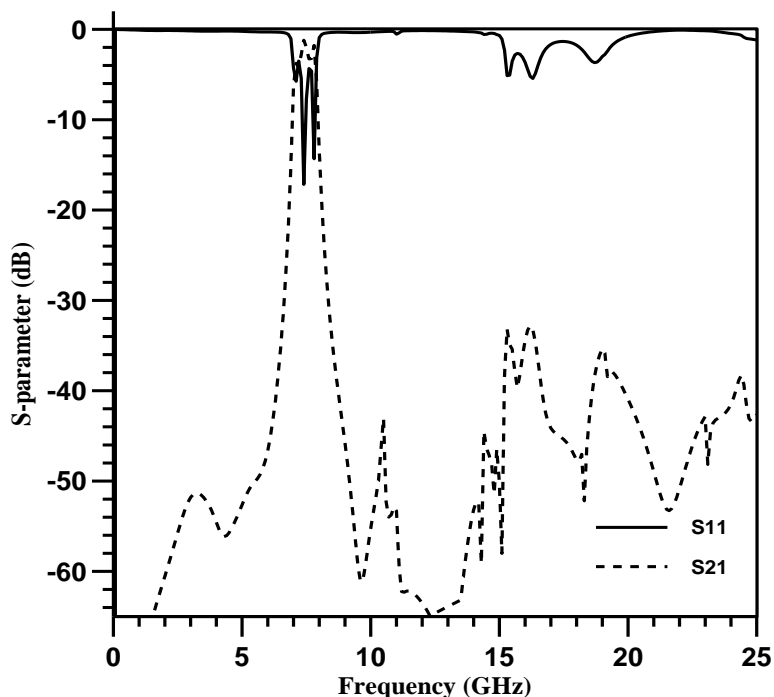


Figure. 5.21: Simulated s-parameter performances of a band pass filter perturbed by chebyshev distributed dumbbell shaped DGS in the ground plane. The substrate is RT/Duroid having height of 25 mils and dielectric constant of 10.2.

No	Band Pass Filter	S-Parameter Performance	Remarks		
			Average 3 dB IL BW (%)	Peak IL (dB) of 2 nd Harmonics	Peak IL (dB) of 3 rd Harmonics
1.			11.11%	5.33	1.99
2.			10.08%	11.81	2.02

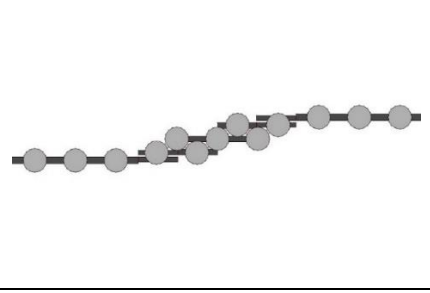
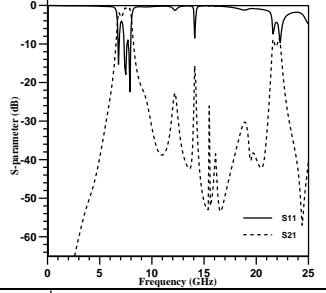
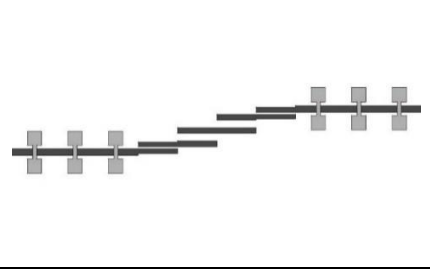
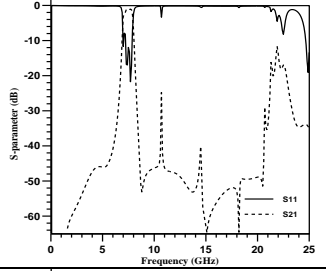
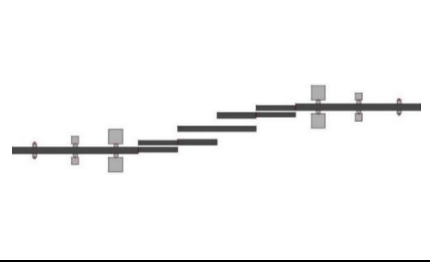
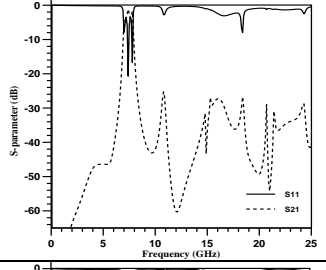
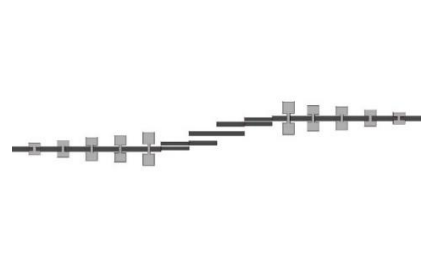
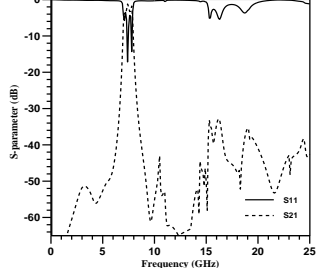
4.			16.91%	15.95	8.63
7.			11.73%	40.30	11.7
8.			7.37%	27.25	28.82
9.			7.23%	33.47	38.41

Table 5.1: A comparison table of the different designs and its s-parameter performances.

5.6 Conclusion

In this chapter reference BPF has reproduced and has investigated its s-parameter performances. Then normal PBG elements are used for harmonic suppression. Both uniform circular and square PBG elements have used during investigation. But they have failed to suppress both 2nd and 3rd harmonics completely. Dumbbell shaped has distinct properties that it can stem wider stopband. For investigating this property on BPF harmonic suppression a design has made and simulated. Expected result has found. Nonlinear distribution in Electromagnetic Bandgap Structures (EBGSs) provides smoother transmission passband and dumbbell shaped defected ground structures (DGSs) provide

wider stopband. These two distinct properties have investigated. The *Chebyshev* distributed structures show better performance than the binomially distributed structures. Both have showed significant stopband and capable of suppressing 2nd and 3rd order harmonics. These novel designs provide the impressive BPFs. The wider stopband can be used to mitigate the surface wave problem and suppression of spurious and leakage transmission. This structure can also find potential application in RF front-ends to isolate transmitters from receiver modules.

Chapter VI

Conclusion

6.1 Conclusion

Designing of a filter in conventional way is very cumbersome. It is observed that designing of a filter in the conventional way by “Insertion Loss” method is very difficult process & it has four long steps, they are: filter specification, low-pass prototype design, scaling & conversion and implementation. At present, to overcome this difficulty EBGs are used for their good performance and potential applications. Using EBGs, filters can be designed by simply etching in the ground plane of a microstrip structure.

It makes the filter circuit so simple. For this, attractive feature, EBGs are now used in microwave filter design. In this thesis work, at first, three lines and single line uniform EBGs are designed and simulated. From s-parameter performances, it is seen that three line EBGs is identical to single line EBGs. Different FF (0.25-0.45) of EBGs (uniform circular and square) is used to observe the S-parameters of this design. From the S-parameter performance it is seen that, with the increase of FF of EBGs the -20 dB rejection BW increases. Intensive investigation on EBGs assisted T-line shows excellent stopband performances.

The main objective of our thesis work is pure harmonic suppression of band pass filter by using different photonic band gap structures. Uniform circular & square EBGs under all lines are used in a four section asymmetric coupled line BPF. The S-parameters of different FF of uniform EBGs are analyzed and the insertion loss 2nd and 3rd harmonic was also compared with each other. But the suppression result was unsatisfactory. Nonlinear distribution in EBGs provides smoother transmission passband and dumbbell shaped DGSs provide wider stopband. In this paper, these two concepts are combined to design EBGs assisted BPF to suppress the 2nd and 3rd order harmonics. For nonlinear distribution binomial and chebyshev distribution is used. Then these two distributions have applied on

dumbbell shaped DGS. After simulating the structure, significant result is found. Both designs can suppress higher order harmonics. Taconic substrate is used in standard four section asymmetric couple line BPF whose dielectric constant is 10.2. For pure harmonic suppression center frequency 15 GHz is used.

6.2 Recommendation for Future Work

In the whole research work, attention has been paid to simulate all the structures by commercial available Method of Momentum (MOM) based EM software Zeland IE3D. The future work can be mentioned in the following manner.

In this paper, harmonic suppression has been analyzed for different FF of uniform circular, square photonic band gap structure and binomial and chebyshev distribution structures. With the non-linear distribution the higher order harmonics have suppressed. The 20dB bandwidth is still narrow. By changing the basic parameter of the reference BPF we can achieve higher bandwidth. Also ring shaped PBG elements can be used to investigate the performance.

The PBGSs are actually complex geometries. For such geometries it is a difficult task to calculate the value of the propagation constant. However the wise solution to the exact eigenvalue equation for the 1-D PBGS can be obtained through the use of the Fourier series. It is known as analytical techniques of the plane wave expansion method. The formulation can be derived for transverse electric or transverse magnetic case. The electric field/magnetic field of periodic structures can be expressed with the propagation constant and the period of the structure. Applying the required useful vector operator yield the simplified differential equation that can be expanded by Fourier series. Fourier series can also represent the dependence of the dielectric constant in a periodic structure. These double representations of Fourier series yield a Kronecker delta function over a unit cell of PBGS. This equation can have a general matrix form. Writing the code in MATLAB can solve a generalized linear Eigen system. Then a correct picture of passband characteristics could be found out, namely the slow wave factor (SWF) that is useful to calculate the value of compactness of the design. The stopband performance can also be explained

nicely by calculating the propagation constant. There is another option to calculate the input impedance of the structure, as at stopband the input impedance will be very larger showing the surface to be perfectly magnetic conductor. In this way the numerical results could be compared with the theoretical and measured results that would give more insight of the present research.

References

- [1] E. Yablonovitch, "Inhibited spontaneous emission in solid-state physics and electronics," *Phys. Rev. Lett.*, vol. 58, no. 20, pp. 2059 - 2063, May, 1987.
- [2] L. H. Weng, Y. C. Guo, X. W. Shi, and X. Q. Chen, "An overview on defected ground structure," *Prog. Electromagn. Resea. B*, vol. 7, pp.173–189, Aug., 2008
- [3] D. Sievenpiper, L. Zhang, R. F. J. Broas, N. G. Alexopolous, and E. Yablonovitch, "High-impedance electromagnetic surfaces with a forbidden frequency band," *IEEE Trans. Microw. Theory Tech.*, vol. 47, no.11, pp. 2059-2074, Nov. 1999.
- [4] K-C. CHEN, C-K. C. TZUANG, Y. Qian and T. Itoh "Leaky properties of microstrip above a perforated ground plane," in *IEEE MTT-S International Microwave Symposium Digest*, Anaheim, CA, 1999, pp. 69-72.
- [5] Y. Qian, R. Coccioli, D. Sievenpiper, V. Radisic, E. Yablnovitch and T. Itoh, "Microstrip patch antenna using novel photonic band-gap structures," *Microw. J.*, vol. 42, no. 1, pp. 66-76, Jan. 1999.
- [6] R. Coccioli, F-R. Yang, K-P Ma, and T. Itoh, "Aperture-coupled patch antenna on UC-PBG substrate," *IEEE Trans. Microwave Theory Tech.*, vol. 47, no. 11, pp. 2123-2130, Nov. 1999.
- [7] R. Gonzalo, P. D. Maagt, and M. Sorolla, "Enhanced patch antenna performance by suppressing surface waves using photonic-bandgap substrates," *IEEE Trans. Microwave Theory and Tech.*, vol. 47, no. 11, pp. 2131 – 2138, Nov. 1999.
- [8] K. M. Shum, Q. Xue, C. H. Chan and K. M. Luck "Investigation of microstrip reflectarray using a photonic using a photonic bandgap structure." *Microw. Opt. Tech. Lett.*, vol. 28, no. 2, pp. 114-116, Jan., 2001.

- [9] P. S. Hui and A. Alphones, "Microstrip patch antenna with annular ring PBG," in *Asia-Pacific Microwave Conference*, Sydney, NSW, 2000, pp. 1347 - 1351.
- [10] E. R. Brown, C. D. Parker, and E. Yablonovitch, "Radiation properties of a planar antenna on a photonic-crystal substrate," *J. Opt. Soc. Amer. B. Opt. Phys.*, vol. 10, no. 2, pp. 404-407, Feb., 1993.
- [11] S. K. Sharma and L. Shafai, "Enhanced performance of an aperture-coupled rectangular microstrip antenna on a simplified unipolar compact photonic bandgap (UC-PBG) structure," in *IEEE Antennas and Propagation Society International Symposium*, Boston, MA, 2001, pp. 498-501.
- [12] A. Byers, I. Rumsey, Z. Popovic, and M-P-May, "Surface-wave guiding using periodic structures," in *IEEE Antennas and Propagation Society International Symposium*, Salt Lake City, UT, 2000, pp. 342 - 345.
- [13] D. Sievenpiper and E. Yablonovitch, "Eliminating surface currents with metallodielectric photonic crystals," in *IEEE MTT-S International Microwave Symposium Digest*, Baltimore, MD, 1998. pp. 663-666.
- [14] R. Kim and H.Y.D. Yang., "Surface waves and leaky waves in integrated circuit structures with planar periodic dipole loading," in *IEEE Antennas and Propagation Society International Symposium*, Salt Lake City, UT, 2000, pp. 346-349.
- [15] R. Coccioli and T. Itoh "Design of photonic band-gap substrates for surface waves suppression," in *IEEE MTT-S International Microwave symposium digest*, Baltimore, MD, 1998, pp. 1259 - 1262.
- [16] K-P. Ma, J. Kim, F-R. Yang, Y. Qian and T. Itoh, "Leakage suppression in stripline circuits using a 2-D photonic bandgap lattice," in *IEEE MTT-S International Microwave symposium digest*, Anaheim, CA, pp.73-76, 1999.
- [17] P. De Maagt, R. Gonzalo, J. Y. Vardaxoglou, "Review of electromagnetic bandgap technology and applications", *The Rad. Sci. Bull.*, no. 309, pp. 11- 25, Jun., 2004.

- [18] Chul-Soo Kim, Jun-Seok Park, Dal Ahn, and Jae-Bong Lim, "A Novel 1-D Periodic Defected Ground Structure for Planar Circuits," *IEEE Microwave and Guided Wave Lett.*, vol. 10, no. 4, pp.131-133, Apr., 2000.
- [19] G. A. Richard. (2010, January 29). *Bragg's Law and Diffraction* [Online]. Available: <http://www.eserc.stonybrook.edu/ProjectJava/Bragg/>
- [20] S. M. S. Hassan, S. M. Anayetullah and M. N. Mollah, "Sinusoidal Appearance of Nonuniform Dumbbell Shape EBGs in Microstrip Transmission Line," in *International Conference on Electrical Information and Communication Technology*, Khulna, 2014, pp. 1-5.
- [21] S. M. S. Hassan, M. N. Mollah, M. A. Rashid, N. H. Ramly, and M. Othman, "Dumbbell shape EBG structure - worth to EBG assisted microwave filter designing," in *IEEE Asia Pacific Conference on Applied Electromagnetics*, Melaka, 2012, pp. 1-5.
- [22] M. N. Mollah and N. C. Karmakar, "Pure harmonic suppression of a bandpass filter using Binomially distributed photonic bandgap structures," *Microwave and Optical Tech. Lett.*, vol. 44, no. 2, pp. 194 - 196, Jan., 2005.
- [23] V. Radisic, Y. Qian, R. Coccioli, and T. Itoh, "Novel 2-D photonic bandgap structures for microstrip lines," *IEEE Microwave and guided wave Lett.*, vol. 8 no. 2, pp. 69 - 71, Feb. 1998
- [24] F-R Yang, K-P Ma, Y. Qian and T. Itoh "A uniplanar compact photonic-bandgap (UC-PBG) structure and its applications for microwave circuits," *IEEE Trans. Microw. Theory Tech.*, vol. 47, no. 8, pp. 1509 - 1514, Aug. 1999.
- [25] M. N. Mollah and N. C. Karmakar, "Investigations into nonuniform photonic-bandgap microstrip line filters," *IEEE Trans. Microw. Theory Tech.*, vol. 51, no. 2, pp. 564 - 572, Feb. 2003.
- [26] M. N. Mollah and N. C. Karmakar, "Harmonic suppression of a bandpass filter using binomially distributed photonic bandgap structures," in *IEEE Antennas and Propagation*

Society International Symposium, Columbus, Jul., 2003, pp. 883 - 886.

[27] A. A. Oliner, "Periodic structures and photonic band-gap terminology: historical perspectives", in *29th European Microwave Conference*, Munich, Ger., 1999, pp. 295 - 298.

[28] M. N. Mollah and N. C. Karmakar, "Optimum filling factor and performances of a transmission line at X-band perturbed by binomially distributed photonic bandgap (PBG) Structure", in *IEEE Pacific Rim Conference on Communications, Computers and signal Processing*, Victoria, BC, 2003, pp. 66 - 69.

[29] F. R. Yang, R. Coccioli, Y. Qian, and T. Itoh, "Planar PBG Structures: Basic Properties and Applications", *IEICE Trans. Electron.*, vol. E83-C, no. 5, pp. 687 - 696, May, 2000.

[30] T. Euler, and J. Papapolymerou, "Silicon Micromachined EBG Resonator and Two-Pole Filter with Improved Performance Characteristics," *IEEE Microwave and Wireless Components Lett.*, vol. 13, no. 9, pp. 373 - 375, Sept., 2003.

[31] H-ju Hsu, M.J. Hill, R.W. Ziolkowski, and J. Papapolymerou, "A Duroid-Based Planar EBG Cavity Resonator Filter with Improved Quality Factor", *Antennas and Wireless Propagation Lett.*, vol. 1 no. 2, pp. 67 - 70, Feb., 2002.

[32] W. J. Chappell, M. P. Little, and L. P. B. Katehi, "High Isolation, Planar Filters Using EBG Substrates," *IEEE Microwave And Wireless Components Lett.*, vol. 11, no. 6, pp. 246-248, Aug., 2001.

[33] W. J. Chappell and X. Gong, "Wide Bandgap Composite EBG Substrates", *IEEE Trans. Antennas Propag.*, vol. 51, no. 10, pp. 2744 - 2750, Oct., 2003.

[34] I. Rumsey, M. Piket-May and P. Kelly, "Photonic bandgap structures used as filters in microstrip circuits," *IEEE Microwave Guided Wave Lett.*, vol. 8, no. 10, pp. 336 - 338, Oct. 1998.

[35] Y. Horii and M. Tsutsumi, "Harmonic control by photonic bandgap on microstrip patch antenna," *IEEE Microwave Guided Wave Lett.*, vol. 9, no. 1, pp. 13 - 15, Jan. 1999.

- [36] R. Coccioli, W.R. Deal, and T. Itoh, "Radiation characteristics of a patch antenna on a thin PBG substrate," in *IEEE Antennas and Propagation Society International Symposium*, Atlanta, GA, 1998, pp. 656 - 659.
- [37] T. Yun and K. Chang, "One-dimensional photonic bandgap resonators and varactor tuned resonators," in *IEEE MTT-S International Microwave Symposium Digest*, Anaheim, CA, 1999, pp. 1629 -1632.
- [38] J. C. Vardaxoglou, A. Chauraya, A. P. Feresidis and P. De. Maagt, "Tunable Metallodielectric Electromagnetic Band Gap Structures with Defects", in *International Conference on Electromagnetics in Advanced Applications*, Torino, 2003, pp. 667 - 670.
- [39] M. J. Hill, R. W. Ziolkowski, and J. Papapolymerou, "A High-Reconfigurable Planar EBG Cavity Resonator," *IEEE Microwave and Wireless Components Lett.*, vol. 11, No. 6, pp. 255 - 257, Jun., 2001.
- [40] V. Radisic, Y. Qian, R. Coccioli and T. Itoh, "Novel 2-D photonic bandgap structures for microstrip lines," *IEEE Microwave and guided wave Lett.*, vol. 8 no. 2, pp. 69 - 71, Feb. 1998.
- [41] T. Lopetegi, M. A. G. Laso, J. Hernandez, M. Bacaicoa, D. Benito, M. J. Garde, M. Sorolla and M. Guglielmi, "New Microstrip Wiggly - Line Filters with Spurious Passband Suppression," *IEEE Trans. Microw. Theory Tech.*, vol. 49, no. 9, pp. 1593 - 1598, Sep., 2001.
- [42] D. Nestic, "A New Type of Slow-Wave 1-D PBG Microstrip Structure without Etching in the Ground Plane for Filter and Other Applications," *Microw. Opt. Tech. Lett.*, vol. 33, no. 6, pp. 440 - 443, Jun., 2002.
- [43] D. Nestic, "A New Type of Slow-Wave 1D PBG Microstrip Band-Pass Filter," *Microw. Opt. Tech. Lett.*, vol. 37, no. 3, pp. 201 - 203, May, 2003.
- [44] F.R. Yang, Y. Qian and T. Itoh, "A novel compact microstrip bandpass filter with intrinsic spurious suppression," in *Asia-Pacific Microwave Conference*, pp. 593 - 596, Dec. 1998.

- [45] F.R. Yang, Y. Qian and T. Itoh, "A novel uniplanar compact PBG structure for filter and mixer applications," *IEEE MTT-S International Microwave Symposium Digest*, Anaheim, CA, 1999, pp. 919 - 922.
- [46] C. Hang, V. Radisic, Y. Qian, and T. Itoh, "High efficiency power amplifier with novel PBG ground plane for harmonic tuning," *IEEE MTT-S International Microwave Symposium Digest*, Anaheim, CA, 1999, pp. 807 - 810.
- [47] W. L. Stutzman and G. A. Thiele, "Electromagnetic BandGap Structures," in *Antenna Theory and Design*, 3rd ed., John Wiley & Sons, 1998.
- [48] F.R. Yang, R. Coccioli, Y. Qian and T. Itoh, "PBG assisted gain enhancement of patch antennas on high-dielectric constant substrate," *IEEE Antennas and Propagation Society International Symposium*, Orlando, FL, 1999, pp. 1920 - 1923.
- [49] R. Coccioli, F.R. Yang, K.P. Ma, and T. Itoh, "Aperture coupled patch antenna on UC-PBG substrate," *IEEE Trans. Microw. Theory Tech.*, vol. 47, no.11, pp. 2123 - 2130, Nov. 1999.
- [50] V. Radisic, Y. Qian and T. Itoh, "Novel architectures for high-efficiency amplifiers for wireless applications," *IEEE Trans. Microw. Theory Tech.*, vol. 46, no. 11, pp. 1901 - 1909, Nov. 1998.
- [51] D. M. Pozar, "Microwave Filters," in *Microwave Engineering*, 4th ed., NJ, John Wiley & Sons, 1998, ch. 8, pp. 380 - 436.
- [52] M. Rahman and M. A. Stuchly, "Transmission line - periodic circuit representation of planar microwave photonic bandgap structures," *Microwave Optical Tech. Lett.*, vol. 30, no. 1, pp. 15 - 19, Jul. 2001.
- [53] M. F. Karim, A. Q. Liu, A. B. Yu and A. Alphones, "MEMS-based tunable bandstop filter using electromagnetic bandgap (EBG) structures," *Asia-Pacific Microwave Conference Proceedings*, 2005, pp. 4 - 7.

- [54] C. A. Balanis, "Microstrip Antennas," in *Antenna Theory Analysis and Design*, 2nd ed., New York, John Wiley, 1997, ch. 14, pp. 722 – 767.
- [55] M. N. Mollah, "Planar electromagnetic bandgap structures and applications," PhD Dissertation, Dept. Elect. & Electron. Eng., N. T. U., Nanyang, 2004.
- [56] Y. Sung., "Tunable BandStop Filter Based Defected Ground Structure using a Metal Plate", *Microwave and Optical Tecnology Lett.*, vol. 51, no. 1, pp. 160 - 163, Jan., 2009.
- [57] M. A. G. Laso, T. Lapetegi, M. J. Erro, D. Benito, M. J. Garde and M. Sorolla, "Multiple-Frequency-Tuned Photonic Bandgap Microstrip Structures," *IEEE Microw. Guided Wave Lett.*, vol. 10, no. 6, pp. 220 - 222, Aug., 2000.
- [58] S. Rogers, W. McKinzie, G. Mendolia, "AMCs Comprised of Interdigital Capacitor FSS Layers Enable Lower Cost Applications," *IEEE Antennas and Propagation Society International Symposium*, Columbus, OH, 2003, pp. 411 - 414.
- [59] S. Tse, B. S. Izquierdo, J. C. Batchelor and R. J. Langley, "Reduced Sized Cells for Electromagnetic Bandgap Structures," *Electron. Lett.*, vol. 39, no. 24, pp. 1699 - 1701, Nov., 2003.
- [60] A. P. Feresidis, G. Apostolopoulos, N. Serfas and J. C. Vardaxoglou, "Closely Coupled Metallodielectric Electromagnetic Band Gap (CCMEBG) Structures Formed By Double Layer Dipole and Tripole Arrays", *IEEE Trans. Antennas Propag.*, vol. 52, no. 5, pp. 1149 - 1158, May, 2004.
- [61] A. P. Feresidis, G. Apostolopoulos and J. C. Vardaxoglou, "Miniaturised Metallodielectric EBG structures", *IET Microw. Antennas Propagat.*, vol. 1, no. 1, pp. 234 - 239, Feb., 2003.
- [62] A. P. Feresidis, A. Chauraya, G. Goussetis, J. C. Vardaxoglou and P. de Maagt, "Multiband Artificial Magnetic Conductor Surfaces," *IEE Seminar on Metamaterials, for Microwave and (Sub) Millimetre Wave Applications*, London, UK, 2003, pp. 2/1 - 2/4.

- [63] G. K. Gopalakrishnan and K. Chang “Novel excitation schemes for the microstrip ring resonator with lower insertion loss”, *Electron. Lett.*, vol. 30, no. 2, pp. 148 - 149, Jan., 1994.
- [64] F. Martin, F. Falcone, J. Bonache, T. Lopetegui, M. A. G. Laso, M. Coderch and M. Sorolla, “Periodic loaded sinusoidal patterned electromagnetic bandgap coplanar waveguides,” *Microw. Optical Technol. Lett.*, vol. 36, no. 3, pp. 181 - 184, Feb., 2003.
- [65] Jia-Sheng Hong and M. J. Lancaster, “Network Analysis,” in *Microstrip Filters for RF / Microwave Applications*, 2nd ed., NY, John Wiley & Sons, 2011, ch. 2, sec. 2.1, pp. 7 - 21.
- [66] Hasegawa and Okizaki, “M.I.S. and Schottky Slow Wave Coplanar Striplines on GaAs Substrates,” *IET Electron. Lett.*, vol.13, no 20, pp. 663 - 664, Oct. 1977.
- [67] D. F. Sievenpiper, “High Impedance Electromagnetic Surfaces,” Ph.D. Dissertation, Dept. Elect. Eng., U. CA., Los Angeles, CA, 1999.
- [68] P. I. Richards, “Resistor-Transmission Line Circuits,” *Proc. IRE*, vol. 36, no. 2, pp. 217 - 220, Feb., 1948.
- [69] S. B. Cohn, “Parallel-Coupled Transmission-Line-Resonator Filters,” *IRE Trans. Microw. Theory Tech.*, vol. 6, no. 2, pp. 223 - 231, Apr., 1958.
- [70] E. M. T. Jones and J. T. Bolljahn, “Coupled-Strip-Transmission Line Filters and Directional Couplers,” *IRE Trans. Microw. Theory Tech.*, vol. 4, no. 2, pp. 75–81, Apr., 1956.
- [71] R. S. Kshetrimayum, L. Zhu, “EBG Design using FSS Elements in Rectangular Waveguide,” *The Applied Computational Electromagnetics Society (ACES) Journal*, vol. 21, no. 2, pp. 149 - 154, Jul., 2006.
- [72] D. W. Prather, S. Shi, A. Sharkawy, J. Murakowski and G. J. Schneider, “Preliminary Concepts Of Electromagnetic Waves And Periodic Media,” in *Photonic Crystals: Theory, Applications, and Fabrication*, 2nd ed., New Jersey , John Wiley & Sons, 2009, ch. 2, sec. 2.2, pp. 73 - 103.

- [73] G. H. Li, X. H. Jiang and X. M. Zhong, "A novel defected ground structure and its application to a lowpass filter," *Microw. Optical Tech. Lett.*, vol. 48, no. 9, pp. 1760 - 1763, Sep., 2006.
- [74] M. R. I. Faruque, M. T. Islam and N. Misran, "Study of specific absorption rate (SAR) in the human head by metamaterial attachment," *IEICE Electron. Express*, vol. 7, no. 4, pp. 240 - 246, 2010.
- [75] J. Shumpert, T. Ellis, G. Rebeiz and L. Katehi, "Microwave and Millimeter-Wave Propagation in Photonic Band-Gap Structures," *IEEE AP-S International Symposium and URSI North American Radio Science Meeting Presentation*, 1997.
- [76] C. M. Soukoulis, "The History and Review of the Modeling and Fabrication of Photonic Crystals," *IOPscience Nanotechnology*, vol. 13, no. 3, pp. 420 - 423, Jun., 2002.
- [77] John D. Joannopoulos, Steven G. Johnson, Joshua N. Winn and Robert D. Meade, "Three Dimension Photonic Crystal," in *Photonic Crystals: Molding the Flow of Light*, 2nd ed., New Jersey, Princeton Uni. Press, 1995, ch. 6, pp. 94 - 105.
- [78] F. Falcone, T. Lopetegi and M. Sorolla, "1-D and 2-D Photonic BandGap Microstrip Structures," *Microw. Optical Tech. Lett.*, vol. 22, no. 6, pp. 411 - 412, Sep., 1999.
- [79] M .N. Mollah and N. C. Karmakar, "A novel hybrid defected ground structure as low pass filter," in *IEEE Antennas and Propagation Society International Symposium*, Monterey, CA, 2004, pp. 3581 - 3584.
- [80] M. N. Mollah, N. C. Karmakar and J. S. Fu, "Investigation into Novel Tapered Hybrid Defected Ground Structure (DGS)," *Int. J. RF Microw. Computer-Aided Eng.*, vol. 15, no. 6, pp. 544 - 550, Nov., 2005

Electromagnetic Bandgap Structures (EBGSs) Assisted Microstrip Bandpass Filter

(Corrections)

Submitted to

Submitted by

Dr. Md. Nurunnabi Mollah

Abu Talha Sadi

Professor


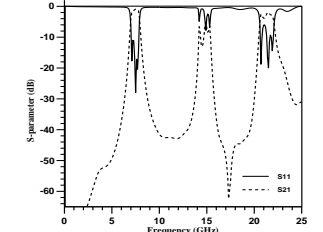
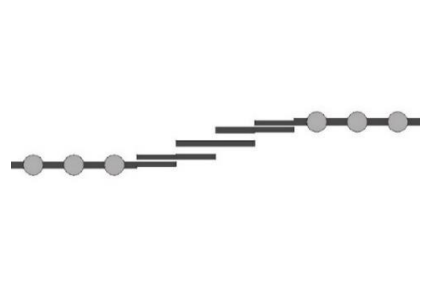
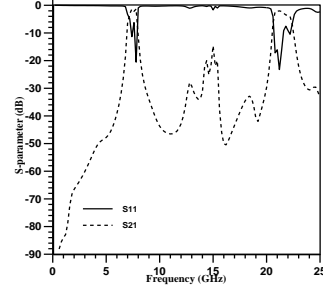
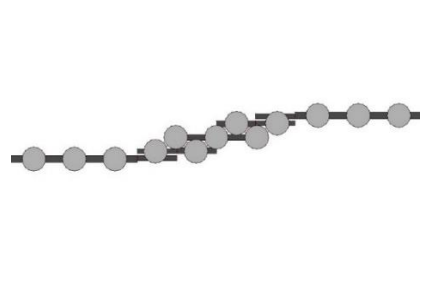
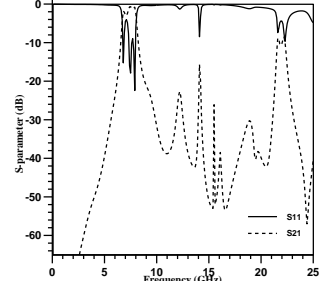
Roll: 1203554


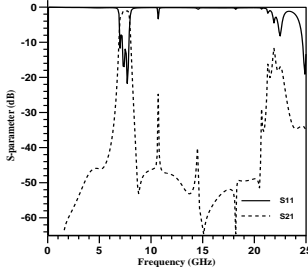

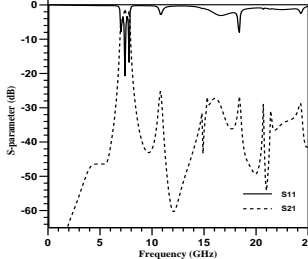
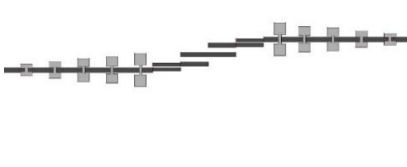
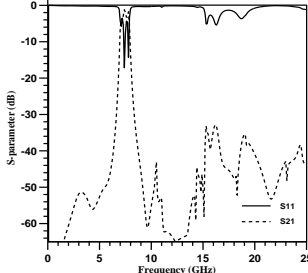
Department of Electrical and Electronic Engineering
Khulna University of Engineering & Technology

Department of Electrical and Electronic
Engineering
Khulna University of Engineering & Technology

Correction 1

Make a comparison table of the designs (Chapter 5, page 103-104).

No	Band Pass Filter	S-Parameter Performance	Remarks		
			Average 3 dB IL BW (%)	Peak IL (dB) of 2 nd Harmonics	Peak IL (dB) of 3 rd Harmonics
1.			11.11%	5.33	1.99
2.			10.08%	11.81	2.02
4.			16.91%	15.95	8.63

7.			11.73%	40.30	11.7
8.			7.37%	27.25	28.82
9.			7.23%	33.47	38.41

Correction 2

I have added 3dB IL bandwidth, average 10 dB RL bandwidth, maximum RL pick at 2nd and 3rd harmonics, maximum IL pick at 2nd and 3rd harmonics (pages 89-103).

Correction 3

Why harmonics are generated in BPF? What is the effect of harmonics in the communication system? (page 86)